PHOTOELECTROCHEMICAL WATER SPLITTING USING PEROVSKITE SEMICONDUCTORS

by
Burcu Oral
B.S., Chemical Engineering, Boğaziçi University, 2017

Submitted to the Institute for Graduate Studies in
Science and Engineering in partial fulfillment of
the requirements for the degree of
Master of Science

Graduate Program in Chemical Engineering
Boğaziçi University
2019

ACKNOWLEDGEMENTS

I would first like to thank my thesis supervisor, dear Prof. Ramazan Yıldırım who guided me in this work and encouraged me to be a better researcher.

Besides my advisor, I would like to thank the rest of my thesis committee: Assist. Prof. Damla Eroğlu Pala, and Assist. Prof. Uğur Ünal, for their valuable time and interest in my thesis.

I would like to thank Elif Can and Beyza Yılmaz, who assisted me for my experimental system set-up and were always open for a discussion about experiment results.

I would like to thank my friends, Pınar Eribol, Ayşegül Karakuş, İlke Kaynakanat, Uğurcan Tozar and Olcay Türkmen; with them I had a great two years and enjoyed my master's degree study.

Finally, I would to like to thank my dear family, my mother Bahriye, my father İbrahim and my sister Ezgi, for their unconditional love and support.

The financial support provided by Boğaziçi University Research Fund through Project 18A05D2 is also gratefully acknowledged.

ABSTRACT

PHOTOELECTROCHEMICAL WATER SPLITTING USING PEROVSKITE SEMICONDUCTORS

In this work, the photoelectrochemical cells with $SrTiO_3$ and TiO_2 photoanodes were constructed and the effects of preparation method, Al and Fe metal doping, the use heterostructure as well as the type, pH and molarity of electrolyte on photoelectrochemical water splitting performance were investigated. Solid state reaction, sol-gel and hydrothermal methods were used in synthetization of catalysts while in-situ coating, spin coating, dip coating and doctor blade methods were utilized in coating of the conductive substrates in fabrication electrodes. In addition, the precursor ratios of Sr and Ti were also changed. Linear sweep voltammetry from -1 to 2 V with scan rate of 10 mV/s was employed to measure the photoelectrochemical performances of the photoelectrodes by construction of the current voltage curves. XRD was used to determine the crystal structure while UV-VIS analysis was used to obtain diffuse reflectance spectra of catalysts; Kubelka-Munk method was applied to calculate the band gap energies. The solid state reaction followed by doctor blade coating method was found to be the best route to prepare an efficient photoelectrode. When the molar ratio of the Sr and Ti precursors were 2:3, the photoelectrochemical performance increased up to 2.5 folds compared to the ratio of 1:1. XRD analysis showed that cubic perovskite $SrTiO_3$ was obtained. The band gap energy of $SrTiO_3$ slightly changed from 3.2 eV to 3.17 eV by Fe-doping, but Al-doping did not change the band gap; no significant improvement observed in the performance. The best electrolyte was found to be NaOH. In addition to photoelectrochemical water splitting, the same materials were also tested in photocatalytic system, in which the particulate catalysts were used; the highest hydrogen production rate, which was with 600 μmol/h.gcat, was observed on the catalyst with the Sr:Ti ratio of 2:3.

ÖZET

PEROVSKİT YARI İLETKENLERİ ÜZERİNDE SUYUN FOTOELEKTROKİMYASAL OLARAK AYRIŞTIRILMASI

Bu çalışmada, $SrTiO_3$ and TiO_2 fotoanotları ile oluşturulan fotoelektrokimyasal hücrelerde, hazırlama methodu, Al ve Fe metal yükleme, çoklu yapı kullanımı, elektrolitin tipi, molaritesi ve pH'ı gibi parametrelerin suyun footoelektrokimyasal olarak ayrıştırlamasına etkisi araştırılmıştır. Katalizörler katı hal sentezi, sol-jel ve hidrotermal sentez yöntemleri ile hazırlanmış, malzeme elektrot üzerine dönel kaplama, daldırıp çıkararak kaplama ve bıçakla sıyırma yöntemleri ile kaplanmıştır. Ayrıca Sr ve Ti öncül maddelerinin oranları da değiştirilmiştir. Fotoelektrotların fotoelektrokimyasal performanslarını ölçmek için, akım-gerilim eğrileri 10 mV/s tarama hızında -1 ile 2 V arasında lineer tarama voltametrisi ile oluşturulmuştur. XRD sonuçları kristal yapının belirlenmesinde kullanılırken, UV-VIS ile elde edilen dağınık yansıma spektrumları kullanılarak Kubelka-Munk yöntemi ile band enerjileri saptanmıştır. Çalışmada, katı hal sentezi ile hazırlanan katalizöerlerin bıçak sıyırma yöntemi ile kaplamasının en uygun elektrod hazırlama yöntemi olduğu saptanmıştır. Sr ve Ti öncül maddelerinin molar oranı sırasıyla 2:3 olduğunda, 1:1 oranına göre fotoelektrokimyasal performansın 2.5 katına kadar arttığı saptanmıştır. Ayrıca XRD analizinden elde edilen SrTiO3'ün kubik yapıda olduğu görülmüştür. Fe yüklemesi $SrTiO_3$'ün bant boşluğu enerjisini çok az (3.2 eV'dan 3.17 eV'ta) değiştirirken Al yüklemesinde band enerjisi değişmemiş, her iki metal varlığında da performansta iyileşme olmamıştır. Deneylerde en iyi elektrolitin NaOH olduğu gözlenmiştir. Suyun fotoelektrokimyasal yöntem ile ayrıştırılması yanında aynı malzemelerden hazırlanmış katalizörler fotokatalitik olarak da test edilmiş, en yüksek hidrojen üretim hızı 600 μmol/s.gr_{cat} ile 2:3 oranıyla hazırlanan katalizörde görülmüştür.

TABLE OF CONTENTS

LIST OF FIGURES

LIST OF TABLES

LIST OF ACRONYMS/ ABBREVIATIONS

3DOM	Three Dimensional Ordered Mesoporous
ABPE	Applied Bias to Photon Efficiency
AM 1.5 G	Air Mass 1.5 Global
APCE	Absorbed Photon-to-Current Efficiency
CB	Conduction band
DSSC	Dye Sensitized Solar Cell
EDTA	Ethylenediaminetetraacetic Acid
HER	Hydrogen Evolution Reaction
IPCE	Incident Photon-to-Current Efficiency
NHE	Normal Hydrogen Electrode
OER	Oxygen Evolution Reaction
PEC	Photoelectrochemical
PV	Photovoltaic
RHE	Reversible Hydrogen Electrode
RTIL	Room Temperature Ionic Liquid
SCLJ	Semiconductor Liquid Junction
SSR	Solid state reaction
STH	Solar to Hydrogen Efficiency
VB	Valence band

LIST OF SYMBOLS

*	Adsorption site
C	Capacitance , F
e^-	Electron
E_f	Fermi Level
E_g	Band Gap Energy, eV
h	Planck's constant, eV.s
h^+	Holes
J	Current Density, mA/cm^2
k	Boltzmann Constant, $m^2\ kg\ s^{-2}\ K^{-1}$
P	Power, mW/cm^2
q	Electronic charge, C
r	Rate of Production ($\mu mol/h.g_{cat}$)
R	Reflectance
v	Frequency, 1/s
V_b	Applied bias, V
V_{fb}	Flat band potential, V
V_{ph}	Photovoltage, V
α	Symmetry Factor
η_F	Faradic Efficiency
η	Overpotential, V
κ	Dielectric constant, F/m

1. INTRODUCTION

The energy demand has been rapidly increasing in recent years with the increasing population. Today, the energy is mostly supplied from fossil fuels such as coal, natural gas and petroleum, which are limited and cause global warming through emitting greenhouse gases. As the results, the researches for new, renewable and clean energy sources are increasing.

In recent years, hydrogen utilization as a clean and sustainable energy source has increased. Hydrogen is an energy carrier such as electricity (Acar & Dincer, 2016); However, in contrast to electricity, it can be stored and this property with many others makes the hydrogen an attractive alternative energy source. Hydrogen can be used as a source for electricity via utilizing fuel cells, which are promising energy conversion devices producing electricity from hydrogen and oxygen emitting only water vapor (Daud *et al.*, 2017). It can be also used to produce synthetic fuels through Fisher- Tropsch type processes (United States Department of Energy, 2015). In petroleum industry, it is widely used in hydrocracking and in chemical industry hydrogen is an important raw material for ammonia and fertilizer production (de Valladares, 2017).

Hydrogen is an abundant element in the nature; however it does not exist in gaseous form, it is found in many substances such as water, organic compounds, biomass, fossil fuels (Acar & Dincer, 2016); therefore it is important to obtain pure hydrogen. There are mainly four energy sources of hydrogen production; by electrical, thermal, biochemical and photonic energy and these energy systems utilizes water, biomass and fossil fuels (Acar & Dincer, 2016).

Currently the most economically feasible method for producing hydrogen is steam reforming of hydrocarbons (Koroneos *et al.*, 2008). However this method uses fossil fuels as source; hence the process emits CO_2, which is a strong greenhouse gas and responsible from environmental problems such as global warming. Recently, the researches about hydrogen production methods are focused on obtaining hydrogen in a clean way, i.e. systems which does not increase CO_2 concentration in the atmosphere.

Figure 1.1 shows the prediction of hydrogen production paths and amounts, as it can be seen, in long-term future the utilization of sun in hydrogen production is expected to be increased. Some of the clean and environmentally friendly methods of hydrogen production and their future plan are given below.

Table 1.1. The hydrogen production methods cost and efficiency targets for 2020. (United States Department of Energy, 2015).

	Production Cost ($/kg)		Efficiency (%)	
	2011 status	2020 target	2011 status	2020 target
Biomass derived liquid reforming	6.6	2.3	68	75
Electrolysis of water	4.2	2.3	67	75
Biomass gasification	2.2	2	46	48
Solar thermochemical water splitting	NA	3.7	NA	20
Photoelectrochemical water splitting	NA	5.7	4 to 12	20
Photobiological processes	NA	9.2	NA	5

Biomass-derived liquid reforming utilizes sources like ethanol and reforming of ethanol is thermally neutral reaction with possibility to have 70% conversion (Hou *et al.*, 2015). In electrolysis, electricity is applied on cathode and anode to produce oxygen and hydrogen gases (Rashid *et al.*, 2015). Electrolysis can be called a clean hydrogen production method if electricity is provided by sources other than CO_2 emitting routes like fossil fuels. In nature and daily life there are several biomass sources like corn, rice, cotton etc. and since they consume CO_2 during growth, biomass gasification would yield zero or very small net CO_2 emission (Koroneos *et al.*, 2008). Solar thermos-chemical route requires higher reaction temperature compared to others but it is possible to decrease the temperatures using two-step cycles and modified catalysts (Rao & Dey, 2017). In photobiological process, generally bacteria are used for production of hydrogen from wastes of food, alcohol or sugar industries (Seifert *et al.*, 2010).

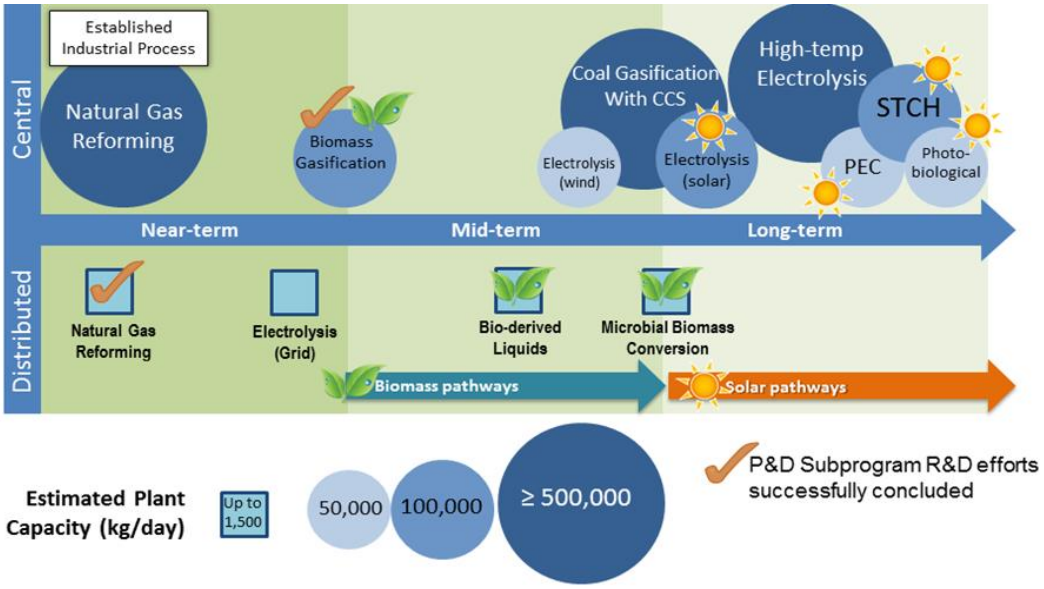

Figure 1.1. Future prediction of hydrogen production methods. (United States Department of Energy, 2015).

Water can be split into hydrogen and oxygen by using electricity, solar light and heat. Sun and water can be considered as renewable and exploitable, therefore production of hydrogen from water using solar light has a big potential for future developments (Kalanoor *et al.*, 2018). The systems uses solar light can be divided into two groups: photocatalytic and photoelectrochemical (PEC) water splitting (Indra, *et al.*, 2018). In photocatalysis, powder form catalyst suspension in water is illuminated and through redox reactions hydrogen and oxygen are produced. In photoelectrochemical cells, the photo electrodes are used to split water with or without an external energy source; in these type of systems hydrogen and oxygen are produced at different sides. For efficient utilization of solar light, utilizing catalysts responsive to visible light is crucial since almost half of the solar energy coming to Earth's surface is in visible light region (Acar & Dincer, 2016). Consequently, the researches on the photoelectrochemical water splitting have been increasing in recent years to improve the efficiency and the stability of photo electrode materials; the efficiency should be minimum 10% to have commercialized photoelectrochemical water splitting application (Minggu *et al.*, 2010; Osterloh, 2017). Currently the research about PEC focuses on increasing the efficiencies and eliminating the need of external bias (Bak *et al.*, 2002).

In a photoelectrochemical cell, the oxygen is produced at anode side while side hydrogen is generated at cathode side with following reactions (Chen, 2013):

Anode (oxidation reaction): $4\,h^+ + 2\,H_2O \rightarrow 4\,H^+ + O_2$ (1.1)

Cathode (reduction reaction): $4\,e^- + 4\,H^+ \rightarrow 2\,H_2$ (1.2)

Overall Water Splitting: $2\,H_2O \rightarrow O_2 + 2\,H_2$ (1.3)

$SrTiO_3$ and TiO_2 are widely used in PEC and photocatalytic water splitting applications. These semiconductors are also used in similar areas; For example they are used in solid-oxide fuel cell applications, waste water treatment and antibiotic removals, photocatalytic reduction of CO_2 and enhancing the hydrogen storage behaviors of materials like $4MgH_2Na_3AlH_6$ and MgH_2 (Chou *et al.*, 2019; Eghbali *et al.*, 2019; Luo *et al.*, 2018; Yahya & Ismail, 2018). Their chemical and physical properties are well established. It is possible to easily alter their electronic and structural properties to increase activity and efficiencies.

In literature, $SrTiO_3$ has been widely studied since it is stable, and it has suitable band edge positions to govern overall water splitting reaction. However, due to its band gap, its solar to hydrogen efficiency is low, and the researchers are focused on improving this by various means. Doping is one way to change the electronic properties of $SrTiO_3$. For example Fe-doping on $SrTiO_3$ in photoelectrochemical applications was done in only few reports even though Fe has suitable ionic radius to replace both Sr and Ti atoms in the structure. Al-doping was used in photocatalytic activity more often and proven to enhance the activity; however, as far as we know, it has not been used in photoelectrochemical water splitting applications. Additionally, the use of different Sr:Ti ratios were also tested; for example Sulaeman, *et al*., (2011) reported an enhancement of photocatalytic activity with larger Sr:Ti ratios than one; however, as far as we know, such a work was not reported for photoelectrochemical water splitting either.

This thesis aims to construct a working photoelectrochemical cell for water splitting and optimizing the conditions for achieving high efficiencies. $SrTiO_3$ and TiO_2 semiconductors are used as photo electrodes to absorb the light to split water into hydrogen and oxygen gases. Au and Pt plates are used as counter electrode and Ag/AgCl reference electrode is used in three-electrode configuration. Effect of preparation method, doping, sacrificial agents, electrolyte type and pH are studied. In addition heterostructure of TiO_2 and $SrTiO_3$ are fabricated and investigated.

In the following chapters literature survey is conducted to understand the current status in photoelectrochemical water splitting (Chapter 2), experimental work is briefly explained (Chapter 3) and results of this work are given (Chapter 4) and finally the conclusions are stated and recommendations for future work are given (Chapter 5).

2. LITERATURE SURVEY

2.1. Fundamentals of Solar Water Splitting

The decomposition of water into hydrogen and oxygen gases is called water splitting. At standard conditions the Gibbs free energy (ΔG) is equal to 237.2 kJ/mol (Navarro Yerga *et al.*, 2009). Since ΔG is positive, water splitting is not a spontaneous reaction, it is thermodynamically unfavorable. According to the Nerst equation, the energy required to split water into hydrogen and oxygen is 1.23 eV. Theoretically, in order to catalyze this reaction, semiconductors must absorb the light with photon energy minimum of 1.23 eV (Kment *et al.*, 2017). Considering energy losses due to the recombination of the charge carriers, electrical connections, resistance of the electrodes and electrolyte etc., an energy of 1.8 eV is needed for water splitting to be spontaneous (Choudhary *et al.*, 2012). Therefore, a semiconductor with band gap in the range of 1.8-2.2 eV will be a suitable choice for unassisted water splitting. Large band gap semiconductors such as $SrTiO_3$, TiO_2, WO_3, ZnO, SnO_2 etc., are stable in electrolytes but due to their band gap they can only absorb UV region of the solar light; intermediate band gap semiconductor like Fe_2O_3 can absorb visible region but suffers from poor charge carrier rates and trapping of electrons in oxygen-deficient iron sites. For the optimum band gap semiconductors like Si, GaAs, CdSe, CdTe, CuO, Cu_2O etc., on the other hand, the corrosion is a serious problem (Yoon *et al.*, 2000; Mishra *et al.*, 2003). The instability of the photoelectrodes is due to the oxidation of semiconductor with photogenerated holes. (Memming, 2001). Solar water splitting reaction can be shown as (Abe, 2010):

$$H_2O + h\nu \rightarrow H_2 + 1/2\ O_2 \qquad (2.1)$$

Generally, solar water splitting can happen through two ways; in particulate photocatalytic system, where photocatalyst is suspended in aqueous solution, the hydrogen and oxygen gases are produced at the surface of catalyst upon irradiation. In photoelectrochemical cells, on the other hand, two electrically wired/contacted electrodes are immersed in aqueous solution and upon irradiation, the hydrogen gas evolves on cathode side while the oxygen is produced over anode (Moniruddin *et al.*, 2016). The efficiencies of

particulate systems are lower compared to photoelectrochemical systems because of poor charge separation and rapid charge recombination (Alfaifi *et al.*, 2018). In Figure 2.1 the main process in photocatalytic (a) and photoelectrochemical (b) water splitting and possible recombination types are shown.

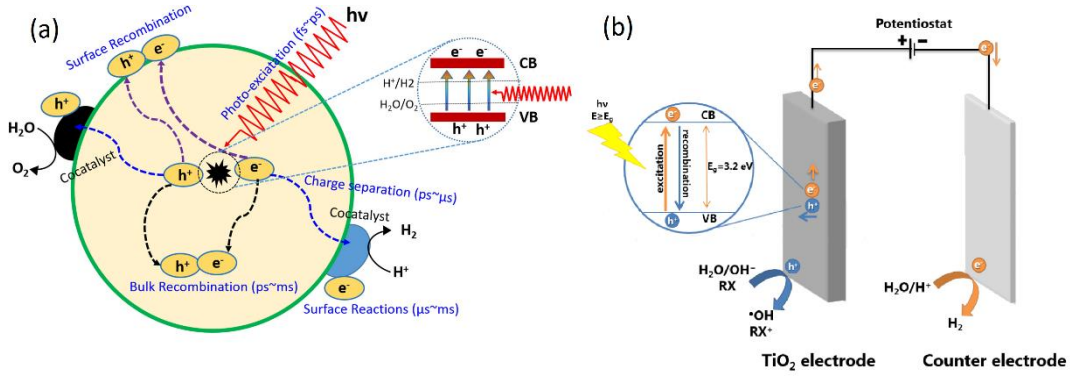

Figure 2.1. Mechanism and recombination in (a) Photocatalytic water splitting on particulate catalyst (b) Photoelectrochemical water splitting on TiO_2 photoanode. (Bessegato *et al.*, 2014; Alfaifi *et al.*, 2018).

When a semiconductor absorbs photons that have higher energy than its band gap, electrons in the valence band is excited to the conduction band leaving mobile holes behind (McEvoy, 2011). These photogenerated electrons and holes drive redox reactions if the positions of bands are appropriate (Hisatomi *et al.*, 2014). Electrons drive hydrogen evolution reaction (HER) while holes drive oxygen evolution reaction (OER). The photogenerated energy carriers can be involved in following reactions (Sharma *et al.*, 2017):

- Holes: $$2h^+ + H_2O \rightarrow 1/2\,O_2 + 2H^+ \quad (2.2)$$

$$2h^+ + OH^- \rightarrow 1/2\,O_2 + H_2O \quad (2.3)$$

- Electrons: $2e^- + 2H^+ \rightarrow H_2$ (2.4)

$2e^- + H_2O \rightarrow H_2 + OH^-$ (2.5)

Along with these reactions, the recombination of photo-excited carries also occur; therefore effective charge separation is important in solar water splitting materials (Hisatomi *et al.*, 2014). Sometimes the holes (or the electrons) causes decomposition by oxidizing (or reducing) the semiconductor itself. This happens when the redox potentials of the semiconductor lies in between the redox potentials of water splitting.

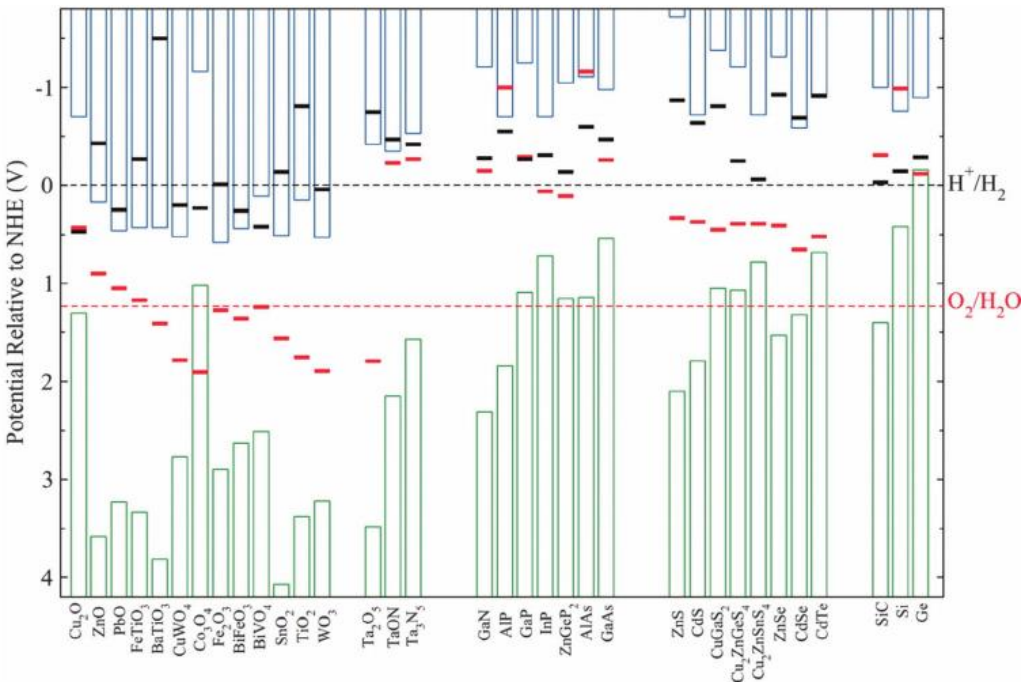

Figure 2.2. The oxidation (red bars) and reduction (black bars) potentials of semiconductors with respect to water splitting redox potentials. (Berardi *et al.*, 2014).

In Figure 2.2, the oxidation and reduction potentials of semiconductors with respect to water splitting redox potentials are given. Green and blue columns represent the valance and conduction band edge positions of the semiconductors at pH=0 respectively. For example, the bars for TiO_2 lies outside of the redox potential of water splitting; therefore instead of reduction or oxidation of TiO_2, reduction and oxidation of water is thermodynamically

preferred. A representative explanation is given for an instable semiconductor, Cu_2O in Figure 2.3. Since the reduction and oxidation of Cu_2O need lower potentials compared to reduction and oxidation of water, instead of water splitting, decomposition of the semiconductor occurs.

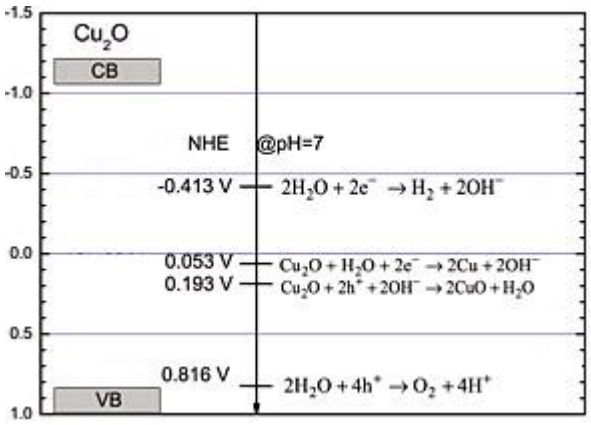

Figure 2.3. The redox potentials of Cu_2O decomposition and water splitting with respect to NHE at pH= 0. (Ying *et al.*, 2016).

The mechanism of photoelectrochemical water splitting can be given as (Iqbal & Siddique, 2018):

- Light is absorbed by the semiconductor according to its band gap
- Electrons in the valance band of the semiconductor are excited and jumped to conduction band leaving holes behind
- For n-type photoelectrode, electrons are transferred to cathode via external circuit (For p-type photoelectrode electrons are withdrawn from anode)
- At (photo)anode surface, oxidation of water to oxygen gas and at (photo)cathode surface, reduction to hydrogen gas occurs

Mainly there can be three different assemblies in a photoelectrochemical cell (Moniruddin *et al.*, 2016):

- n-type semiconductor as photo node and a metal cathode

- p-type semiconductor as photocathode and a metal anode
- n-type semiconductor as photoanode and p-type semiconductor as photocathode connected in series

Configurations a and b can be also called as Schottky type cell and configuration c is also called as tandem cell. (Kment *et al.*, 2017). The schematics of these three configurations can be found in Figure 2.4.

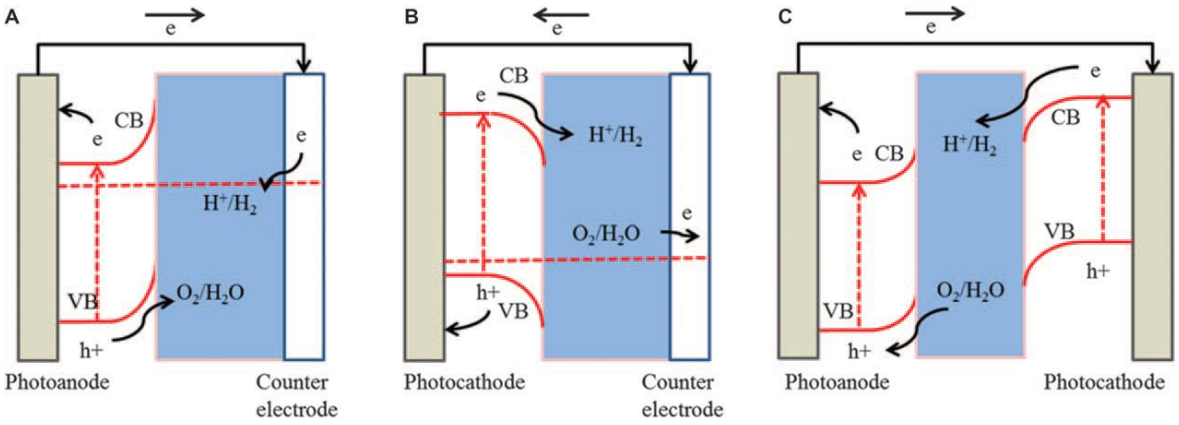

Figure 2.4. The schematics of assemblies in photoelectrochemical cells (A) n-type semiconductor as photoanode (B) p-type semiconductor as photocathode and (C) tandem type where both electrodes are photoactive. (Moniruddin *et al.*, 2016).

When electrodes are immersed in electrolytes, their Fermi levels are equilibrated (Sivula, 2013). Fermi level is the representation of chemical potential of electrons in the semiconductor (Nozik, 1980). When the semiconductor is n-type, E_f, fermi energy level, is closer to the conduction band whereas, in p-type semiconductors, E_f is closer to valance band (Peter, 2016). When Fermi level of a semiconductor is different than that of electrolyte, electrons transfer happens till the levels become the same (Dias & Mendes, 2018). Figure 2.5, shows the equilibration of fermi levels at semiconductor-electrolyte interface.

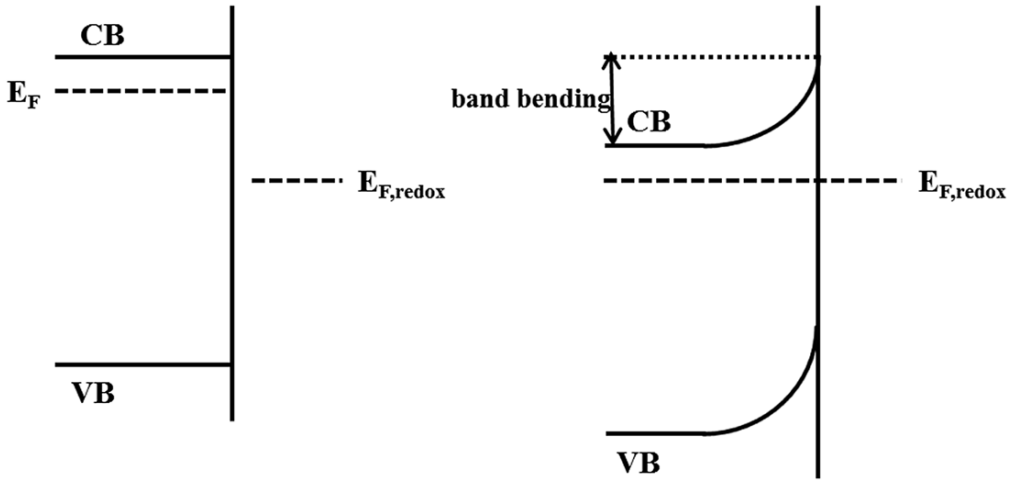

Figure 2.5. Equilibration of Fermi levels and band bending for a n-type semiconductor in contact with electrolyte. (Peter, 2016).

When fermi level of the electrode is moved because of disturbances (electron transfer in this case), valence and conduction bands move along with the fermi level but the energy level at the semiconductor- electrolyte junction (SCLJ) is fixed, therefore band bending is observed (Sivula, 2013). The amount of band bending depends on the initial difference between the Fermi levels of the semiconductor and the electrolyte (Peter, 2016). Bending acts as a potential barrier for further electron transfer (Nozik, 1980).

Band bending can be induced by many types of interactions: (i) metal/semiconductor contact induced band bending happens due to the difference of the work functions of metal and semiconductor, (ii) surface state induced band bending occurs due to the difference between the energy levels at the surface and the fermi level, (iii) absorption induced band bending happens because of the molecules adsorbed by the semiconductor surface, (iv) applied-bias induced band bending occurs depending on the type of bias i.e. anodic or cathodic; for n-type semiconductor application of anodic bias (positive bias, reverse bias) increases space charge layer and causes upward bending and finally (v) semiconductor/electrolyte junction induced bending happens because of the difference between the fermi level of the semiconductor and redox potential of the electrolyte (Jiang *et al.*, 2017).

The interfacial electron transfer creates also a space charge layer (also known as depletion layer) in the semiconductor and this layer induces an electric field which plays an important role in charge separation (Nozik, 1980; Sivula, 2013). Depending on the amount of band bending and conductivity of the semiconductor, the space charge layer can be in the range of 100 Å to microns, and in the solution side Helmholtz double layer in the order of 1 Å is generated due to adsorption of counter ions on the surface of the electrode (Schoonen & Xu, 2000). Without Helmholtz layer the band bending is expected to be equal to the difference of initial fermi levels of semiconductor and electrolyte (Nozik, 1980). Helmholtz layer creates additional potential drop in the space charge layer so that band bending is adjusted to make the net rate of electron transfer equal to zero. When zero net electron transfer is established, equilibrium is reached (Schoonen & Xu, 2000).

Flat band potential is an important character of a semiconductor in photoelectrochemistry, it is the potential of the electrode when bands are flat, i.e. zero space charge in the semiconductor (Nozik, 1980). For estimation of conduction and valence band positions of semiconductors, the flat band potentials are important. Since flat band depends strongly on the pH, the band positions of the semiconductors are expected to shift with the change of pH (Gomes & Cardon, 1982).

When SCLJ is illuminated, photogenerated electron-holes are separated by the influence of the electric field present in the space charge layer (Nozik, 1980). Upon illumination, electrons and holes become mobile and Fermi level is split into quasi-fermi levels which represent the occupation of states by electrons and holes (McEvoy, 2011). The difference between quasi fermi levels is the generated photovoltage and acts as the driving force for water splitting (McEvoy, 2011; Sharma *et al.*, 2017). Figure 2.6 shows the band alignment in SCLJ under illumination. Photovoltage (V_{ph}) is regarded as the actual driving force because it carries all the losses that can arise such as incomplete light trapping, and non-radiative recombination, and therefore it is always less than the band gap of the semiconductor (Chen *et al.*, 2013). The maximum possible open circuit photovoltage is equal to the difference between the flat band potential of the semiconductor and the redox potential of the electrolyte, i.e. the band bending (Nozik, 1980).

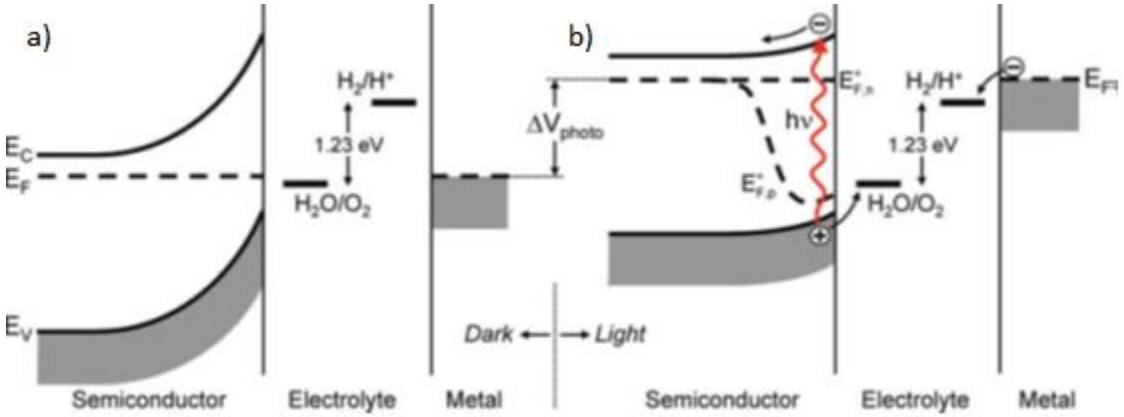

Figure 2.6. Changes in SCLJ (a) under equilibrium in dark and (b) under illumination. (Krol, 2012).

In Figure 2.6, n-type semiconductor in an electrolyte is depicted. When the equilibrium is disturbed by illumination, the Fermi level is divided into two quasi fermi levels, representing electrons and holes respectively (Van de Krol, 2012). The fermi level of electrons is shifted by the amount of the photovoltage produced in semiconductor and band bending decreases.

When bias is applied to a semiconductor, the position of fermi level changes and the potential difference is distributed over space charge and Helmholtz layer (Bak *et al.*, 2002; Jiang *et al.*, 2017). Applying negative bias to a n-type semiconductor can act against band bending and cause bands to be flat (Jiang *et al.*, 2017). Further increase in negative potential will cause upward band bending and cathodic current will start to flow as depicted in Figure 2.7 (Rajeshwar, 2007).

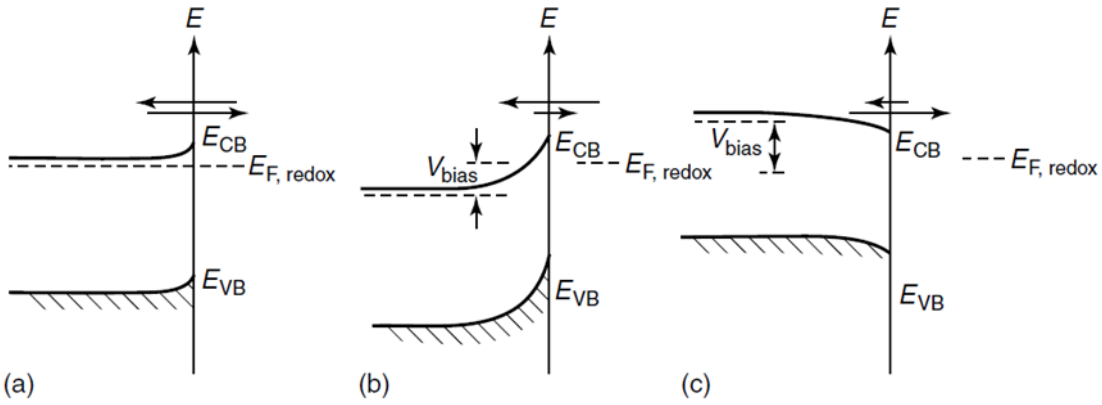

Figure 2.7. Effect of applying (b) positive bias and (c) negative bias to an n-type semiconductor in equilibrium (a). (Rajeshwar, 2007).

In Figure 2.7, the arrows represent flow of the currents and their magnitudes. When a positive bias is applied (b), anodic current it observed while the cathodic currents are observed when negative bias is applied (c) (Rajeshwar, 2007).

In ideal conditions, when flat band potential of a semiconductor is (exceeded)passed, the electrocatalytic reactions start and current is observed; however in practical applications the potential at which current is observed (onset potential) does not match with flat band potential and the difference of these potentials is called overpotential (Rajeshwar, 2007; Sivula, 2013). Overpotentials are required due to energy losses in electron transfer from the external circuit and holes passing through space charge region (Jiang *et al.*, 2017).

2.2. Materials used in Solar Water Splitting

The semiconductors can be classified as n-type or p-type according to the electronic properties and the majority carrier types (electron or hole) (Kment *et al.*, 2017). Most oxide, nitride and sulfide semiconductors have anion defects hence n-type conductivity is observed (Moniruddin *et al.*, 2016). In photoelectrochemical water splitting, generally p-type semiconductors, hole abundant semiconductors, are suitable for H_2 generation whereas n-type semiconductors, electron abundant semiconductors, are suitable for O_2 generation

(Kalyanasundaram, 2013). The ability of reducing water to hydrogen or oxidizing to oxygen depends on the positions of valance and conduction bands of the semiconductor.

An efficient and effective photocatalyst/photoelectrocatalyst should have: good chemical stability, low electron-hole recombination rates, low cost of production, rapid charge transfer and to govern overall water splitting; the conduction band edge should be more negative than redox potential of reduction to hydrogen and valance band edge should be more positive than redox potential of oxidizing to oxygen (Kment *et al.*, 2017). Below in Figure 2.8 the band edges with respect to water splitting redox potentials for several semiconductors are given. When the band edges are not positioned at the required potentials, an external bias is needed to overcome the potential deficiency and drive the reaction (Moniruddin *et al.*, 2016)

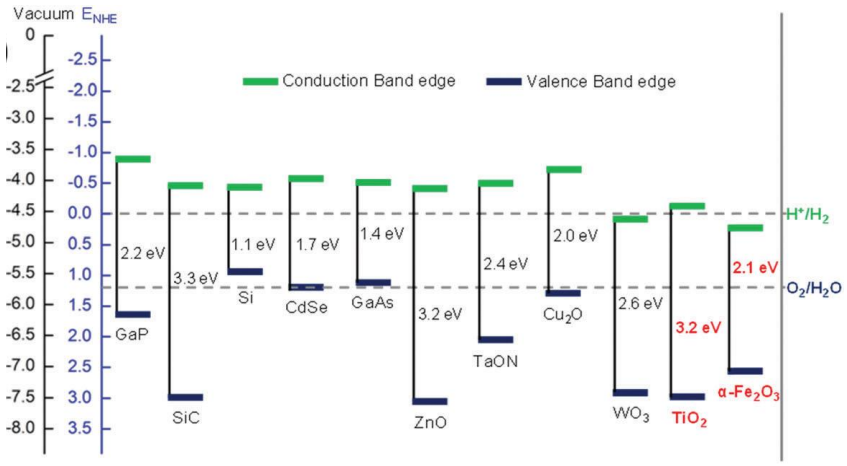

Figure 2.8. Band positions of several semiconductors with respect to Vacuum and Normal Hydrogen Electrode at pH=0. (Kment *et al.*, 2017).

2.2.1. Photoanodes

Despite the large band gap and fast electron-hole recombination rate, metal oxides are regarded as most viable options for water splitting applications due to their low cost and high stability (Kment *et al.*, 2017). Several metal oxides have d^0 electronic configured metal ions and hence are photosensitive in the UV region of solar spectra (Moniruddin *et al.*, 2016).

TiO_2 is most studied material for PEC applications, it is found in three phases with different band gap and activities; tetragonal rutile, tetragonal anatase and orthorhombic brookite (Shen *et al.*, 2018). Rutile phase is thermodynamically most stable phase with 3 eV band gap whereas anatase phase is more active with band gap of 3.2 eV (Luttrell *et al.*, 2015). TiO_2 as photoanode has good (photo)corrosion resistance in aqueous environments (Nowotny *et al.*, 2007). The properties of TiO_2 can be altered by defect chemistry and oxygen non-stoichiometry (Bak *et al.*, 2002). Its reserves are abundant and it is less expensive and environmentally friendlier than other semiconductors (Fujishima *et al.*, 1999).

Titanate based perovskites ($MTiO_3$; M = metal) are mostly large band gap, stable and photoactive materials that are used in photocatalytic applications (Bin Adnan *et al.*, 2018). $NiTiO_3$ (2.10 eV) and $CoTiO_3$ (2.28 eV) are narrow band gap perovskites but due to their band positions, they are not considered as suitable materials for PEC applications (Qu *et al.*, 2014). $FeTiO_3$ (2.8 eV) and $PbTiO_3$ (2.75) are mid-band gap perovskites and due to their ferroelectric behavior, charge separation is better at the interface (Li *et al.*, 2017). $SrTiO_3$ (3.2 eV) is the most widely studied titanate perovskite (Sanwald *et al.*, 2018). After TiO_2, this semiconductor was considered as a suitable photoelectrode for overall water splitting, since it has one of the smallest anodic value flat band potential compared to other semiconductors (Sivula *et al.*, 2011). Due to its band gap, $SrTiO_3$ is active mostly in UV region so doping, sensitization, p-n junction formation and defect engineering are investigated for improving the absorption in visible region (Pinheiro *et al.*, 2014).

ZnO is an inexpensive and environmentally friendly semiconductor with band gap of 3.2 eV and high carrier mobility (Kolodziejczak-Radzimska & Jesionowski, 2014).However its application in PEC water splitting is limited due to low conductivity and insufficient light absorption (Paulauskas *et al.*, 2008). In order to change electronic properties of ZnO

electrodes doping, heterojunction formation and controlled oxygen vacancies introduction are studied (Wang *et al.*, 2018).

WO_3 photoanodes are widely studied in PEC water splitting. It has band gap of 2.5-2.8 eV and it is nontoxic, stable in acidic environments and inexpensive (Liu *et al.*,2012). WO3 photoanodes generate H_2O_2 instead of oxygen by photo-oxidation and this product causes dissolution of WO_3, causing instability in some cases (Seabold & Choi, 2011).

With band gap of 2.2 eV, hematite (α-Fe_2O_3) can absorb light in the visible range, around 40% of the solar spectrum (Li *et al.*, 2013). But due to its band positions without external bias it is not possible to produce hydrogen on hematite electrodes (Duret & Grätzel, 2005). The efficiency is lower because Fe_2O_3 has excited state life time of 10 ps, short hole diffusion distance of 5 nm, therefore the transfer and collection of holes in SCLJ is limited (Tryk *et al.*, 2000). Fe_2O_3 has potential to generate H_2O_2 instead of O_2 like WO_3 photoanodes depending on the surface hole density, hence interface engineering is crucial in hematite electrodes (Kuang *et al.*, 2017).

$BiVO_4$ photoanodes have band gap of 2.4 eV and suitable band levels for reduction potential and low onset potential for oxygen evolution (Pihosh *et al.*, 2015). However, low photocurrent efficiency, fast recombination of electron hole pairs, slow charge transfer and low oxidation kinetics are the drawbacks of the $BiVO_4$ photoanodes (Huang *et al.*, 2014). In addition, $BiVO_4$ is found to be instable in acidic and neutral phosphate buffer solutions and strong basic electrolytes (Kuang *et al.*, 2016; Lichterman *et al.*, 2013). However, it is also reported that monoclinic phase is thermodynamically stable (Kudo *et al.*, 1999).

Copper tungstate ($CuWO_4$), also known as copper tungsten oxide has band gap of 2.3 eV, ideal for PEC applications but absorption of light is low and it has high bulk charge transfer resistance (Yourey & Bartlett, 2011). Construction of heterojunctions and surface modifications are some approaches to increase the efficiency of $CuWO_4$ (Alfaifi *et al.*, 2018).

Nitride or oxynitride compounds considered as promising materials for PEC applications (Zou *et al.*, 2001). Their valence bands are more negative than that of oxides due to the hybridization of N 2p with O 2p orbitals and this results in having proper band

levels for overall water splitting with narrower band gap but it also causes instability because of the oxidation of N ions to N_2 (Jian *et al.*, 2018).

TaON has band gap of 2.5 eV and suitable band positions for overall water splitting but the activity for hydrogen production is low and has low stability due to N 2p orbitals (Higashi *et al.*, 2012).

Ta_3N_5 has small band gap and band positions to perform spontaneous water splitting and has theoretical solar to hydrogen efficiency around 15% but it has low photocurrent efficiency and poor charge transport (Alfaifi *et al.*, 2018). PEC performance of Ta_3N_5 photoanodes is limited because of the growth of a thin oxide layer on the surface due to photooxidation (He *et al.*, 2016).

N-type semiconductors like ZnS, CdS and CdSe are also studied as photocatalysts for solar water splitting (Jang *et al.*, 2007). Except ZnS, they can absorb visible light but they are sensitive to oxidation which results in corrosion (Lianos, 2011). These materials can be in the form of core-shell structures which increases the stability (Wang *et al.*, 2010). They are sometimes used in combination with large band gap catalyst as sensitizers to absorb visible light and reduce electron hole recombination (Chi *et al.*, 2010). CdS offers proper band gap and band edge positions for overall water splitting but the efficiency of separation and transfer of photogenerated carriers (electrons & holes) is low (Pareek *et al.*, 2016). ZnS, despite its band gap, is promising material due to generation of mobile photo-excited charge carriers and fast electron transfer abilities (Monroy *et al.*, 2003). It is found that overall efficiency of ZnS can be improved by transition metal doping and defect engineering (Kurnia *et al.*, 2016; Öztaş *et al.*, 2006).

2.2.2. Photocathodes

Earlier studies on photocathodes mainly focused on p-type materials such as p-silicon and group III-V semiconductors like InP and GaP and recently p-type oxides and sulphide gain attraction too (Alfaifi *et al.*, 2018).

Cuprous oxide (Cu_2O), cupric oxide (CuO), and nickel oxide (NiO) are widely used in solar water splitting since they are low cost, abundant and ideal band-gap materials (Alfaifi *et al.*, 2018). Cu_2O has a band gap of 1.9-2.2 eV but suffers from photocorrosion (Hara *et al.*, 1998). It is possible to decrease the photocorrosion by adding a protective layer on the surface, the best performance of Cu_2O was achieved where TiO_2 is used as passivation layer (Paracchino *et al.*, 2011). CuO has band gap of 1.2-1.8 eV, which can result in higher photocurrents than Cu_2O but it has received less attention since its conduction band is more positive (Chauhan *et al.*, 2007). NiO has wide band gap of 3.6 eV to 4 eV, it is favorable for p-n junction and has low resistance, high hole mobility and low lattice mismatch (Gupta *et al.*, 2009).

There are some bimetallic semiconductors that are used in PEC systems. $CuFeO_2$ has band gap of 1.5 eV and it is earth abundant and stable in aqueous solutions but it has poor charge transfer which limits its performance (Read *et al.*, 2012). $CaFe_2O_4$ has small band gap and favorable band positions for overall water splitting but its photo response is low due to poor charge separation and charge carrier mobility (Kim *et al.*, 2013).

Cu containing chalcogenide materials such as $CuGaSe_2$ and Cu_2ZnSnS_4 exhibit p-type behavior but they are prone to photocorrosion and they are insufficient for oxidation of water (Hisatomi *et al.*, 2014). $CuInS_2$ and $CuGaS_2$ are small band gap chalcogenides but it is hard to fabricate uniform films (Kang *et al.*, 2015).

Crystalline silicon has attractive properties to be a suitable candidate for PEC applications such as small band gap, high mobility carrier property and its applications in PV and electronic areas but under anodic conditions, the surface is oxidized which creates surface defects and a passivation layer which inhibits photocurrent production in PEC systems (Myamlin & Pleskov, 1967). The Si electrodes can be protected by depositing metal clusters or oxide layers (Lana-Villarreal *et al.*, 2007).

GaP and InP are two of the III-V semiconductors that are widely studied for solar water splitting. GaP (2.2 eV) can exhibit both n-type and p-type properties. N-type is unstable in water but under cathodic conditions p-type is stable for long periods in electrolytes (Memming & Schwandt, 1968). InP (1.35 eV) has conduction band edge slightly above

hydrogen evolution potential, which makes it a good photocathode; but in acidic conditions, the photocorrosion inhibits its performance (Alfaifi *et al.*, 2018). The instability problem can be solved by coating a protective oxide layer (Lin *et al.*, 2015).

2.3. Preparation Methods of Catalysts and Electrodes

2.3.1. Preparation of Catalysts

Catalyst activity strongly depends on its morphology, surface area, crystallinity, crystal phase and particle size (Phoon *et al.*, 2019). It is important to have a control over these properties to achieve high catalytic activities. There are many ways to synthesize catalysts, and the chemical and the physical properties of the catalyst greatly depends on the preparation method. Some of the catalyst preparation methods are sonochemical, co-precipitation, direct oxidation, molten salt synthesis, chemical vapor deposition, physical vapor deposition and electrodeposition method etc. (Iqbal & Siddique, 2018); in the following part, the frequently used preparation methods in photocatalytic and photoelectrochemical studies will be discussed briefly.

Hydrothermal Reaction. In order to achieve small particle sizes and have a better control over shape and size distributions, the hydrothermal method is widely used. The reaction takes place in a stainless steel-Teflon vessel, also known as autoclave, and the reaction takes place under vapor saturation pressure (Phoon *et al.*, 2019). $SrTiO_3$ can be prepared by hydrothermal process through following mechanism with the Sr and Ti precursors (such as Strontium hydroxide, $Sr(OH)_2$, and Titanium dioxide, TiO_2 respectively) (Huang *et al.*, 2014): Sr precursor is hydrolyzed to produce Sr ions and $[Ti(OH)_6]^{2-}$ complex is formed by the reaction of TiO_2 precursor and hydroxide ions. Sr ions and Ti complex are then precipitate mutually to form $SrTiO_3$ phase. Dissolution and precipitation reaction continues till all TiO_2 is consumed. After the reaction, uniformly sized nanoparticles are produced.

The shape of $SrTiO_3$ particles can be tuned by adjusting temperature, pH or time of the reaction. It is reported that alkaline medium is critical for formation of Ti complex from TiO_2 precursor (Zhang *et al.*, 2015).

Kalyani *et al.* created mesocrystals of $SrTiO_3$ with sizes 100-200 nm by hydrothermal reaction using ethanol and polyethylene glycol as organic additives (Kalyani *et al.*, 2012). Mourão *et al.* incorporated mechanical stirring with hydrothermal reaction and produced $SrTiO_3$ microspheres with sizes from 30-46 nm (Mourão *et al.*, 2015).

Phoon *et al.* formed $SrTiO_3$ nanocubes with 30-56 nm size and optimized reaction temperature for obtaining higher photoelectrochemical activity (Phoon *et al.*, 2018). *Zhao et al.* produced core-shell microspheres of $SrTiO_3/TiO_2$ heterostructure with a hierarchical surface with particle size of 700 nm (Zhao *et al.*, 2017).

Huang *et al.* showed that increasing reaction temperature increases the particle size and further increase in temperature may lead to aggregation of particles and non-homogeneity in the product structure. They suggested that, in order to produce high purity of nanocrystals, high pH and Sr/Ti mole ratio larger than one is required (Huang *et al.*, 2014).

In addition to conventional hydrothermal reaction, microwave assisted hydrothermal reaction (MAH) is another way to produce $SrTiO_3$ with shorter reaction time and lower temperatures (Moreira *et al.*, 2008). For example, Souza *et al*. produced crystalline $SrTiO_3$ nanoparticles in 4 mins by MAH (Souza *et al.*, 2012).

As $SrTiO_3$, TiO_2 can be also synthesized as nanoparticles, nanotubes, nanobelts and nanowires with hydrothermal reaction by altering reaction conditions (Wang *et al.*, 2014). For example, with the addition of corrosive additives, Liu *et al.* prepared low density and large surface area TiO2 hollow nanospheres (Liu *et al.*, 2007).

Solvothermal Reaction. This synthesis reaction is similar to hydrothermal reaction; however, instead of water, various solvents such as ketones, alcohols, carboxylic acids and toluene are used (Wang *et al.*, 2014). When organic solvents with high boiling points are chosen, nanoparticles with uniform particle size can be produced by solvothermal reaction. High

crystallinity can be achieved when the low dielectric organic solvents are employed in the reaction (Phoon *et al.*, 2019).

By solvothermal method, better size control of nanoparticles, higher crystallization and less agglomeration can be achieved in preparation of TiO_2 nanomaterials (Wang *et al.*, 2014). The mechanism of solvothermal reaction in TiO_2 synthesis was summarized by (Lü *et al.*, 2011): First etherification of TiO_2 precursor and alcohol solvent will take place and this reaction will produce water. The produced water will then lead to hydrolysis of TiO_2 precursor, and Ti-O-Ti bridges will be formed. When amount of water is limited, the TiO_2 particles will have a smaller structure such as microspheres. When reaction temperature is increased, the etherifying reaction will produce more water and this will result in larger TiO_2 particles.

Sol-gel. Sol-gel method can be used in fabrication of high purity, fine-scale and homogeneous catalysts with controllable morphology (Wang *et al.*, 2014). The process starts with hydrolysis and condensation of metal alkoxides. After that with temperature treatment polymerization is promoted and metal oxide network is formed (Phoon *et al.*, 2019).

Downsides of the sol-gel method are that the metal alkoxides precursors are generally expensive, and in order to get crystalline product high temperature, the calcination is required (Liu *et al.*, 2008). In some cases, the aging, drying and annealing are needed after the reaction (Xie *et al.*, 2007).

The morphology of the final product depends on molar ratios of the reactants, reaction pH, temperature and time (Chen *et al.*, 2010; Tseng *et al.*, 2010). In sol-gel hydrolysis, the reaction between the Ti precursor and water/alcohol is a critical step, and molar ratios of reactants can affect hydrolysis speed and result in different structures and properties of TiO_2 (You *et al.*, 2012). In 2001, Bao synthesized sol-gel derived $SrTiO_3$ thin films with high crystallinity, and observed that the high crystallinity results in lower band gap energy, which promotes the photocatalytic activity (Bao *et al.*, 2001). Liu *et al.* synthesized $SrTiO_3$ by both sol-gel method and solid state reaction; catalyst prepared by sol-gel reaction had smaller $SrTiO_3$ particle size (30 nm), uniform morphology and higher photocatalytic activity than $SrTiO_3$ prepared with SSR (150 nm size) (Liu *et al.*, 2008).

Solid Sate Reaction (SSR). SSR is known as an environmentally friendly route since it does not involve any solvent therefore there is no need for waste disposal at the final stage of the synthesis. In addition, it is cost effective since it involves only solid precursors which are generally cheap. Downsides of SSR are the need of high reaction temperatures, nanoparticles agglomeration, non-uniformity and large nanoparticles size (Schwarz *et al.*, 1995). There are some modifications in SSR, incorporation of ball milling decreases the particle size of catalyst to improve the activity (Phoon *et al.*, 2019). In SSR, the precursors are mixed and grounded to decrease particle size and heated up to high temperatures to allow diffusion of atoms (Dulian, 2016).

Anodization (anodic oxidation). To fabricate in situ nanotube arrays, the anodization is widely used. The metals such as Al, Ti, Zr and Ta can be anodized to nanotube arrays (Wang *et al.*, 2014). Metal foils are used as anodes for oxidation and a cathode, generally Pt is used for construction of two-electrode electrochemical cell. A potential of 10-20 V is applied to the electrolyte for a determined amount of time and nanotube arrays are obtained (Wender *et al.*, 2011). The morphology and size of TiO_2 nanotubes can be controlled by electrolyte type and concentration, pH, applied potential, anodization duration and temperature (Su & Zhou, 2011). At low chemical dissolution rate longer nanotube arrays are obtained (Yang *et al.*, 2010). For photoelectrochemical applications, Ti sheets are often anodized as well.

2.3.2. Preparation of Electrodes

Mainly there are two ways to obtain an electrode for photoelectrochemical application, they are in-situ coating or coating after the catalyst is prepared. Powder catalyst can be coated simply by preparing a paste and coating the conductive substrate by doctor blade, spin coating, drop casting or dip coating techniques. In these techniques, the choice of binders, coating conditions and post-treatments are important for the bulk and surface properties (Aroutiounian *et al.*, 2005; Park *et al.*, 2016). Spin coating uses angular speed to coat uniform layers of thin films on substrates and as the speed increases, the thickness of the film decreases (Schubert & Dunkel, 2003). Drop casting offers a very simple and low material waste in coating of substrates. In drop casting process, the solution is dropped on the surface, and after the solvent is evaporated, the thin film is coated on the substrate. However there are some drawbacks such as poor uniformity, hard thickness control and inability to cover

large areas. Some of these drawbacks can be overcome by using combination of solvents, speeding up evaporation rate and optimizing the solution concentration (Grimoldi, 2015). In doctor blade method, also known as tape casting, the solution is spread on the substrate with a blade and good uniformity and precise thickness control is achieved. The thickness of the layer depends mainly on surface tension, viscosity, coating speed and wetting of the solution (Mennig *et al.*, 2004). Dip coating can be used in both powder or sol-gel derived catalyst coating. The conductive substrate is dipped in to the catalyst containing solution and withdrawn at a constant speed, and the thin and layers can be coated on both sides of the substrate (Grimoldi, 2015).

Electrodeposition and atomic layer deposition (ALD) are other methods to coat conductive substrates to prepare electrodes. In ALD, it is possible to obtain uniform layers of thin films with well controlled thickness on complex surfaces and 3D structures (Guan & Wang, 2016). Electrodeposition or electrochemical deposition methods offer a simple, low temperature and low cost operations (Acar & Dincer, 2016). With electrodeposition and dip coating, it is possible to obtain large surface area photoelectrodes for industrial applications (Dilger *et al.*, 2019).

Spray pyrolysis is used for coating of conductive substrates on the electrodes and has several advantages: (i) applicability to large scales, (ii) no restrictions in type of element or compound, their proportions and size or profile of substrate, (iii) no need for vacuum, high temperature or pressure, (iv) efficient control over film thickness, (v) no chemical side products (Patil, 1999). Spray coating is a fast and cheap way to fabricate layers of nanoporous films of photoelectrodes and results in better photoelectrode activity compared to doctor blade method (Chen & Ting, 2013). In spray coating, the vaporized solution flux is hit to substrate and the thickness and morphology are controlled by pressure, viscosity, solvent type, single or multiple pass coating etc. (Grimoldi, 2015).

Sometimes the electrodes can be prepared during the catalyst synthesis. Physical or chemical vapor deposition, sol-gel and hydrothermal reactions are the methods used to prepare the electrode coated with the catalyst. Chemical vapor deposition is suitable for fabricating single or multi component films with controlled morphology and stoichiometry

(Tahir *et al.*, 2010). In hydrothermal and sol-gel techniques, the conductive substrate is placed in autoclave and in-situ coating occurs during the reaction (Sun *et al.*, 2017).

2.4. Efficiencies in Photoelectrochemical Systems and Ways to Improve Them

There are mainly four types of efficiency which can be categorized in two titles; benchmark efficiency, reporting stand-alone water splitting capability and diagnostic efficiencies which characterize materials system/interface performance (Chen, 2013). Solar to hydrogen conversion efficiency is in former category; applied bias photon-to-current efficiency, internal quantum efficiency and external quantum efficiency are in latter.

Solar to hydrogen (STH) efficiency is the most important type of efficiency that can be used to compare the PEC devices reliably (Khaselev *et al.*, 2001). Since it is a standard efficiency for PEC systems, there are some requirements for the measurement of STH. Most importantly, the system must be under zero-bias conditions (no applied voltage), working and counter electrodes must be immersed in same pH electrolyte (no chemical bias). In addition, photocurrent or hydrogen production rate must be recorded under Air Mass 1.5 Global illumination (AM 1.5 G) in the absence of any sacrificial agents (electron donors or acceptors). Direct measurement of STH efficiency are done under short-circuit conditions where voltages versus reference electrode or open circuit voltage are not relevant (Chen, 2013).

STH efficiency can simply be defined as chemical energy of produced hydrogen divided by solar energy coming from sunlight, in the form of (Kuang *et al.*, 2017):

$$STH = \left[\frac{r_{H_2} \frac{\text{mmol}}{\text{s}} \times 237\,000 \frac{\text{J}}{\text{mol}}}{P_{total} \left(\text{mW}/\text{cm}^2 \right) \times Area\ (\text{cm}^2)} \right]_{AM\ 1.5\ G} \tag{2.6}$$

STH also relates photocurrent density with hydrogen production by formula:

$$STH = \left[\frac{j_{SC} \left(\text{mA}/\text{cm}^2 \right) \times 1.23\text{V} \times \eta_F}{P_{total} \left(\text{mW}/\text{cm}^2 \right)} \right]_{AM\ 1.5\ G} \tag{2.7}$$

In equations 2.6 and 2.7, j_{sc} represents short circuit photocurrent density, when there is zero voltage in the external circuit. P_{total} is the intensity of illumination, 1.23 V and 237 kJ/mol are thermodynamic water splitting potential and Gibbs free energy respectively and ηF represents the faradic efficiency of the system.

Faradic efficiency describes the relation of charge used for evolution of gases in the system (Shi *et al.*, 2015). Most systems assume it as one, saying that all the generated charges (current) are used for gas evolution but there are reports showing that experimental hydrogen or oxygen evolution amounts does not always match the amounts calculated by produced photocurrent densities (Hisatomi *et al.*, 2014).

Applied Bias Photon-to-Current Efficiency (ABPE) is measured when there is an external potential applied to working and counter electrodes. It is important to report this efficiency with a bias versus a reference electrode and not counter electrode and without a chemical bias or sacrificial agents since it should represent overall water splitting performance of the system (Chen, 2013).

The formula for ABPE is (Shi *et al.*, 2015):

$$ABPE = \left[\frac{j_{ph}\left(\mathrm{mA}/\mathrm{cm}^2\right) \times (1.23 - |V_b|)\mathrm{V} \times \eta_F}{P_{total}\left(\mathrm{mW}/\mathrm{cm}^2\right)}\right]_{AM\ 1.5\ G} \tag{2.8}$$

In this formula, j_{ph} represents photocurrent achieved under applied bias of V_b.

External quantum efficiency (EQE) is also known as Incident Photon-to-Current Efficiency (IPCE). IPCE describes the ratio of the number of electrons passing through as photocurrent to the number of photons irradiating the photoelectrode (Hisatomi *et al.*, 2014). IPCE assumes faradic efficiency as unity and measured under monochromatic wavelengths (Chen *et al.*, 2013) . IPCE can be found by:

$$IPCE = \left[\frac{j_{ph}\left(\mathrm{mA}/_{\mathrm{cm}^2}\right) \times 1239.8\ (\mathrm{V\ x\ nm})}{P_{mono}\left(\mathrm{mW}/_{\mathrm{cm}^2}\right) \times \lambda(\mathrm{nm})}\right]_{AM\ 1.5\ G} \quad (2.9)$$

Where, the value of 1239.8 is the multiplication of Planck's constant, h, and speed of light, c. Pmono is the intensity of the monochromatic light and λ is the wavelength. It is possible to measure IPCE values under bias.

Absorbed Photon-to-Current Efficiency (APCE) is a measure of Internal Quantum Efficiency (IQE) in PEC cells. It does not include the losses from reflected or transmitted photons, it is based on the photons that are absorbed (Chen, 2013). It can simply be found by dividing IPCE to absorptance ($1\text{-}10^{-A}$), where A is absorbance, fraction of electron-hole pairs generated per photon flux:

$$APCE = \frac{IPCE}{1 - 10^{-A}} \quad (2.10)$$

The efficiency of a photoelectrochemical cell is strongly depends on the electron transfer in the semiconductor, band gap energy and the band structure (Jing *et al.*, 2010). In order to improve efficiencies and overcome above stated problems in semiconductors various studies are conducted. The modifications of the photoelectrodes can be done by doping, metal ion loading, creating composites of mixed oxides and heterojunction systems, sensitization etc. (Choudhary *et al.*, 2012).

Preparation method is an important parameter in improving efficiencies in PEC since it has impact on size and morphology of catalysts. Xu *et al.* (2015) studied the effect of annealing temperature in electronic structure of $SrTiO_3$ thin films. The highest photocurrent density is achieved by the catalyst which is annealed at 750°C. They observed that thin films begin to crystallize at 550°C and after 800°C, a secondary phase is formed and hinders the photoelectrochemical activity. Zhang *et al.* (2017) compared the PEC performances of SSR and solvothermal route $SrTiO_3$, and by increasing surface area of particles, they obtained two folds increase in photocurrent density. Klusáčková *et al.* (2019) investigated the effect of $SrTiO_3$ nanocubes size on the PEC activity and observed that at 30 nm the photocurrent

density increased by 10 fold compared to 8 nm. Lu *et al.* (2019) synthesized flowerlike $SrTiO_3$ on Ti foil by hydrothermal reaction and achieved 3.38 mA/cm^2 current density at 0.6 V vs RHE. Peng *et al.* (2015) showed that the crystal facet of TiO_2 precursors have significant impact on the activity of $SrTiO_3$ prepared by hydrothermal method.

Doping and defect engineering are methods to change the electronic structures of the semiconductor. Oxygen vacancy fabrication is an effective method to increase charge transport and donor density up to an optimum level since excess amounts of vacancies act as recombination centers. It is possible to introduce oxygen vacancies to $SrTiO_3$ semiconductor by controllable solid-state reaction of $NaBH_4$ and $SrTiO_3$ nanocrystals (Tan *et al.*, 2014). Another method to modify the semiconductor to enhance the photocatalytic activity is doping an ion or incorporation of cocatalyst. $SrTiO_3$ is doped with many metals and non-metals to reduce the band gap. Interestingly, doping $SrTiO_3$ by rhodium creates p-type conductivity and shows cathodic photocurrents (Iwashina & Kudo, 2011). Doping with Ag, due to plasmonic effect, is found to be efficient method to increase the current density and activity of $SrTiO_3$ (Liu *et al.*, 2018). Al, In, Ga, Mg, Na, Nb, Cr and Zn are other ions that are used in doping of $SrTiO_3$ (Jing *et al.*, 2019; Wang *et al.*, 2010). Among these materials doping of alkali such as Na and Mg is reported to enhance the activity up to 20 times (Han *et al.*, 2017; Sakata *et al.*, 2016). Co-doping of Cr-B, Bi-Ga, In-V and Cr-La are also studied to increase the activity of $SrTiO_3$ in water splitting (Hara & Irie, 2012; Yu *et al.*, 2014). Non-metal doping is done by N doping on $SrTiO_3$ (Xu *et al.*, 2014). It is found that significant reduction in band gap is observed when N is doped on $SrTiO_3$ which resulted in better activity (Atkinson *et al.*, 2019). Cocatalysts can be used to prevent electron hole recombination or to be hydrogen or oxygen evolution sites in solar water splitting applications (Hisatomi *et al.*, 2014). Usually noble metals such as Pt, Pd and Au are used as cocatalyst in photocatalytic and photoelectrochemical water splitting but researchers are working on developing cheaper alternatives (Colón, 2016). For oxygen evolution, the cocatalyst such as IrO_2 and RuO_2 are preferentially replaced with cheaper and earth abundant materials such as cobalt phosphate (Kanan & Nocera, 2008). In addition to Co-based catalysts, NiFe was also studied for oxygen evolution and exhibit excellent electro catalytic activity and durability (Gong *et al.*, 2013). In general MnO_x, IrO_x, CoO_x,RuO_x materials can be applied as oxygen evolution co catalyst (Obregón & Colón, 2014; Yang *et al.*, 2013). Several transition metal oxides like NiO_x,NiO, Cu2O and CuO and sulphides like CuS, NiS

and MoS cocatalysts are employed as hydrogen evolution cocatalyst (Ran *et al*., 2014; Wang *et al.*, 2013).

Solid solutions and composites are widely studied as they enhance charge transfer properties. Yu *et al.* (2019) prepared solid solutions of $AgTaO_3$ and $SrTiO_3$ and observed plasmonic effect of Ag particles. In photoelectrochemical analysis, the charge separation was higher than that of pure components and under optimized ratio, the band edge positions of the solids were suitable for solar water splitting reactions. Luo *et al.* (2018) produced NiS/g-C_3N_4/$SrTiO_3$ composites by hydrothermal method and tested its photoelectrochemical activity in 0.5 M Na_2SO_4 aqueous solution. At 2% NiS content, the photocurrent density was maximum at 46 $\mu A/cm^2$, almost 6 times higher than pristine $SrTiO_3$. They suggested that NiS cocatalyst would increase H_2 evolution on CN/STO electrode. Wysmulek *et al.* (2017) worked on $SrTiO_3$-TiO_2 eutectic rods that were grown by the micro-pulling-down method and reached photocurrents up to 8.5 mA/cm^2 at 1.5 V vs. NHE. Furthermore, they observed that the photocurrent was sustained for 30h in H_2SO_4 and Na_2SO_4 solution and pH was 1.6.

Z-schemes and heterojunctions are widely investigated for TiO_2 and $SrTiO_3$ semiconductors. In heterojunction systems, a hole-accepting semiconductor (generally n-type) and an electron-accepting semiconductor (generally p-type) with well aligned band edges and high charge transfer properties are coupled (Choudhary *et al*., 2012). Due to the unique junction zone, the charge separation and transfer is greatly increased in heterojunction systems (Wang *et al*., 2016; Yan *et al*., 2017). Figure 2.9 shows the charge transport in different kinds of heterojunctions.

Coupling $SrTiO_3$ and TiO_2 are very common in PEC applications. Mostly $SrTiO_3$/TiO_2 heterostructure is formed by hydrothermal reaction and Zhou *et al.* (2015) showed that the optimum reaction time is 1 hour. Forming heterojunction between $SrTiO_3$ and TiO_2 reduces recombination of charge carriers and band gap, therefor obtaining photocurrents as high as 1.2 mA/cm^2 and 33% increase in hydrogen production rate is possible (Khemakhem *et al*., 2017; Wu *et al*., 2015). During synthesis of heterojunction it is possible to observe Ti^{3+} self-doped $SrTiO_{3-x}$/TiO_{2-x} heterostructure and this doping results in 20 times increase in the photocurrents (Hou *et al*., 2016).

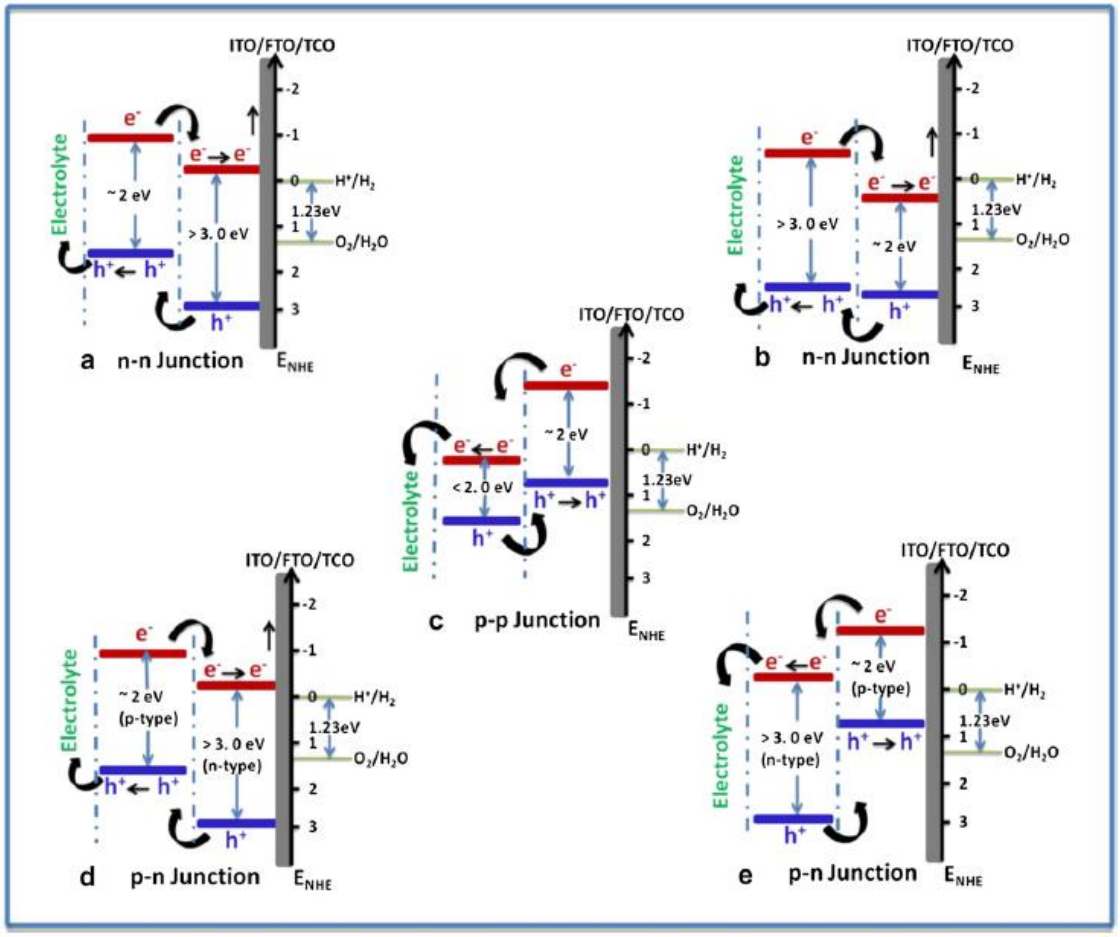

Figure 2.9. Possible charge transfer mechanism across heterojunctions under illumination with redox potential of water. (Choudhary *et al.*, 2012).

Yan *et al.* (2017) investigated the effect of hydrogen treatment on the $SrTiO_3/TiO_2$ heterojunction for PEC performance and concluded that hydrogen treatment introduced oxygen vacancies, which increased the electron-hole separation hence yielded higher photocurrents. In addition to hydrogen treatment, sensitization and doping is also applied to heterostructures; Nb doping, Ag nanoparticle decoration and CdS sensitization are some of the attempts to further increase the photoelectrochemical activities (Zhang *et al.*, 2010; Yang *et al.*, 2012; Liu & Ma, 2019).

Besides TiO_2, $SrTiO_3$ can be also coupled with many different materials. Cen *et al.* (2016) created Nb-$SrTiO_3/SrTiO_3$ n-n homojunction structure and achieved IPCE over 70%. Che *et al.* (2016) fabricated different weight percentages of $SrTiO_3/Bi_2O_3$ heterostructure by micro-wave process and observed that in 0.5 M Na_2SO_4, 50% $SrTiO_3/Bi_2O_3$ has the highest photocurrent almost 4 times higher than that of $SrTiO_3$ and concluded that introduction of

$SrTiO_3$ to Bi_2O_3 increases interfacial charge separation and transfer. Guo *et al.* (2014) studied the effect of layer thickness, concentration and reaction temperature on the photoelectrochemical performances of $ZnO/SrTiO_3$ nanomaterials. Under optimum conditions, the maximum photocurrent density was 7.53 mA/cm^2 in 1M Na_2S at 1.5 V vs SCE and the hydrogen generation efficiency was 1.4%. They concluded that increasing thickness and concentration had a negative impact on photocurrent density. Luo *et al.* (2019) worked on $g\text{-}C_3N_4/SrTiO_3$ nanocomposites and its advantageous interfacial effects. The photocurrent density has remarkably increased with coupling $g\text{-}C_3N_4$ and $SrTiO_3$. However, they observed recombination of photogenerated carriers. He *et al.* (2016) fabricated $SrTiO_3$-RGO (reduced graphene oxide) heterostructure and observed that by increasing amount of RGO the bang gap has changed from 3.16 to 2.99 eV. Wang *et al.* (2016) investigated photoelectrochemical performance of $SrTiO_3$ nanocubes coupled with NiO nanoparticles. At 0 V vs Ag/AgCl, the photocurrent of p-NiO/n- $SrTiO_3$ reached 7 times higher than that of $SrTiO_3$. They concluded that p-n junction accelerated holes migration and hence decrease recombination of electron hole pairs.

Sensitization is another way to improve PEC performance of catalysts. Sensitization can be done by dyes or quantum dots. Sensitization materials by relatively narrow-band-gap semiconductors, such as Cu_2O, CdS and MoS_2 have been widely applied to increase efficiencies in systems (Yin *et al.*, 2019). Sharma *et al.* (2014) fabricated $SrTiO_3$ thin films sensitized by Cu_2O and compared its photoelectrochemical activity with pristine $SrTiO_3$ and Cu_2O. The heterojunction of $SrTiO_3$ and Cu_2O exhibited 30 times higher photocurrent density than that of $SrTiO_3$. And maximum IPCE is found as 6.5% at 0 V vs SCE. Sensitization of $SrTiO_3$ are also done by carbon quantum dots, CdSe quantum dots and all sensitizations increased photoelectrochemical performance of $SrTiO_3$ (Han *et al.*, 2019; Wang *et al.*, 2012). Safranin, Fluorescein and Eriochrome black T were used as sensitizer in Zr-doped $SrTiO_3$ photoanode and efficiency was increased 2-3 times (Elzayat, 1998).

In Z-scheme systems, charge transfer is different from p-n heterojunctions as seen in Figure 2.10 (Peerakiatkhajohn *et al.*, 2016). Balanced photocatalytic activity of hydrogen and oxygen evolution catalyst under shared electrolyte is needed for Z-scheme water splitting (Hisatomi *et al.*, 2014). The advantage of creating a Z-scheme is that the energy

required to activate each photocatalysts is lower compared to one step water splitting systems (Maeda, 2013).

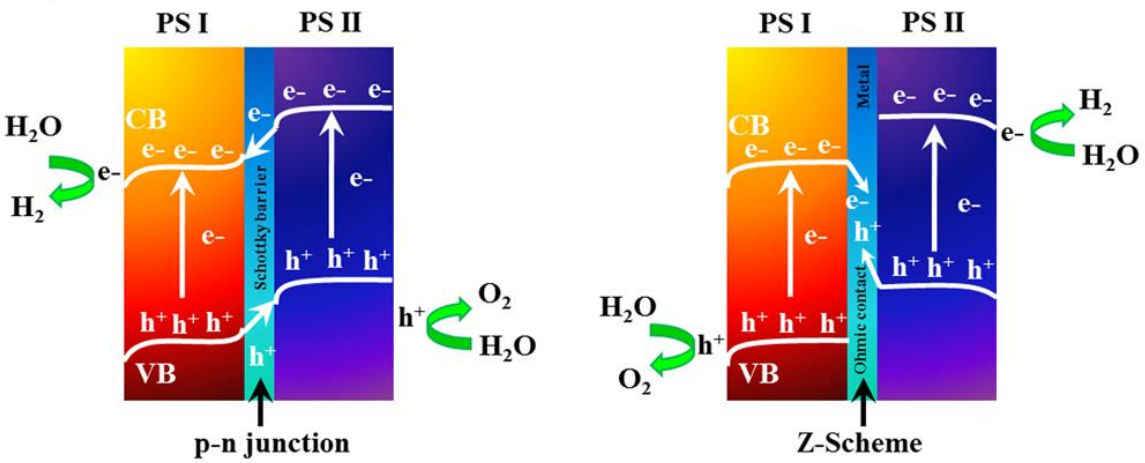

Figure 2.10. Charge transfer in p-n junction and Z-scheme configuration. (Peerakiatkhajohn *et al.*, 2016).

The redox mediator in Z-schemes can be both liquid and solids. The first example all-solid state was CdS-Au-TiO_2 nanojunction (Chang *et al.*, 2017). Three-Dimensional Ordered Macroporous (3-DOM) structures are widely used for creating Z-Schemes involving $SrTiO_3$ (Chang *et al.*, 2019). 3DOM-$SrTiO_3$/Ag/Ag_3PO_4 and CdS/Au/3DOM-$SrTiO_3$ photocatalysts are synthesizes successfully for efficient overall water splitting (Chang *et al.*, 2017; Zhang *et al.*, 2017).

Another way of improving efficiency is construction of tandem type cells where both electrodes are photoactive or combining the PEC system with PV/DSSC systems. Tandem approach allows to decrease the dependence of PEC systems to external energy sources other than sun. Tandem cells created by photoanode and photocathode coupling was first done with n-TiO2 and p-GaP system (Nozik, 1976). As for photo anode/PV tandem cell, TiO_2 photo anode is combined with thin film Cu (In, Ga) Se_2/CdS based PV device and produced 0.052 μL cm^{-2} s^{-1} hydrogen (Neumann *et al.*, 2009). In addition, a-Si:Ge PV is coupled with WO_3 and Fe_2O_3 electrodes for improving efficiency (Stavrides *et al.*, 2006). The corporation

of photoanodes with DSCC is more attractive than PV coupling because there is usually a problem of corrosion in PV-photoelectrode applications (Sivula & Grätzel, 2013). Arakawa *et al.* connected two DSSC in series to produce the energy needed for overall water splitting (Arakawa *et al*., 2007). Developments in dyes and DSSC structures are increasing the efficiencies of these tandem systems day by day (Sivula & Grätzel, 2013).

2.5. Design and Setup of Photoelectrochemical Devices

In reactor design, the main concern is to separate gases and collecting sufficient amount of light for semiconductors. There are various shapes and configurations of reactors that can be used in photoelectrochemical water splitting: simple open beaker setup, single chamber vessel, closed vessels equipped with membranes, H-type cells monolithic structure and dual beds. (Fujishima & Honda, 1972; Minggu *et al.*, 2010; Chen *et al.*, 2010).

The window is an important factor for fabrication of an efficient photoreactor, it should transmit the incoming light with minimum reflection. A normal soda lime glass cannot transmit the wavelengths lower than 350nm, where a quartz window will transmit the light till 250 nm (Lopes *et al*., 2014). Quartz windows are expensive but cheaper materials with similar performances can be used; fused silica or Pyrex has 90% visible light transmittance and has good stability in both acidic and alkaline media (Chen *et al.*, 2010).

Electrode assembly is a crucial part of a PEC cell because the water splitting occurs on the surface of electrodes. At least one of the electrodes is composed of semiconductors or photosensitizers. These photoactive materials, i.e. photoelectrodes, absorb light and facilitate redox reactions via production of electron and hole pairs (Bosserez *et al*., 2015). These electrodes are submerged in an electrolyte which is responsible for ion conductivity, reaction centers and molecular transport (Rongé *et al*., 2014). The electrode assembly can be wired or wirelessly connected with physical contact in one compartment or two as shown in Figure 2.11 Each configuration has its own advantage and disadvantage; in wired configuration, the electron path length is larger due to electrical wires, but ionic path length can be minimized by placing the electrodes close; for wireless configuration, electron path length is small but ionic path length is increased (Bosserez *et al*., 2015).

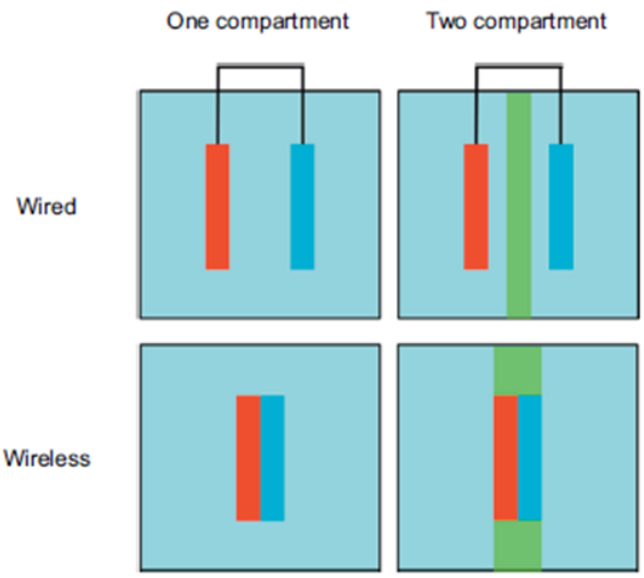

Figure 2.11. Possible Configurations of Simple PEC cells. (Bosserez *et al.*, 2015).

As stated before, the most desirable photoelectrode should have proper band positions and sufficient band gap for spontaneous solar water splitting applications. When these criteria are not met, an external bias is needed to govern overall water splitting reaction. This external bias can be given in several ways; grid bias, pH bias, PV or DSSC bias and internal bias as given in Figure 2.12 (Minggu *et al.*, 2010). Honda & Fujishima used chemical bias, i.e. pH bias for photoelectrochemical water splitting on TiO_2 photoanode, the pH of the anode side and cathode side of the cell was different (Fujishima & Honda, 1972). The pH bias is hard to maintain because, as the reactions carry on, pH difference decreases due to neutralization, and therefore supply of fresh solution is required (Ong, 2013). The grid biased systems are not considered as an attractive option because most of the electricity produced are coming from fossil fuels (Minggu *et al.*, 2010). DSCC and PV biased systems utilizes solar energy to produce the current which will be transferred to PEC system where water splitting occurs (Van De Krol & Grätzel, 2012). Internal bias is achieved when layered, stacked or hybrid structures are used for creating bias potential within the photoelectrode (Minggu *et al.*, 2010). There are numerous combinations of semiconductors with appropriate band gap and band edges for direct water splitting; however, the stacking different semiconductors makes the system more complex (Miller *et al.*, 2003).

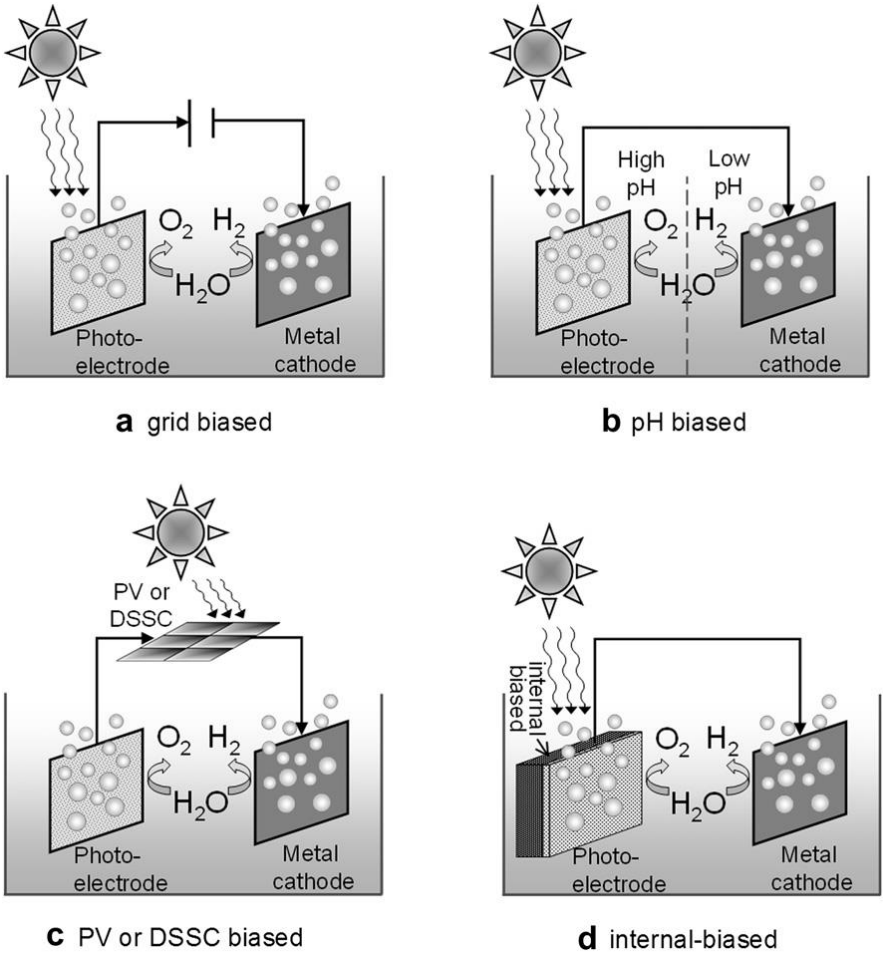

Figure 2.12. Possible Bias Types in PEC cells. (Minggu *et al.*, 2010)

Since mixture of hydrogen and oxygen can be explosive, it is crucial to separate these gases in the water splitting system. For this reason, different reactor designs and ion exchange membranes can be used (Walter *et al*., 2010). Use of membranes enables to have two different electrolyte types at the electrode sides, and it can increase charge transfer and act as a chemical bias (Minggu *et al.*, 2010). Nafion and Teflon membranes can be used as ion exchange membrane that allows ions to pass without mixing the anode and cathode side electrolytes and produced gases (Lopes *et al*., 2014).

2.6. Electrolytes Used in Photoelectrochemical Applications

Electrolytes are aqueous salt solutions that supply additional ions and electrons to the system. They also act as a medium for electron transfer and prevent electron-hole

recombination (Abe, 2010). Solutions containing Li^+, Na^+, K^+, Ba^{2+}, Cl^-, $H_2PO_4^-$ and NO_3^- can be used as electrolytes; their electrical resistance can be minimized by adjusting their concentrations (Bak *et al*., 2002). Some of the solutions can be listed as: NaOH, KOH, Na_2SO_4, Na_2S, H_2SO_4 and Na_2CO_3 (Osterloh, 2017). For TiO_2 photoelectrode, the PEC water splitting performance is highest with Li^+ containing alkaline electrolytes compared with Na^+ and K^+ containing alternatives (Ding *et al*., 2015). Crawford *et al.* showed that anions like iodine and bromide should not be used since they are oxidized easier than water; however, Cl^- ions can be used because the required potential to oxidize is 1.33 V, which is higher than that of water (Crawford *et al.*, 2009). Saito *et al.* studied the $BiVO_4/SnO_2/WO_3$ multi-composite anode in Na_2CO_3 and Na_2SO_4 electrolytes and observed that photocurrent achieved in carbonate electrolyte was 2.4 times higher than that of in sulfate electrolyte (Saito *et al.*, 2012).

Electrolyte choice is important in photoelectrochemical processes since the concentration, pH and type of ions affects the surface of the catalyst (Ding *et al*., 2017). As the conductivity of the electrolyte increases, the photocurrent increases due to the diffusion is facilitated (Crawford *et al*., 2009). Ren *et al.* studied the solutions of alcohols, polyols and electrolyte pollutants such as ethylene glycol, ethanol, ammonia, glycerol, urea and Na_2S as electrolyte for TiO_2 photoanodes, and observed that increase of concentration results in an activity decrease for polyols and alcohols due to the change in mobility of ions and viscosity (Ren *et al*., 2013).

The half reactions, hydrogen and oxygen evolution reactions greatly depend on the pH of the electrolyte (Hilliard, 2016). In acidic environment the reactions are:

$$H_2O + 4h^+ \leftrightarrow O_2 + 4e^- + 4H^+ \quad \text{with } E_0\text{=1.23 V vs NHE} \qquad (2.11)$$

$$4H^+ + 4e^- \leftrightarrow 2H_2 \qquad \text{with } E_0\text{=0.00 V vs NHE} \qquad (2.12)$$

In basic environment on the other hand, the following reactions occurs:

$$2\,H_2O\ +\ 4e^-\ \leftrightarrow 4OH^-\ +2H_2 \quad \text{with } E_0\text{= -0.82 V vs NHE} \qquad (2.13)$$

$$4\,OH^-\ +\ 4h^+\ \leftrightarrow\ O_2\ +2\,H_2O \quad \text{with } E_0\text{= 0.40 V vs NHE} \qquad (2.14)$$

The rate determining steps are different in acidic and alkaline environments *(Ding et al.*, 2017):

$$H_3O^+ + e^- + * \leftrightarrow H^* + H_2O \qquad \text{Acidic conditions} \qquad (2.15)$$

$$H_2O\ +\ e^- + * \leftrightarrow H^* +\ OH^- \qquad \text{Basic conditions} \qquad (2.16)$$

In equations 2.15 and 2.16, * represents the adsorption site (semiconductor surface that is used for adsorption of species.)

The activities of semiconductors change with pH because of the change of position in their Fermi level. When excess H^+/OH^- species are adsorbed on the surface, semiconductors the fermi level shifts up (Van De Krol & Grätzel, 2012). The equation for the change of potential with respect to pH can be written as (Hilliard, 2016):

$$E_f = E_f^0 - 0.059 \times pH \qquad (2.17)$$

In Figure 2.13, the change of flat band potential with respect to pH of electrolyte for $SrTiO_3$ and TiO_2 electrodes are given.

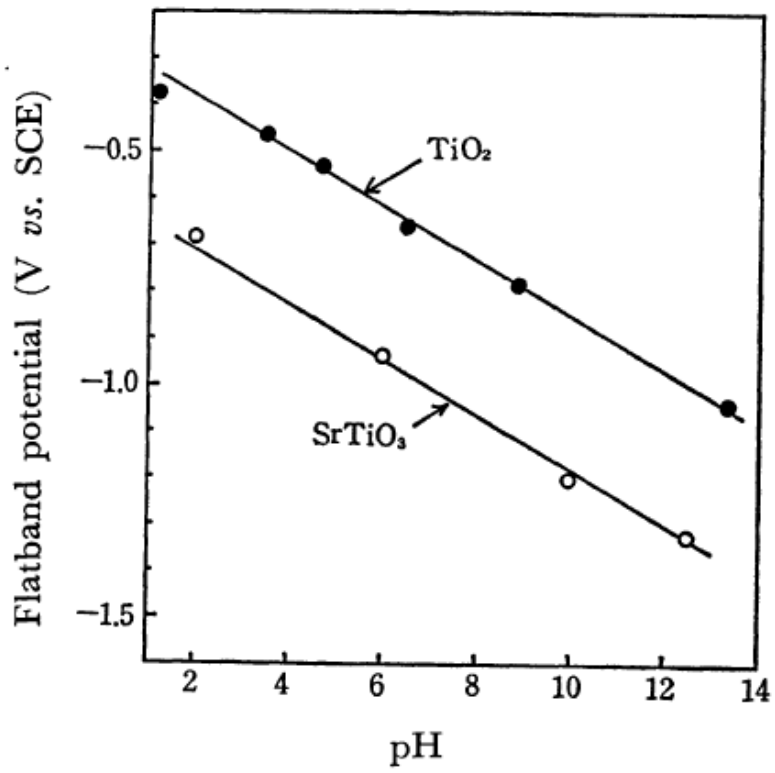

Figure 2.13. The flat band dependence on pH for $SrTiO_3$ and TiO_2 electrodes**.** (Watanabe *et al.*, 2006)

Tayyebi *et al.* investigated the activity of $BiVO_4$ in three different pH values as acidic, neutral and alkaline media, and found that increasing pH increased the activity. Increasing the pH of electrolyte increases the reducing power of the electrons, i.e. electrode potential becomes more negative. Hence, as the flat band potential becomes more negative than the redox potential, the driving force for hydrogen production increases (Tayyebi *et al.*, 2019).

When total decomposition of water cannot be achieved, for charge balancing, in order to promote photo-reduction of water to H_2 sacrificial electron donors such as ethanol, methanol, EDTA, ascorbic acid or triethanolamine are used; for photo-oxidation to O_2, sacrificial electron acceptors such as silver nitrate and persulphate are used (Kalyanasundaram, 2013). Sacrificial agent increases charge separation within the PEC process and are used to measure activity of the catalyst for the half reactions (i.e. hydrogen and oxygen evolution reactions) (Hisatomi *et al.*, 2014). Methanol is one of the most

common electron donor and hole scavenger used in photocatalytic processes, and it is also used in PEC applications (Pinheiro *et al*., 2014). Methanol is a suitable electron donor to be used in PEC applications since it is transparent, does not corrode the electrodes like H_2O_2 does and its oxidation is relatively easy compared to water (Kuo & Klabunde, 2012). Yourey and Bartlett showed that methanol is a strong electron donor and cathodically shifted the onset potential by 0.2 V for $CuWO_4$ photoelectrode (Yourey & Bartlett, 2011). Guo *et al.* studied the PEC water splitting activity of ZnO nanowires in both Na_2SO_4 and Na_2SO_3 electrolytes and observed that using Na_2SO_3 electrolyte resulted in 4.5 times higher photocurrents because SO_3^{2-} acted as hole scavenger (Guo *et al*., 2018).

Silver nitrate is one of the additive that is used as an electron acceptor. Thermodynamically, silver cation is easily reduced than hydrogen so it can be used to measure the activity for oxygen evolution reaction (Hisatomi *et al.*, 2014).

In addition to all of the electrolytes stated above, room temperature ionic liquids (RTIL) can also be used as ion transfer media in PEC water splitting (Matsumoto, 2005). Singh *et al.* showed that employing chloro-aluminate based RTILs can inhibit the photocorrosion of GaAs photoanode for 720 hours of irradiation (Ohno, 2005). The major problem of using RTILs in PEC applications is that their high viscosity limits the mobility of electrochemically active ions in the system (Matsumoto, 2005).

2.7. Characterization Methods

Current-voltage (I-V) curves are widely used for evaluation of the photo electrochemical performance (Duret & Grätzel, 2005). The resistances of the film, substrate, electrical connections and electrolyte affect the measurement and hydrogen production cannot be measure directly (Bell, 2012). Linear Sweep Voltammetry or Cyclic Voltammetry modes in potentiostat create I-V curves for 2-electrode and 3-electrode configurations (Shi *et al.*, 2015). The I-V curves should fit Butler -Volmer equation given as (Van de Krol, 2012):

$$j = j_0(\exp\left(\frac{(1-\propto)e\eta}{kT}\right) - \exp\left(\frac{-\propto e\eta}{kT}\right)) \qquad (2.18)$$

A Tafel plot can be constructed by plotting $\log(j/j_0)$ vs. η (overpotential) and it can be used for construction of reaction mechanism and analyzing kinetics of the reaction (Van de Krol, 2012). In addition, for observing the stability and the saturated current density, the current-time curves are also obtained at a fixed potential (Shi *et al*., 2014). The Figure 2.14 shows a I-t curve with light on and off cycles for TiO_2 photoanode (Liang *et al*., 2017). A decrease in photocurrent is attributed to some type of corrosion of the electrode (Shi *et al*., 2015). In time-resolved spectroscopy, the photocurrent is recorded as a function of time, and it represents the defects that are responsible for the change the concentration of the charge carriers within the system (Paulauskas *et al*., 2008).

Since the observed current may not result in hydrogen gas production due to energy losses, it is important to measure amount of gas evolved in the PEC system (Magesh *et al*., 2014). The faradic efficiency is the measure of the ratio between the charges used in gas evolution in the system to the overall charge flows in the external circuit of system (Shi *et al*., 2015). Faradic efficiency may be smaller than 100% in a practical photoelectrochemical cell due to side reactions and the inhibition of proton reduction (Augustynski *et al*., 2006).

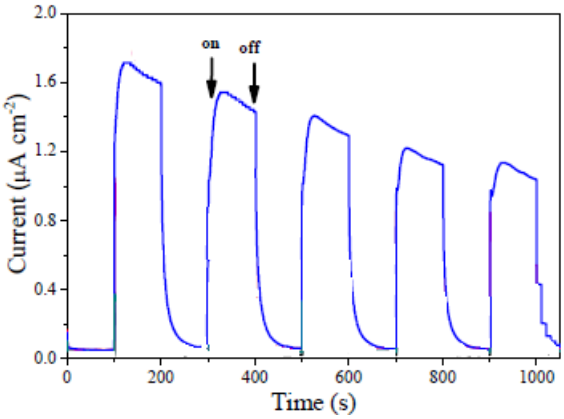

Figure 2.14. An example I-t curve for an n-type photoanode.

X-ray powder diffraction (XRD) characterizes the crystallographic structure (Ong, 2013). It is used to identify the phases that are present in a catalyst, and it can give complete description of the structure (Haber *et al.*, 1995). In principle, X-rays are sent to sample and

the angle of diffraction of the rays from the sample are recorded. Distance between atoms can be found by applying Bragg's Law (Schields, 2004).

X-ray photoelectron spectroscopy (XPS) analyzes the kinetic energy distribution of ejected core level photoelectrons, enables the observation of oxidation states and the chemical environment with a resolution of 0.2 mm (Haber *et al.*, 1995). The analysis gives the binding energies, and it represents the energy required to remove an electron from cores. Hence, when oxidation stated of an atom is changes, the electrostatic attraction between an electron and nuclei is also changed; if the atom is more oxidized, the larger binding energy is observed while the binding energy gets smaller when the atom is reduced more (Ohtani, 2010).

Surface morphology of the materials can be analyzed used scanning electron microscope (SEM) (Ong, 2013). SEM is useful in examining the mesoporous structures and the distribution of sizes (Haber *et al.*, 1995). High energy electrons are sent to the sample, and the interactions are recorded to determine texture, crystal structure, shape and chemical composition (Swapp, 2017). Another surface characterization method is transmission electron microscopy (TEM), which gives information about particle size and distributions, support morphology and particle location in resolution of 2-3 nm size range (Haber *et al.*, 1995). Fourier transform infrared spectroscopy (FTIR) is a rapid, non-destructive and easy characterization technique, which gives information about the interactions and structures present in the sample (Petit & Madejova, 2013). It can be used for identification of chemical groups on the surface of a sample (Berthomieu & Hienerwald, 2009). Molecular vibrations are recorded, and each molecule/functional group has unique infrared absorption band (Colthup *et al.*, 1990; Griffiths & De Haseth, 2007).

Brunauer–Emmett–Teller, BET, method is used to determine the specific surface area of materials by nitrogen adsorption-desorption process (Zsolt, 2011).

The band gap of semiconductors can be determined from UV-VIS Spectroscopy. The absorption of light as a function of wavelength gives information about electronic transitions in the semiconductor. In this analysis method, the modes of transmission, diffuse reflectance (DRS) or absorption can be used; for particulate samples, the diffuse reflectance provides

better results (Chen, 2013). The Tauc plot can be used to find the band gap (E_g) of a semiconductor with recorded data since (Wood & Tauc, 1972):

$$\alpha h\nu \propto (h\nu - E_g)^{1/n} \tag{2.19}$$

where n can be 3, 2, 3/2 or 1/2 for indirect (forbidden), indirect (allowed), direct (forbidden), and direct (allowed) transitions, respectively (Chen, 2013). In order to find the band gap from diffuse reflectance data, Kubelka-Munk plot is constructed by recorded reflectance vs wavelength data (Deutsch *et al.*, 2006):

$$f(R) = \frac{(1-R)^2}{2R} = \frac{\alpha}{s} \tag{2.20}$$

where *f(R)* is the Kubelka–Munk function and s is the scattering coefficient. The band gap energy of a semiconductor can be found by plotting $h\nu$ vs $(\alpha h\nu)^n$ and extrapolating the straight line part to x axis (Chen, 2013).

Photoluminescence spectra is used for analysis of charge and semiconductor/electrolyte junction potential distribution (Kelly *et al.*, 1999). The recombination of electron and holes gives emission peaks, and enhanced charge carrier separation should give rise to low-intensity peak.

Electro impedance spectroscopy is used to characterize the major internal resistances in the photo electrochemical cell and depends on the light intensity. In this technique, the amplitude and phase shift of the current response of the system is measured under small potential sinusoidal perturbation. Electrical circuit analogs are used to determine the resistances and the double layer capacitances (Lopes *et al.*, 2010). After finding the capacitance of a semiconductor, Mott Schottky plots are derived from electrochemical impedance measurements (Ong, 2013).

Mott-Schottky equation is (Gelderman *et al.*, 2007):

$$\frac{1}{C_s^2} = \frac{2}{q\kappa\varepsilon_0 N_D}(V - V_{fb} - \frac{kT}{q}) \quad (2.21)$$

where , κ is dielectric constant, q is electronic charge, ε_0 is permittivity of vacuum, ND is the charge carrier density, V is electrode potential and V_{fb} is flat band potential. By fitting a linear line to above equation ($1/C^2$ vs V), it is possible to obtain flat band potential and charge carrier density; these values are used in detailed analysis of the PEC performance (Shi *et al*., 2015). The slope of the tangent line gives information about the conductivity type of the semiconductor, the positive slope indicates n-type while the negative slope indicates p-type semiconductor (Zhong *et al*., 2008).

3. EXPERIMENTAL WORK

3.1. Equipment and Chemicals

The list of equipment used in experiments:

- Keithley 2401 source meter
- Shimadzu GC 2014
- ABET Solar Simulator
- Sciencetech Solar Simulator
- pH meter

Glasses are purchased with resistivity <10 Ω/square from TEKNOMA or SIGMA-ALDRICH, and TiO_2 blocking layer electrode and TiO_2 nanoparticle paste is purchased from SOLARONIX. Pure Argon and Nitrogen gases are purchased from Linde gas. Ag/AgCl reference electrode is purchased from SI Analytics. The other chemicals used are given in Table 3.1.

Table 3.1. Chemicals used.

Name	Formula	Molecular Weight (g/mol)
2- propanol	C_3H_8O	60.10
Acetone	C_3H_6O	58.08
Aluminum oxide	Al_2O_3	101.96
Citric acid monohydrate	$C_6H_8O_7.H2O$	210.14
Ethanol	C_2H_5OH	46.07
Glacial Acetic Acid	CH_3COOH	60.05
Iron nitrate nonahydrate	$Fe(NO_3)_3.9H2O$	403.95
Methanol	CH_3OH	32.04
Mono ethylene glycol	$C_2H_6O_2$	62.07
Sodium Hydroxide Pellets	NaOH	39.99
Polyethylene glycol 2000	$HO(C_2H_4O)_nH$	20000
Sodium Sulfide	Na_2S	78.04

Table 3.1. Chemicals used (cont.)

Name	Formula	Molecular Weight (g/mol)
Strontium Carbonate	$SrCO_3$	147.63
Strontium Nitrate	$Sr(NO_3)_2$	211.63
Sulfuric Acid	H_2SO_4	98.08
Titanium butoxide	$Ti(OCH_2CH_2CH_2CH_3)_4$	340.32
Titanium dioxide	TiO_2	79.86

3.2. Preparation of Catalysts/Electrodes

TiO_2 nanoparticle solution is coated on ITO glass by doctor blade method. $SrTiO_3$ catalyst is prepared by solid state reaction described elsewhere (Abass, 2018). Briefly, stoichiometric (Sr:Ti ratio 1:1) and non-stoichiometric (Sr:Ti ratio 2:3) amounts of precursors $SrCO_3$ and TiO_2 are put into a grinding mortar and mixed. Then they are transferred to an aluminum crucible. The synthesis temperature was 1000^oC for 10 hours. For doped $SrTiO_3$ catalyst, same procedure is repeated with addition of Fe and Al precursors. The prepared samples are coated on ITO glass, Au coated glass and TiO_2 blocking layer coated ITO glass.

The coating of powder catalysts on ITO is done by doctor blade method. Coating solution is prepared as described elsewhere (Abass, 2018). PEG-2000 is dissolved in water and added to the solution of powder catalyst and ethanol and these mixtures are sonicated till a uniform solution is achieved. Then the solution is coated on cleaned ITO glasses via doctor blade. In addition to coating by doctor blade method, spin coating is also used for coating of prepared catalysis. The catalyst solution is coated in 3000 rpm for 30 seconds and dried at 80^o C for 30 mins, and the procedure is repeated to increase the layer thickness (Said *et al.*, 2017).

For comparison psurposes, $SrTiO_3$ is also prepared by two different sol-gel routes (Visuttipitukul *et al.*, 2013; Chang *et al.*, 2017), and by hydrothermal route. In sol-gel route

1, 2 M $SrNO_3$ is mixed with 0.5 M titanium butoxide in isopropanol and acetic acid is used as chelating agent, the reaction is conducted at room temperature and cleaned ITO glasses are dipped into the solution and dried on hot plate. In route 2, titanium butoxide is mixed with acetic acid and distilled water is dropped on the mixture, after rigorous stirring 1 M $SrNO_3$ solution is added and finally 2 M of citric acid solution is prepared. In modified hydrothermal method, titanium butoxide is mixed with ethylene glycol and 0.5 M $SrNO_3$ solution is added to the mixture dropwise. After stirring 5M NaOH solution is added and the solution is transferred to autoclave and cleaned ITO glass is placed with conducting face down and the reaction took place at 180^oC for 24 hours. The ITO glasses are also coated with spin coating of the prepared $SrTiO_3$ solutions.

The coated samples are calcined at 500^oC for 3 hours. After they are cooled to room temperature, electrical wire is attached to conductive surface of electrodes and epoxy resin is applied to the electrodes leaving predetermined area for reaction. Figure 3.1 shows the prepared electrodes.

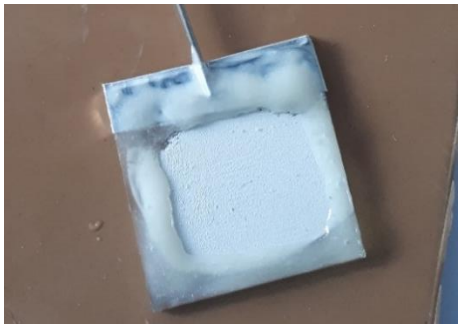

Figure 3.1. Un-doped $SrTiO_3$ prepared by SSR, coated by doctor blade.

3.3. Catalyst Characterization

The band-gap of the catalysts are determined by Shimadzu UV-VIS spectrophotometer. Kubelka-Munk method is used to obtain band gap energy from reflectance data. The crystal structure and the phases of prepared catalysts are analyzed by Rigaku D/MAX-Ultima+/PC X-Ray diffraction (XRD) equipment.

3.4. Design of Photoreactor

A photo reactor is designed for the purpose of monitoring the hydrogen and oxygen evolution form the photoelectrochemical system. The two-compartment system is designed so that it can be used with a membrane to promote product separation. The compartments are designed as identical so that they can be used individually. For one of the compartments, three ports are opened for working, counter and reference electrodes and two ports are opened for gas inlet and outlets. By centralizing the working electrode, a flat window is placed in the center of the reactor and the diameter is adjusted so that the light coming from the source is directly transferred to the solution. Figure 3.2 and Figure 3.3 show the schematic of the reactor and the created reactor.

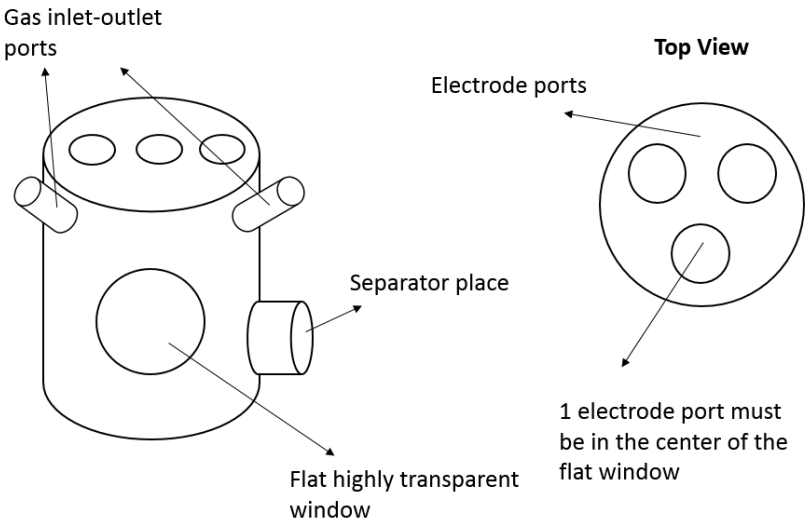

Figure 3.2. Schematics of the designed reactor.

Figure 3.3. The designed photo reactor.

3.5. Electrochemical Analysis

Figure 3.4 shows the open beaker system used for preliminary analysis of the system. three-electrode configuration is used for half-cell analysis. Prepared catalysts are used as working electrode, Pt plate is used as counter electrode and Ag/AgCl is used as reference electrode. Electrolyte is prepared by mixing distilled water with various salts such as NaS_2, NaOH, H_2SO_4 or mixture of them and pH is controlled by pH meter. The solution is purged with N_2 30 mins prior to tests to remove oxygen. The electrodes are immersed in electrolyte and after equilibrium is reached, the open circuit voltage is recorded. The linear sweep voltammetry is performed between -1 and +2 volts under dark conditions. After that the light is turned on and the same sweep is done under light conditions. Xe lamp with 150W power equipped with AM.1.5G filter is used as solar simulator.

Figure 3.4. The open beaker photoelectrochemical setup for three electrode configuration.

3.6. Hydrogen Evolution Analysis

The photocatalytic activities of prepared catalysts are tested in a Pyrex glass reactor irradiated from one side; for product analysis Gas Chromatography is used. Pt is used as cocatalyst and loaded on the catalyst surface by incipient-to-wetness impregnation method. After impregnation the catalyst is dried overnight and calcined at 400^{o} C for four hours. Two grams of catalyst is suspended in one liter 20 vol. % methanol-water mixture and stirred with magnetic stirrer. Argon is used as carrier gas and is bubbled through the reaction solution. The amount of evolved gas is determined with calibration curves. The illumination is done by 300W Xe lamp with AM.1.5G filter. The setup of photocatalytic water splitting is given in Figure 3.5.

Figure 3.5. The setup of photocatalytic water splitting.

3.7. Preliminary Work

As preliminary work, the different coating and preparation of $SrTiO_3$ catalysis are studied. Different preparation are used for in-situ coating of ITO glass. The optimization of paste concentration and thickness for doctor blade method is done to have defect free electrodes.

4. RESULTS AND DISCUSSION

The aim of this study was to develop a working photoelectrochemical cell based on TiO_2 and $SrTiO_3$ photoelectrodes. Ag/AgCl reference electrode and Au or Pt counter electrodes were used. There was no difference in the results obtained with Au and Pt counter electrodes, i.e. similar photocurrents were generated. The Au counter electrode was fabricated by deposition of Au layer on a micro slide and had an area of 2 cm^2 while Pt electrode was a metalic plate with dimensions 1cm x 2.5 cm. Since Pt plate had both faces that were conductive, the remaining experiments were carried out with Pt counter electrode to prevent any current loss associated with small area; it is suggested that the surface area of the counter electrode must be higher than that of working electrode so that the half reaction occurring at the counter electrode is fast enough to not limit the reaction occurring at the working electrode (Bard & Faulkner, 2001).

In addition to developing a working photoelectrochemical cell, the effect of preparation method, electrolyte type, molarity and pH, doping and heterostructure were also investigated. The photocatalytic hydrogen productions of the photocatalysts prepared using the same materials were also studied. As stated in Section 2, the different preparation methods coating methods were used in the fabrication of photoelectrodes. The electrodes synthesized by sol-gel and hydrothermal method was spin and dip coated on the ITO glass. The coating of sol-gel derived catalysts resulted in crack formation, which eliminated the possibility of utilization in a photoelectrochemical cell. Hydrothermal derived catalyst was coated by in-situ techniques and dip coating. For in-situ coating the ITO glass was placed in the autoclave and reaction occurred on the conductive surface of the ITO glass, as for dip coating after the hydrothermal reaction, ITO glasses were dipped in the solution and dried. The coated ITO glasses were calcined at 500^oC for 3 hours to establish crystal structure. However, on the surface of dip coated samples, the cracks were formed while the in-situ prepared electrodes did not exhibit any photocurrent in photoelectrochemical cell. The stability of ITO glasses are limited to 600^oC (Troyan *et al.*,2018); this also limited the calcination temperature, which is important parameter for catalytic activity. If the temperature was not sufficient to create $SrTiO_3$ crystals, the photoelectrochemical performance cannot be observed. The best result and stability is found in $SrTiO_3$ prepared

by SSR and coated by doctor blade method since the thickness of coating was uniform and no crack formation is observed. Hence the remaining experiments were performed with the electrodes obtained this way.

Some of the electrodes prepared successfully were also deformed and inactivated by the electrolyte solution as shown in Figure 4.1. Figure 4.1a is electrode with $SrTiO_3$ on TiO_2 blocking layer used in H_2SO_4 solution; its color has turned from white to black. This may be attributed to the hydrogenation of TiO_2 layer. In literature, hydrogen treated TiO_2 catalyst has black color (Wang *et al.*, 2011; Wang *et al.*, 2017; Shen *et al.*, 2018) and in the solution there is excess H^+ ions, that can result in generation of hydrogen gas on TiO_2 surface and hydrogenate the layer. In Figure 4.1. b and c, $SrTiO_3$ coated ITO photoelectrode in NaOH were given. Due to exposition of ITO layer to the electrolyte due to a small starch on the $SrTiO_3$ layer (Figure 4.1.b), the reduction of ITO was observed and resulted in color change (Figure 4.1.c). Under strong acidic or basic conditions reduction of ITO was also reported by other investigators observed (Liu *et al*., 2015). Corrosion, color change or dissolution of other electrodes were not observed hence, electrolyte choice was not effected; for acidic conditions 0.1 M H_2SO_4, for alkaline conditions 0.1 M NaOH solutions were used as electrolytes.

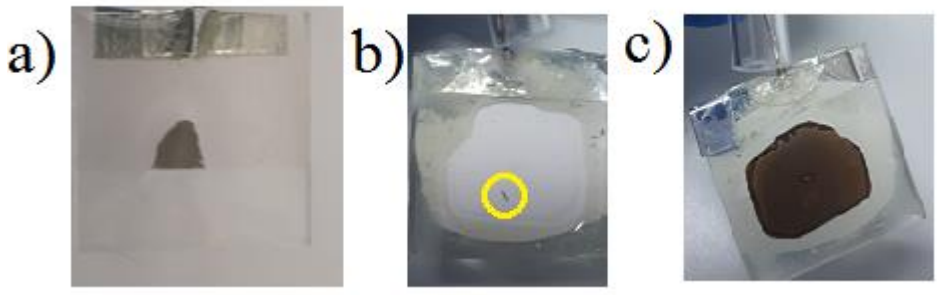

Figure 4.1. Electrodes deformed during photoelectrochemical analysis (a) TiO_2 blocking layer electrode and (b) $SrTiO_3$ electrode (front) with starched surface and (c) $SrTiO_3$ electrode (back) changed color.

The photovoltage generated by the cell is recorded in 0.1 M NaOH solution with Pt counter electrode given in Table 4.1. The difference between the open circuit potentials in light and dark conditions represents the generated photovoltage. The photovoltage is highest in heterostructure form ($SrTiO_3$ /TiO_2) due to increased charge separation. TiO_2 has higher photovoltage compared to $SrTiO_3$ because it has more uniform structure due to the preparation method and it has more transparent nature which increases the amount of particles involved in photo absorption; all $SrTiO_3$ samples were not transparent indicating that only the top most layer absorbs the light. Possibly, recombination of photogenerated charges is less important in TiO_2 anode. All of these photovoltage values are not sufficient to govern spontaneous water splitting, therefore additional bias was required.

Table 4.1. The photovoltage generated by the cell in 0.1 M NaOH solution.

Anode	**open circuit voltage under dark (V vs Ag/AgCl)**	**open circuit voltage under light (V vs Ag/AgCl)**	**Photovoltage (V)**
TiO_2	-0.94	-0.44	0.50
$SrTiO_3$	-0.28	-0.18	0.10
Al-$SrTiO_3$	-0.85	-0.75	0.10
Fe-$SrTiO_3$	-0.55	-0.50	0.05
$SrTiO_3$/TiO_2	-0.53	-0.45	0.08

In the remaining sections, the photocurrent generated with these semiconductors were analyzed under different conditions.

4.1. Effect of Precursor Ratio

The ratio of Sr and Ti precursors are important for the morphology of of $SrTiO_3$. As given in Figure 4.13, the present phases are different in Sr:Ti ratio of 1:1 and 2:3 $SrTiO_3$. TiO_2 phase is significantly higher and other Sr-Ti compounds such as Sr_2TiO_4 are vanished in $SrTiO_3$ prepared by Sr:Ti ratio of 2:3. This structural difference resulted in different photoelectrochemical performances as seen in Figure 4.2. The photocurrent increases up to 2.5 folds higher values in Sr:Ti ratio of 2:3. Their photon absorption properties are similar since they have the same band gap energy (3.2 eV) as seen in Table 4.3, but their charge transfer properties are different due to structural differences and this difference results in higher photocurrent values.

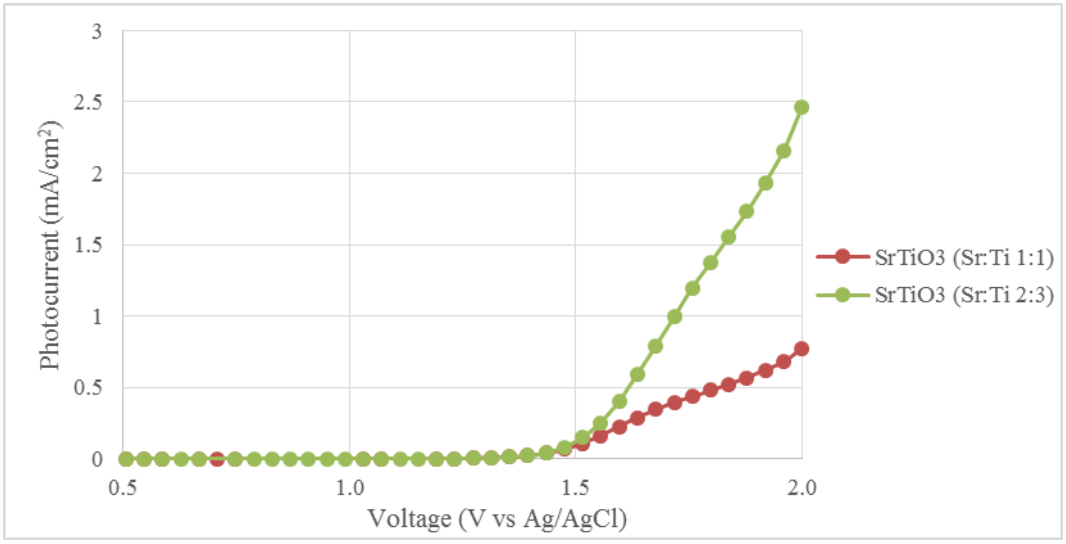

Figure 4.2. I-V curve of $SrTiO_3$ prepared by different precursor ratios in 0.1 M NaOH.

4.2. Photoelectrochemical Performance of TiO_2 photoanode

TiO_2 nanoparticles are coated on ITO by doctor blade method and its I-V curve in 0.1 M NaOH is given in Figure 4.3. Compared to $SrTiO_3$, TiO_2 nanoparticles exhibited nearly 1.5 folds increased photocurrents.

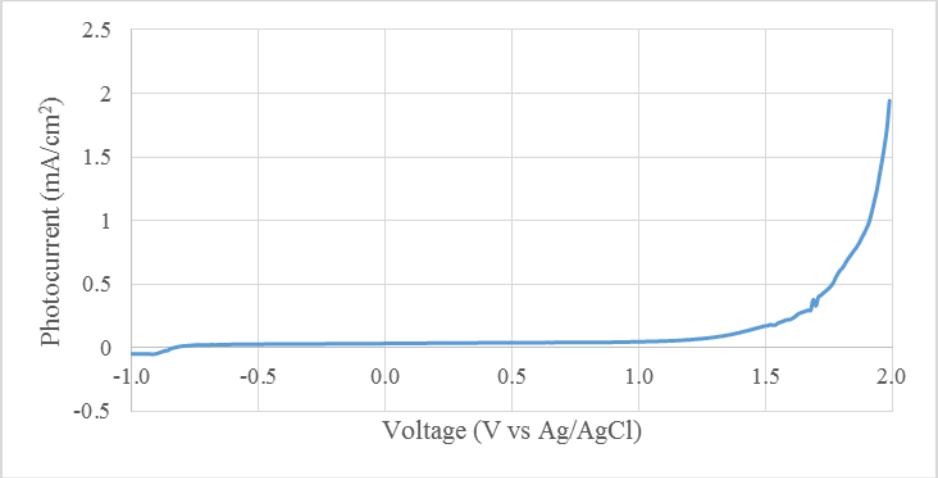

Figure 4.3. I-V curve of TiO_2 nanoparticle photoanode in 0.1 M NaOH.

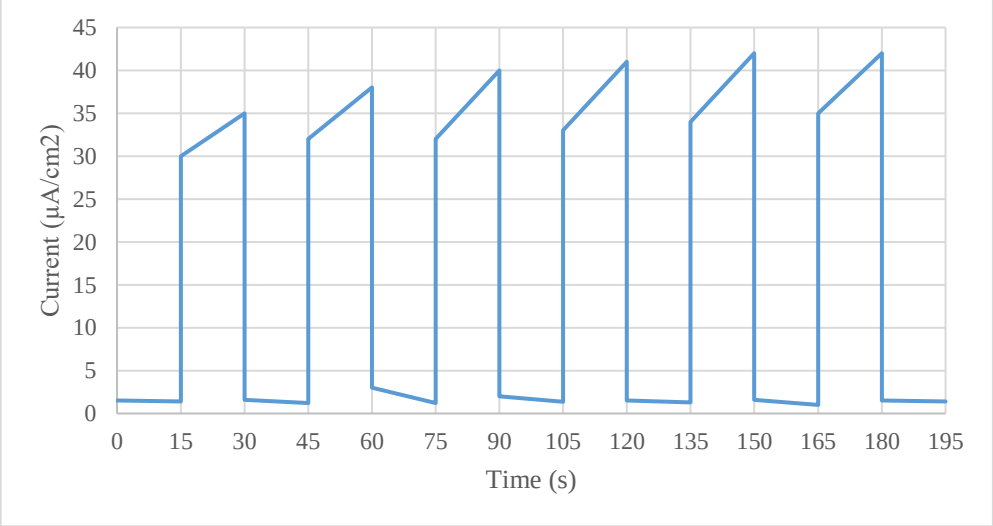

Figure 4.4. I-t curve for TiO_2 nanoparticle photoanode in 0.1 M NaOH at 0 V vs Ag/AgCl with 15 seconds light on-off cycles.

Figure 4.4 shows I-t curve for TiO_2 photoanode at 0 V vs Ag/AgCl in 0.1 M NaOH electrolyte. 15 seconds of light on-off cycles show that there is an increase in photocurrent with respect to time which suggests that the charge recombination is low and does not decrease the current. The maximum attainable photocurrent is 41 $\mu A/cm^2$, which is comparable to literature, the photocurrent response of TiO_2 structures in NaOH electrolyte at 0 V vs Ag/AgCl were reported to change from 75 to 200 $\mu A/cm^2$, depending on electrolyte

molarity, thickness and preparation method (Kitano *et al*., 2007; Kment *et al*., 2017; Kumari *et al*., 2007; Shen *et al*., 2018).

The stability of photocurrent generated by TiO_2 photoanode is given in Figure 4.5. After one hour, the photocurrent decreased by 12% and become stable around 35 $\mu A/cm^2$. Upon irradiation, the equilibrium is disturbed and photogenerated charge carriers are transferred at higher rates. When irradiation continued, the recombination of charges was developed and the generation of photocurrent was decreased as expected (Cheng *et al*., 2016). In addition, the corrosion or instability of the photoanode may have caused the decrease in the photocurrent but no visible change was observed after the reaction.

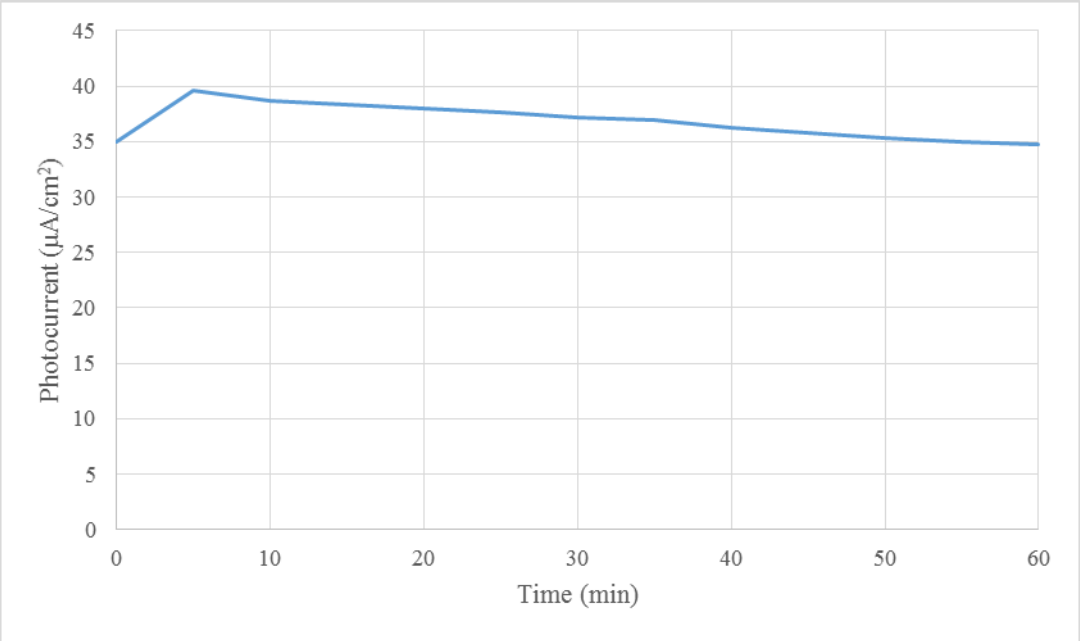

Figure 4.5. I-t curve for TiO_2 nanoparticle photoanode in 0.1 M NaOH at 0 V vs Ag/AgCl.

4.3. Effect of Doping

In this study, 1wt% aluminum and iron were doped to $SrTiO_3$ to observe the effect of metal ion doping on the photoelectrochemical and photocatalytic activity of $SrTiO_3$.

In Figure 4.6 the photocurrent responses of Fe-doped and un-doped $SrTiO_3$ in 0.1 M $NaCO_3$ solution is given. The photocurrent on set potential of $SrTiO_3$ and Fe-$SrTiO_3$ were at 0.9 V and 1V vs Ag/AgCl respectively. Even though the generation of current for $SrTiO_3$ sample started at lower potentials, its overall performance was lower compared to Fe-doped $SrTiO_3$. Fe doping reduced the band gap to 3.17 eV as given in Table 4.3. and therefore Fe-doped $SrTiO_3$ absorbs larger portion of the solar spectrum; in addition, due to introduction of Fe atom to the $SrTiO_3$ crystal lattice might improve the charge transfer and reduce the recombination of charges hence increase the photocurrent.

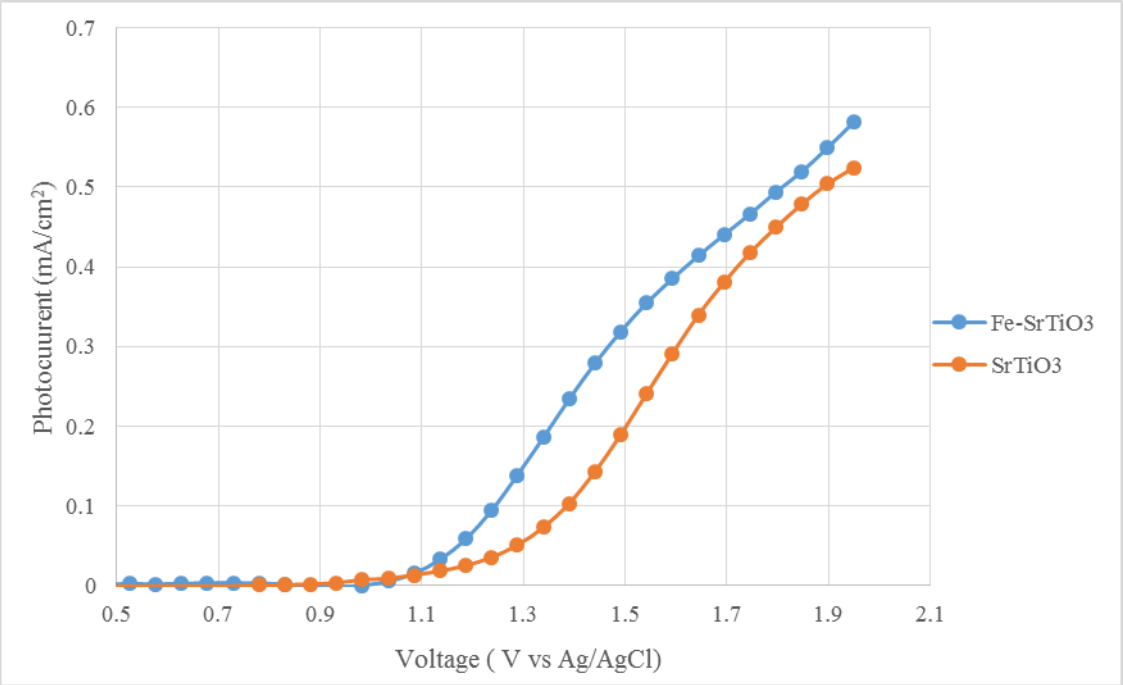

Figure 4.6. I-V curve for $SrTiO_3$ and Fe-$SrTiO_3$ photoanodes in 0.1 M Na_2CO_3.

The differences of photocurrent responses of Al-doped and un-doped $SrTiO_3$ in 0.1M NaOH is given in Figure 4.7. The onset potentials are 1 V and 1.4 V for Al-$SrTiO_3$ and $SrTiO_3$ respectively. Even though between 1 and 1.5 V current generated by Al-$SrTiO_3$ was larger, $SrTiO_3$ developed higher photocurrent values after 1.5 V. Al-$SrTiO_3$ photoanode reached a limiting current first at 0.13 mA/cm^2 but after 1.76 V, the current continues to increase since around that potential aluminum oxidation happens.

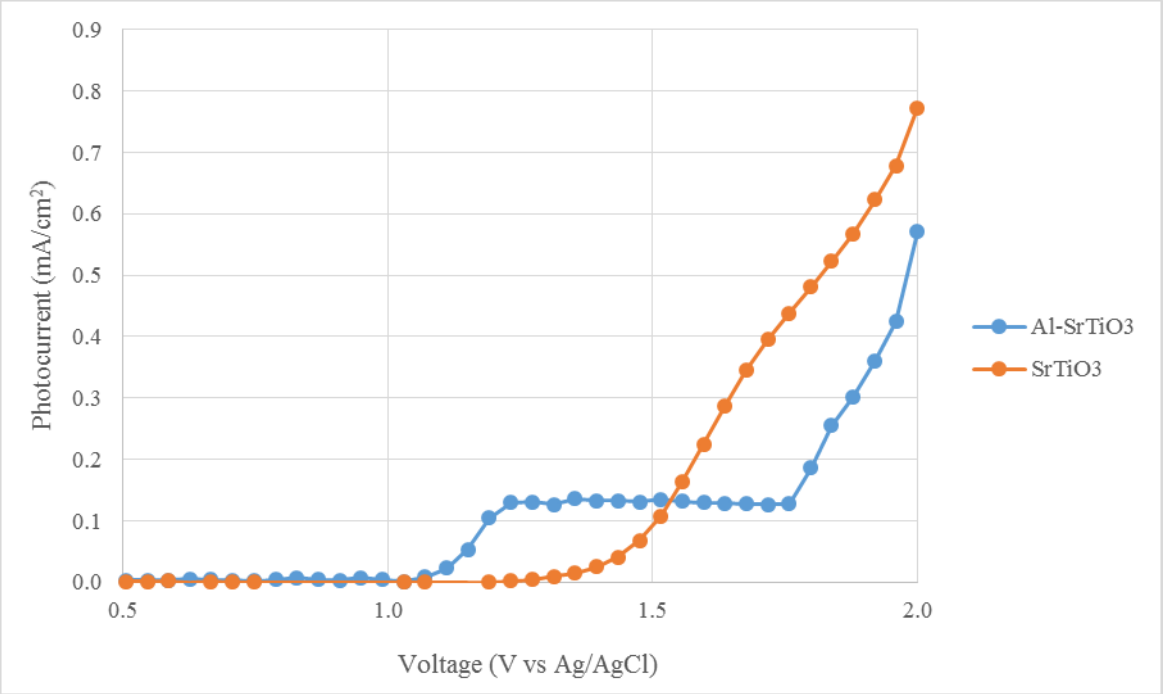

Figure 4.7. I-V curve for $SrTiO_3$ and Al-$SrTiO_3$ photoanodes in 0.1 M NaOH.

4.4. Effect of Electrolyte

Different pH and molarity of common electrolytes as well as a sacrificial agent (Na_2SO_3) electrolyte was investigated. The comparison of the photocurrent values of $SrTiO_3$ in these electrolytes can be found in Table 4.2.

In order to observe the effect of pH of the electrolyte, 0.1 M H_2SO_4 (pH~1) and NaOH (pH ~13) were compared because, as stated in section 2.5, the pH of medium may change the rate limiting steps and favored reactions. In addition, the fermi level and flat band potentials are pH dependent.

Table 4.2. Comparison of electrolytes used in the photoelectrochemical cells.

Cell (WE//CE)	Electrolyte	Photocurrent at 1.5 V vs Ag/AgCl (mA/cm^2)	Photocurrent at 2 V vs Ag/AgCl (mA/cm^2)
$SrTiO_3$//Pt	0.1 M Na_2CO_3	0.0011	0.019
$SrTiO_3$//Pt	0.1 M Na_2SO_3	0.0292	0.059
$SrTiO_3$//Pt	0.1 M NaOH	0.0586	1.556
$SrTiO_3$//Pt	0.1 M H_2SO_4	0.0482	0.866
$SrTiO_3$//Pt	1 M Na_2CO_3	0.0754	3.248

Under acidic conditions, HER (hydrogen evolution reaction) is enhanced whereas OER (oxygen evolution reaction) is faster in alkaline conditions (Hilliard, 2016). At pH value higher than 12, the oxidation of hydroxide ions dominates; hence, the anodic current increases. In contrast, the higher cathodic currents are observed at low pH values due to decreased overpotential (Ding *et al.*, 2017). Both NaOH and H_2SO_4 have good ionic conductivity and additional OH^- and H^+ ions to facilitate water splitting reactions, respectively. As seen in equations 2.11 to 2.14, even though the overall reaction requires 1.23 V, the potentials of half reactions change in alkaline media. There is almost two-folds increase in the photocurrent in NaOH solution compared to H_2SO_4 at 2 V, and this difference is due to the hydroxide oxidation is preferred instead of water oxidation. As compared to Na_2CO_3 and Na_2SO_3 electrolytes, both NaOH and H_2SO_4 solutions generate higher photocurrents because of the nearly four-folds difference in their conductivities (Haynes, 2016).

Na_2CO_3 is a soluble salt with pH of 11 and 12 in 0.1 M and 1 M aqueous solutions respectively. As the concentration of Na_2CO_3 increases, the conductivity of ions increases and it is expected to have increased current values (Crawford *et al.*, 2009). Indeed, there wasa significant increase in the photocurrent values in 1 M Na_2CO_3 electrolyte (Table 4.2.).

As concentration increases, the diffusion of ions are facilitated in addition to the increases in pH; therefore the enchancement is observed due to both pH and concentration increase. Na_2SO_3 has pH value around 10 in 0.1 M aqueous solution, which is widely used as hole scavenger since oxidation of SO_3^{-2} ions have smaller potential with respect to oxidation of water to oxygen (Guo *et al.*, 2018). Compared to 0.1 M Na_2CO_3, there was an increase in photocurrent due to hole scavenging property of SO_3^{-2} ions; however, 0.1 M NaOH solution exhibited higher photocurrents. This difference between Na_2SO_3 and NaOH comes mainly from pH difference and oxidation potentials of SO_3^{-2} and OH^- (0.72 V and 0.4 V, respectively) (Das *et al.*, 2002; Hilliard, 2016).

4.5. Attempts to Improve Photocurrent Response of $SrTiO_3$

Apart from doping and preparation method modifications, two other modifications on the photoanode were also performed to increase the photocurrents: (1) Au interlayer was used for increased charge transfer and (2) $SrTiO_3$ on TiO_2 layer is fabricated to investigate the effect of heterostructure form.

In Figure 4.8 I-V curve of $SrTiO_3$ coated on Au layer in 0.125 M NaOH is given while the pictures of $SrTiO_3$ coated on Au layer before and after the photoelectrochemical reaction are presented. And in Figure 4.9 as the voltage is swept from -1 V to 2 V, the dissolution of $SrTiO_3$ layer was observed. Since Au layer was exposed, the photoelectrochemical behavior in the cell decreased as well. This suggests that the current observed was associated with the dissolution of $SrTiO_3$ layer but not water splitting; having no difference between the dark and light conditions also supports this argument. The dissolution of $SrTiO_3$ may be due to the problems in the interaction of Au and $SrTiO_3$ layer. When stable contact is not established between conductive layer and semiconductor, the alkaline electrolyte or application of electricity may have caused the $SrTiO_3$ removal. Although it was expected to have increased photocurrent due to increased charge transport in Au layer (Ginsburg *et al*., 2018; Wang *et al*., 2016), this did not happen probably due to the instability of the anode.

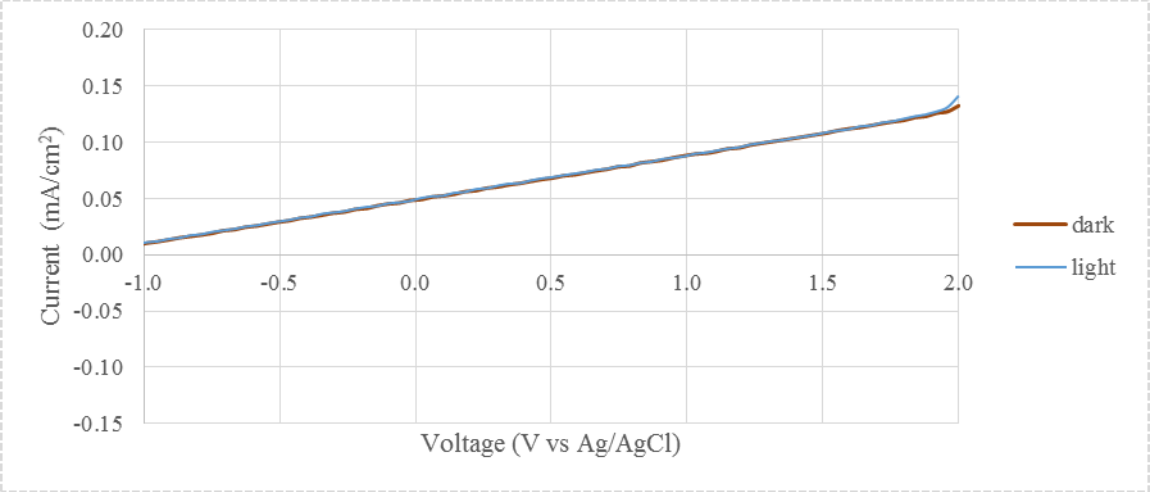

Figure 4.8. I-V curve for $SrTiO_3$ coated on Au layer in 0.125 M NaOH.

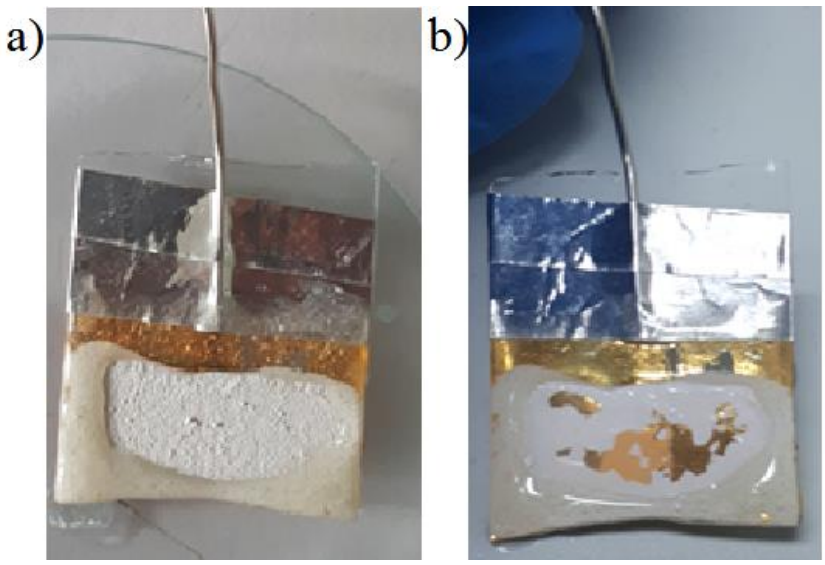

Figure 4.9. The $SrTiO_3$ electrode coated on Au layer (a) before and (b) after the experiment.

In Figure 4.10, I-V curve of $TiO_2/SrTiO_3$ heterostructure and $SrTiO_3$ in 0.05 M H_2SO_4 solution were compared. The photocurrent onset potential of heterostructure and $SrTiO_3$ are -0.3 V and 0.1 V vs Ag/AgCl respectively. The heterojunction starts generating photocurrent at lower potential but the generated photocurrent values are lower compared to $SrTiO_3$. The coating of $SrTiO_3$ layer was done on TiO_2 blocking layer electrode and additional thickness

of $SrTiO_3$ in the structure may have caused charge recombination and decreased the performance. In addition, the $SrTiO_3$ layer was not transparent and since no TiO_2 is exposed to light or the electrolyte, the effect of heterostructure could not be observed clearly since TiO_2 only acted as electron transfer layer.

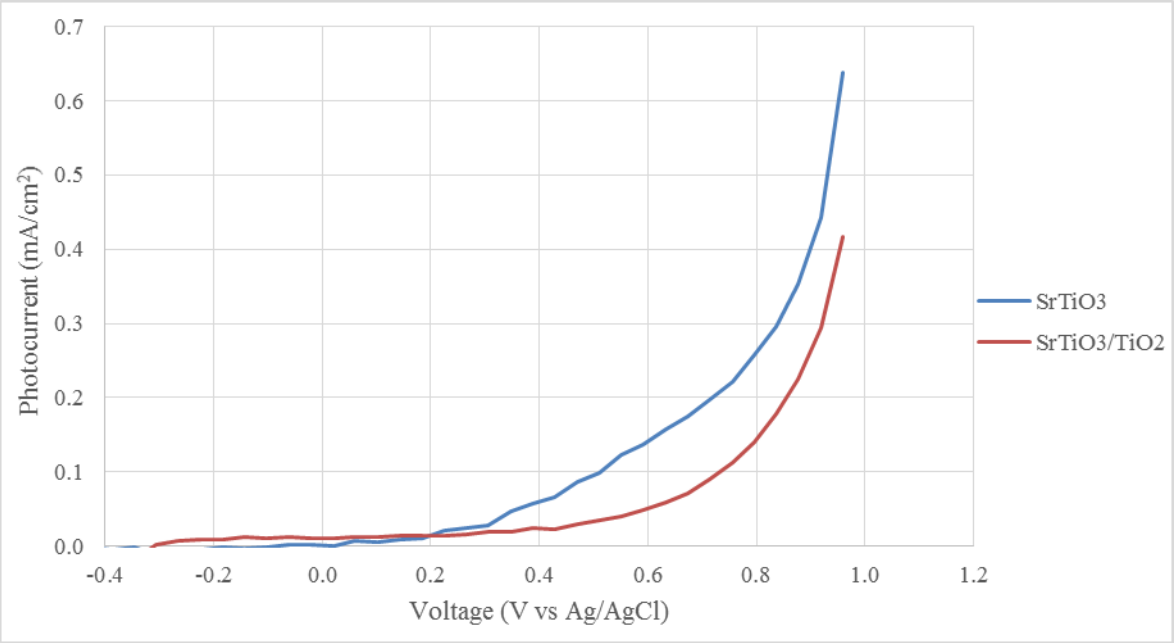

Figure 4.10. The $SrTiO_3$ electrode coated on Au layer (a) before and (b) after the experiment.

4.6. Photocatalytic Hydrogen Production from Aqueous Methanol Solution

In Figure 4.11, the hydrogen production rates of prepared catalysts using the same materials with different precursor ratios and dopant are given. As in photoelectrochemical results, the Sr:Ti ratio of 2:3 gave much better results compared to Sr:Ti ratio of 1:1. Since the crystal structure of catalysts are different, their electronic properties are expected to be different as well. Even though the band gap energy of these catalyst are the same (3.2 eV) as seen in Table 4.3, it is possible for Sr:Ti ratio of 2:3 have better charge separation, which results in better photocatalytic activities, due to structural differences. On the other hand, it was also observed that increasing Sr to Ti ratio from 0.8 to 1.25, increases the photocatalytic

activity of $SrTiO_3$ (Sulaeman *et al.*, 2011). In addition to differences in crystal structures, the amount of TiO_2 in the catalyst with the Sr:Ti ratio of 2:3 is higher, this may lead to a formation of a composite like structure which utilizes both $SrTiO_3$ and TiO_2 photocatalytic properties (Liu & Ma, 2019).

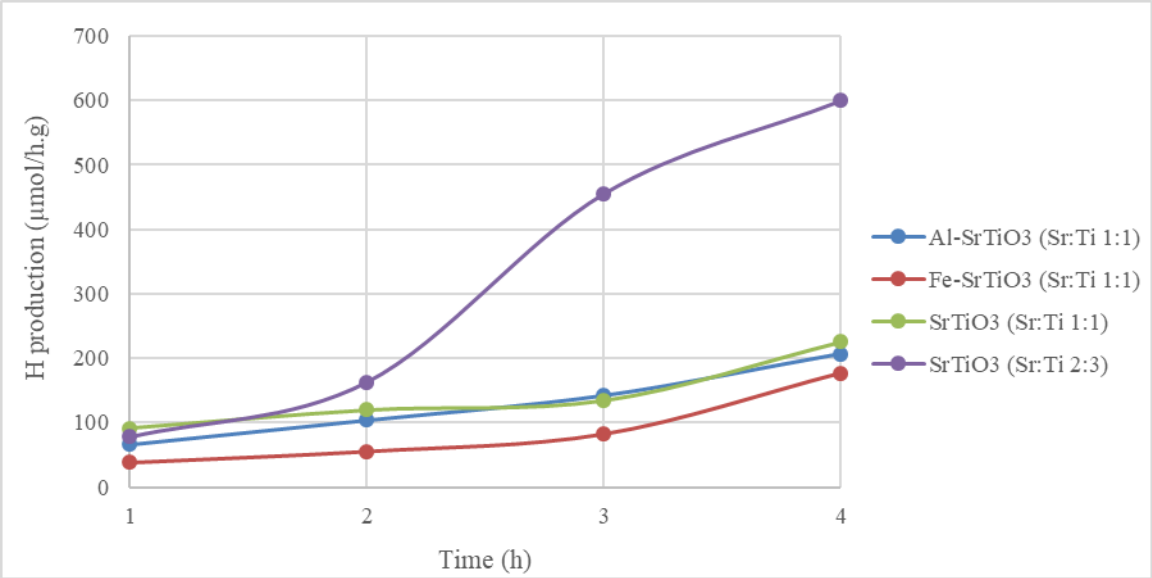

Figure 4.11. The photocatalytic hydrogen production rates of prepared catalysts.

When effect of doping is inspected, no significant change in hydrogen production was observed. Even though Fe doped $SrTiO_3$ has lower band gap energy, as will be discussed below in section 4.8, suggesting higher hydrogen production rate due to the adsorption of larger portion of solar light; the production rate is lowest in Fe-doped $SrTiO_3$. This suggests that the crystal structure of the catalyst promotes charge recombination. The oxidation state of Fe can be different depending on the oxygen vacancies present in the $SrTiO_3$ lattice. Due to its ionic radius, Fe replaces Ti atoms and Fe can have +2 or +3 oxidation state where Ti has +4; this difference causes oxygen vacancies for charge neutralization in the crystal (Lobacheva *et al.*, 2014). Normally these oxygen vacancies enhance the photocatalytic activity up to an optimum concentration (Tan *et al.*, 2014); it is possible to have excess oxygen vacancies in Fe-doped samples which leads to lower photocatalytic activity due to increased charge recombination at these vacancies. Al-$SrTiO_3$ had similar photocatalytic

performance with $SrTiO_3$, since their band gap is the same (Section 4.8), their light absorption abilities are similar. The structure ad oxidation states are generally changed with doping, therefore a change in photocatalytic activity is expected (Atkinson *et al*., 2019; Sanwald *et al*., 2018; Wang *et al*., 2010). Observing no significant difference suggests that implementing Al atom in the $SrTiO_3$ structure may not be successful or efficient. Al has ionic radius smaller than Sr and Ti atoms and this enables the substitution of Al in both Sr and Ti sites (Yu *et al*., 2011). In addition, as presented in Section 4.7, in XRD results strontium hydroxide peaks were higher than other samples, if aluminum caused $SrTiO_3$ to hold the humidity in the structure, this additional phase may have reduced the photocatalytic activity.

4.7. XRD Results

Figure 4.12 shows the XRD spectra of pristine $SrTiO_3$ samples that were prepared with Sr:Ti molar ratio of 1:1. It is seen that the dominant peaks are strontium titanates, hence it can be said that after solid state reaction at 1000^{o}C, the strontium titanate phasewas obtained. The cubic perovskite phase of $SrTiO_3$ was achieved in all samples. The dominant faces of $SrTiO_3$ were at 32^o (110), at 47^o (200) and at 58^o (211) planes.

The quantitative analysis showed presence of other peaks of impurities, which were coming from the precursors; no contamination from alumina crucible was present. Using SSR to prepare $SrTiO_3$ may result in incomplete reaction or different Sr-Ti compounds depending on reaction temperature and time. As seen in Figure 4.12, SrO, $SrCO_3$ and TiO_2 phases were found due to incomplete reaction. There are several reports that also observed impurites like $SrCO_3$ and TiO_2 in XRD analysis of $SrTiO_3$ catalyst (Kalyani *et al.*, 2012; Souza *et al.*, 2012). In the mechanism of SSR preparation of $SrTiO_3$, $SrCO_3$ is converted to SrO and it combines with TiO_2 where CO_2 is released. Coonrod, investigated the effect of reaction temperature and time on the structure of $SrTiO_3$ and observed that samples prepared at 1000^{o}C for 10 hours may have impurities such as TiO_2 and Sr_2TiO_4 (Coonrod, 2014). The longer reaction times and higher temperature would result in elimination of impurity peaks such as $SrCO_3$, SrO and TiO_2. Sr_2TiO_4 and $Sr_3Ti_2O_7$ were other possible forms that can be produced by combination of SrO and TiO_2.

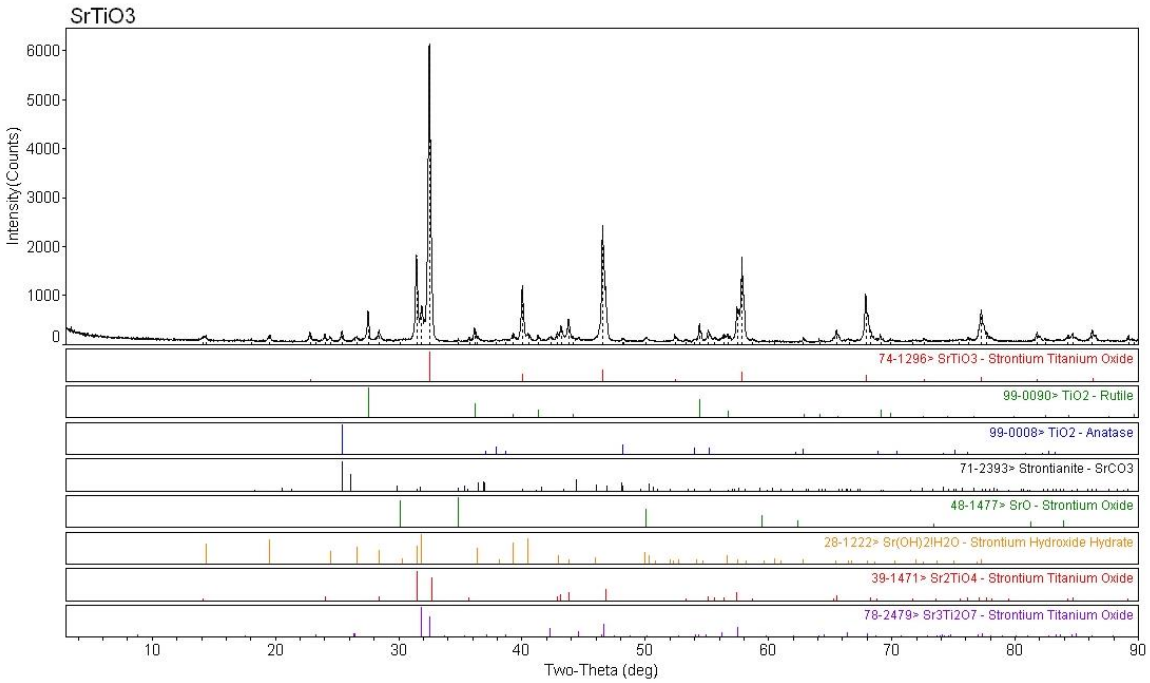

Figure 4.12. XRD result for $SrTiO_3$ electrode.

It can be said that anatase phase of TiO_2 was not present in prepared $SrTiO_3$ catalyst; its corresponding peaks are very low; , the peaks at 26 degree coincides with $SrCO_3$. Rutile TiO_2 was expected to be observed because the irreversible transformation from anatase to rutile is observed for TiO_2 at temperatures higher than 600^oC (Hanaor & Sorrell, 2011).

In Al doped samples (Figure 4.13), Sr hydroxide peaks were higher than other samples. This may be atrributed to the ability of Al to draw the humidity present in air (Sin *et al.*, 2011). In doped samples, the oxide phases of Al and Fe are not observed, which shows that Al and Fe are homogeneously incorporated in the structure. When doped and pristine samples are put on top of each other, a slight shift in peaks are observed. This phenomena was reported by other investigotors as well (Fuentes *et al*., 2015). The peaks of Fe doped $SrTiO_3$ shifts to higher degrees, and this was attributed to the replacement of Ti by Fe ions.

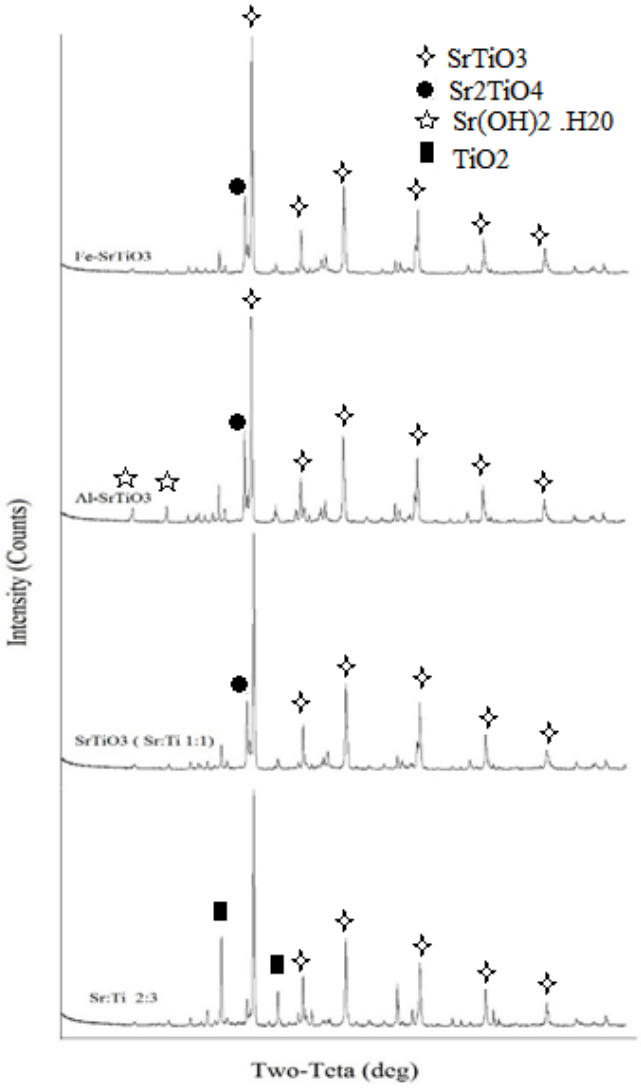

Figure 4.13. XRD results of prepared catalysts.

When the molar ratio of Sr and Ti precursors were 2:3, the XRD spectra changes significantly (Figure 4.13). Since TiO_2 is excess with respect to $SrCO_3$, the TiO_2 phase is more in this sample, and it is seen that the amount of other Sr-Ti compounds like Sr_2TiO_4 decreased remakably indicating that all produced SrO molecules were combined with TiO_2 to produce $SrTiO_3$ phase.

4.8. UV-VIS Characterization Results

In PEC water splitting, the band gap of the semiconductor is an important property that determines whether the reaction will be spontaneous or not. As stated before, the minimum energy required to split water is roughly 1.8 eV if the loses were also considered. A semiconductor that can be used in spontaneous water splitting should have minimum band gap energy of 1.8 eV, but due to recombination of charges and other energy loses under illumination, the generated energy by semiconductor is less than its band gap energy. Therefore, using a semiconductor with large band gap is a way to achieve spontaneous solar water splitting; however, as the band gap value gets larger, the percentage of light that it can absorb gets smaller. For example, if the band gap is larger than 3 eV, the semiconductor will be active in the UV region and this corresponds to only 4% of the solar spectrum (Yerga *et al.*, 2009). Due to absorption of small percentage of the solar spectrum, efficiencies are lower in large band gap semiconductors.

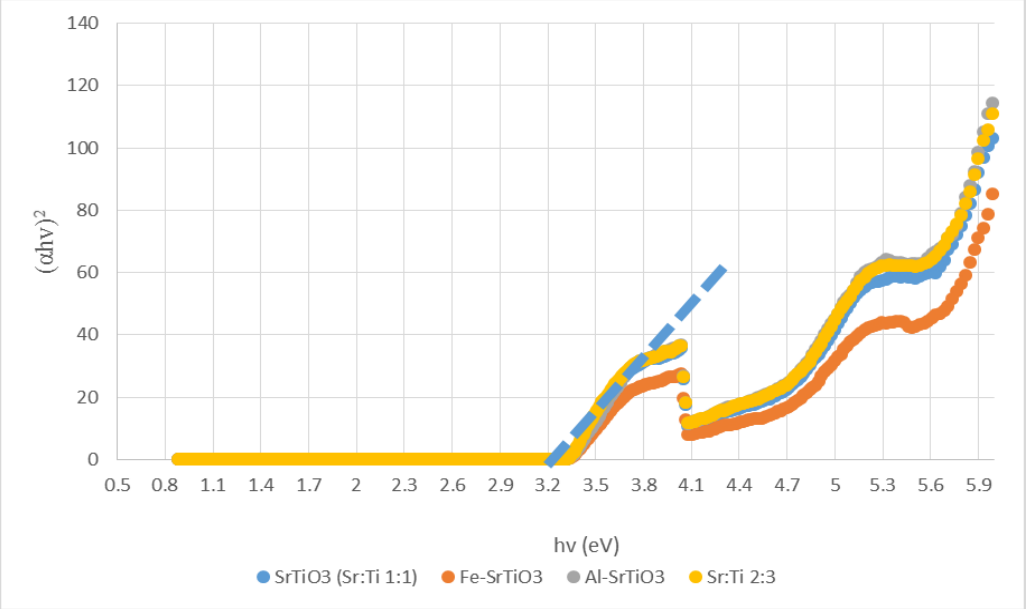

Figure 4.14. Tauc plots of prepared catalysts.

$SrTiO_3$ and TiO_2 are large band gap semiconductors with band gaps of 3.2 eV and 3 eV, respectively (Wysmulek *et al.*, 2017). Kubelka-Munk method was used to calculate band gap energies of samples prepared in this work. In Figure 4.14, the Tauc plots generated by

reflectance data is presented. The graph is plotted by using equations 2.19 and 2.20 with n=2. The intersection of the gradient line with x axis gives the band gap value of the catalyst. The band gap values of the studied semiconductors prepared were given in Table 4.3. The indirect, allowed band gap of prepared $SrTiO_3$, 3.2 eV, matches with literature (Jiang *et al*., 2017). Generally doping of semiconductors results in band gap reduction (Konta *et al*., 2004); However, Al doping did not result in band gap reduction in our sample, and Al doped $SrTiO_3$ was also reported to have a band gap of 3.2 eV in literature (Sanwald *et al.*, 2018). In Fe doped sample, there was a small reduction in bandgap (to 3.17 eV). Even though, the calculated band gap is around 2.8 eV (Xie *et al.*, 2008). Apparently, 1 wt% Fe doping was not sufficient to change the band gap of $SrTiO_3$ significantly. The oxidation state of Fe ions in the structure also affects the band gap energy (Lenser, 2013). If the Fe ions was not properly replaced Sr or Ti atoms, this may be the reason for observing 3.17 eV instead of 2.8 eV.

Table 4.3. Band Gap Energies of Prepared catalysts.

Sample	**Band Gap Energy (eV)**
$SrTiO_3$ (Sr:Ti 1:1)	3.20
$SrTiO_3$ (Sr:Ti 2:3)	3.20
Al doped $SrTiO_3$	3.20
Fe doped $SrTiO_3$	3.17

5. CONCLUSION AND RECOMMENDATIONS

5.1. Conclusion

A working photoelectrochemical cell for water splitting with TiO_2 and $SrTiO_3$ phtotanodes as working electrodes, Pt plate as counter electrode and Ag/AgCl as reference electrode was constructed. Factors affecting the photoelectrochemical performance were investigated. Sol-gel and modified hydrothermal routes were ineffficient due to instability of electrodes. Preparing catalysts by SSR and coating by doctor blade method gave the most efficient and stable electrodes.

UV-VIS analysis showed that the band gap of $SrTiO_3$ and Al-$SrTiO_3$ was 3.2 eV where Fe-$SrTiO_3$ was 3.17 eV. XRD analysis showed that cubic perovskite $SrTiO_3$ was synthesized by SSR with some impurities. Changing the precursor ratio changed the amount of impurities in the structure.

As concentration of the electrolyte increased, much higher photocurrents were observed, in 1M Na_2CO_3 solution at 2 V vs Ag/AgCl, the photocurrent of $SrTiO_3$ increased to 3.2 mA/cm^2. pH is found to have a significant effect on the photoelectrochemical performance. At same molarity values, the NaOH electrolyte gave the best anodic photocurrent values due to oxidation of OH^- . At low pH values, the photocurrent was also increased due to shifts in Fermi levels and increased conductivity. The photocurrent values of $SrTiO_3$ in acid and alkaline electrolytes were 0.87 and 1.56 mA/cm^2, at 2 V vs Ag/AgCl respectively. 1 M concentration and NaOH with pH= 13 is found to be optimum electrolyte for maximum photocurrent values. Effect of scavenger agent was studied with Na_2SO_3; higher photocurrent values was observed compared to Na_2CO_3 electrolyte due to oxidation of SO_3^{2-} ions.

Ratio of precursors of Sr and Ti had a significant effect on the photoelectrochemical and photocatalytic activity, at 2 V vs Ag/AgCl, the photocurrents of Sr:Ti 2:3 and Sr:Ti 1:1 were 2.5 mA/cm^2 and 0.7 mA/cm^2 respectively.

TiO_2 photoanode exhibited 2 mA/cm^2 where $SrTiO_3$ 1.57 mA/cm^2 in 0.1 M NaOH at 2 V vs Ag/AgCl bias. TiO_2 photoelectrode had stablized photocurrent at 35 $\mu A/cm^2$ at 0V vs Ag/AgCl in 0.1 M NaOH solution.

Photocatalytic activities in 20 vol% aqueous methanol solution showed that Sr:Ti ratio of 2:3 showed best activity of 600 $\mu mol/h.g_{cat}$ hydrogen production rate after 4 hours whereas Sr:Ti ratio of 1:1 yielded in 226 $\mu mol/h.g_{cat}$. Doping with Fe reduced the rate to 177 $\mu mol/h.g_{cat}$ and doping with Al did not change the acitivity.

5.2. Recommendations

In order to achieve further insight about the presented topic following improvements can be useful:

- Using Ti sheets as substrates and heterojunctions
- Optimization of sol-gel and hydrothermal synthesis methods for effective in-situ or spin coating
- Understanding electron-hole recombination characteristics by PL spectra
- Further analyzing the resistances of the system with EIS and developing Mott-Schottky plots for flat band potential calculations
- Separation with membrane and recording amount of evolved gas (e.g. Nafion). Care must be taken in implementing an ion membrane because there is a possibility to obtain pH difference in compartments and since ionic and electron path length is larger compared to other configurations, a careful design of the setup is necessary (Yu *et al.*, 2011; Berger *et al.*, 2014; Bosserez *et al.*, 2015).
- Integrating DSSC or PV for renewable energy supply
- Investigating the effect of cations to the activity, it is reported that Li^+ ions has ability to weaken HO-H bonds (Dias & Mendes, 2018).
- Fabricating tandem type cells, both photoactive anode and cathode to eliminate the need of external bias.
- Fabricating heterostructure by sol-gel might result in more transparent and thinner layers of $SrTiO_3$ and increase the performance.

REFERENCES

Abass, A. K. (2018). Synthesis of CdTiO3 thin films and study the impact of annealing temperature on their optical, morphological and structural properties. *Eurasian Journal of Analytical Chemistry, 13*(5).

Abe, R. (2010). Recent progress on photocatalytic and photoelectrochemical water splitting under visible light irradiation. *Journal of Photochemistry and Photobiology C: Photochemistry Reviews*, *11*(4), 179–209.

Acar, C., & Dincer, I. (2016). A review and evaluation of photoelectrode coating materials and methods for photoelectrochemical hydrogen production. *International Journal of Hydrogen Energy*, *41*(19), 7950–7959.

Alfaifi, B. Y., Ullah, H., Alfaifi, S., Tahir, A. A., & Mallick, T. K. (2018). Photoelectrochemical solar water splitting: From basic principles to advanced devices. *Veruscript Functional Nanomaterials, 2*.

Arakawa, H., Shiraishi, C., Tatemoto, M., Kishida, H., Yamaguchi, D. U., Suma, A., … Yamaguchi, T. (2007). Solar hydrogen production by tandem cell system composed of metal oxide semiconductor film photoelectrode and dye-sensitized solar cell. *Solar Hydrogen and Nanotechnology II, 665*.

Aroutiounian, V. M., Arakelyan, V. M., & Shahnazaryan, G. E. (2005). Metal oxide photoelectrodes for hydrogen generation using solar radiation-driven water splitting. *Solar Energy, 78*(5), 581–592.

Atkinson, I., Parvulescu, V., Pandele Cusu, J., Anghel, E. M., Voicescu, M., Culita, D., … Fruth, V. (2019). Influence of preparation method and nitrogen (N) doping on properties and photo-catalytic activity of mesoporous SrTiO3. *Journal of Photochemistry and Photobiology A: Chemistry, 368*, 41–51.

Augustynski, J., Solarska, R., Hagemann, H., & Santato, C. (2006). Nanostructured thin-film tungsten trioxide photoanodes for solar water and sea-water splitting. *Solar Hydrogen and Nanotechnology*, *634*.

Bak, T., Nowotny, J., Rekas, M., & Sorrell, C. . (2002). Photo-electrochemical hydrogen generation from water using solar energy. Materials-related aspects. *International Journal of Hydrogen Energy*, *27*(10), 991–1022.

Bak, T., Nowotny, J., Rekas, M., & Sorrell, C. C. (2003). Defect chemistry and semiconducting properties of titanium dioxide: I. Intrinsic electronic equilibrium. *Journal of Physics and Chemistry of Solids*, *64*(7), 1043–1056.

Bao, D., Yao, X., Wakiya, N., Shinozaki, K., & Mizutani, N. (2001). Band-gap energies of sol-gel-derived SrTiO3 thin films. *Applied Physics Letters*, *79*(23), 3767–3769.

Bard, A. J., & Faulkner, L. R. (2001). *Electrochemical Fundamentals and Applications* (2nd ed.).

Bell, S. J. (2012). *Effect of Light Intensity and Temperature*. Queensland University of Technology.

Berardi, S., Drouet, S., Francàs, L., Gimbert-Suriñach, C., Guttentag, M., Richmond, C., … Llobet, A. (2014). Molecular artificial photosynthesis. *Chemical Society Reviews*, *43*(22), 7501–7519.

Berger, A., Segalman, R. A., & Newman, J. (2014). Material requirements for membrane separators in a water-splitting photoelectrochemical cell. *Energy and Environmental Science*.

Berthomieu, C., & Hienerwald, R. (2009). Fourier Transform Infrared (FTIR) Spectroscopy. *Photosynthesis Research*, (July 2009), 145–178.

Bessegato, G. G., Guaraldo, T. T., & Zanoni, M. V. B. (2014). Enhancement of Photoelectrocatalysis Efficiency by Using Nanostructured Electrodes. In *Modern*

Electrochemical Methods in Nano, Surface and Corrosion Science.

Bin Adnan, M. A., Arifin, K., Minggu, L. J., & Kassim, M. B. (2018). Titanate-based perovskites for photochemical and photoelectrochemical water splitting applications: A review. *International Journal of Hydrogen Energy*, *43*(52), 23209–23220.

Bosserez, T., Rongé, J., van Humbeeck, J., Haussener, S., & Martens, J. (2015). Design of Compact Photoelectrochemical Cells for Water Splitting. *Oil & Gas Science and Technology*, *70*(5), 877–889.

Chang, Y., Xuan, Y., Zhang, C., Hao, H., Yu, K., & Liu, S. (2019). Z-Scheme Pt@CdS/3DOM-SrTiO3 composite with enhanced photocatalytic hydrogen evolution from water splitting. *Catalysis Today*, 315–322.

Chang, Y., Yu, K., Zhang, C., Yang, Z., Feng, Y., Hao, H., … Liu, S. (2017). Ternary CdS/Au/3DOM-SrTiO3 composites with synergistic enhancement for hydrogen production from visible-light photocatalytic water splitting. *Applied Catalysis B: Environmental*, *215*, 74–84.

Chauhan, D., Satsangi, V. R., Dass, S., & Shrivastav, R. (2007). Preparation and characterization of nanostructured CuO thin films for photoelectrochemical splitting of water for photoelectrochemical splitting of water. *Bulletin of Materials Science*, *29*, 709–716.

Chen, C.-C., & Ting, C.-C. (2013). Photoelectrode Fabrication of Dye-Sensitized Nanosolar Cells Using Multiple Spray Coating Technique. *International Journal of Photoenergy*, *2013*, 1–8.

Chen, C., Cai, W., Long, M., Zhang, J., Zhou, B., Wu, Y., & Wu, D. (2010). Template-free sol-gel preparation and characterization of free-standing visible light responsive C,N-modified porous monolithic TiO2. *Journal of Hazardous Materials*, *178*(1–3), 560–565.

Chen, Z. (2013). Photoelectrochemical Water Splitting - Standards, Experimental Methods,

and Protocols. In *Springer Briefs in Energy*.

Chen, Z., Jaramillo, T. F., Deutsch, T. G., Kleiman-Shwarsctein, A., Forman, A. J., Gaillard, N., … Dinh, H. N. (2010). Accelerating materials development for photoelectrochemical hydrogen production: Standards for methods, definitions, and reporting protocols. *Journal of Materials Research*, *25*(1), 3–16.

Cheng, B. Y., Yang, J. S., Cho, H. W., & Wu, J. J. (2016). Fabrication of an Efficient BiVO4-TiO2 Heterojunction Photoanode for Photoelectrochemical Water Oxidation. *ACS Applied Materials and Interfaces*.

Chi, C. F., Liau, S. Y., & Lee, Y. L. (2010). The heat annealing effect on the performance of CdS/CdSe-sensitized TiO2 photoelectrodes in photochemical hydrogen generation. *Nanotechnology*, *21*(2).

Chou, Y. J., Sucipto, K. I., Ningsih, H. S., Moriga, T., & Shih, S. J. (2019). Inhibition of secondary phase formation with orientation-controlled SrTiO3 nanoparticles. *Ceramics International*, *45*(7), 9197–9202.

Choudhary, S., Upadhyay, S., Kumar, P., Singh, N., Satsangi, V. R., Shrivastav, R., & Dass, S. (2012). Nanostructured bilayered thin films in photoelectrochemical water splitting - A review. *International Journal of Hydrogen Energy*, *37*(24), 18713–18730.

Colón, G. (2016). Towards the hydrogen production by photocatalysis. *Applied Catalysis A: General*, *518*, 48–59.

Colthup, N. B., Daly, L. H., & Wiberley, S. E. (1990). *Introduction to Infrared and Raman Spectroscopy* (3rd ed.).

Coonrod, S. S. (2014). *Solid State Synthesis of the SrTiO3 Nano-particle*. University of Arkansas.

Crawford, S., Thimsen, E., & Biswas, P. (2009). Impact of Different Electrolytes on Photocatalytic Water Splitting. *Journal of The Electrochemical Society*, *156*(5).

Das, T. N., Huie, R. E., & Neta, P. (2002). Reduction Potentials of SO3 - , SO5 - , and S4O6 3- Radicals in Aqueous Solution. *The Journal of Physical Chemistry A*, *103*(18), 3581–3588.

Daud, W. R. W., Rosli, R. E., Majlan, E. H., Hamid, S. A. A., Mohamed, R., & Husaini, T. (2017). PEM fuel cell system control: A review. *Renewable Energy*, Vol. 113, pp. 620–638.

de Valladares, M.-R. (2017). *Global Trends and outlook for hydrogen*. IEA Hydrogen Technology Collaboration Program (TCP).

Deutsch, T. G., Koval, C. A., & Turner, J. A. (2006). III-V nitride epilayers for photoelectrochemical water splitting: GaPN and GaAsPN. *Journal of Physical Chemistry B*, *110*(50), 25297–25307.

Dias, P., & Mendes, A. (2018). Hydrogen Production from Photoelectrochemical Water Splitting. In *Fuel Cells and Hydrogen Production* (pp. 1003–1053).

Dilger, S., Trottmann, M., & Pokrant, S. (2019). Scaling Up Electrodes for Photoelectrochemical Water Splitting: Fabrication Process and Performance of 40 cm LaTiO2N Photoanodes. *ChemSusChem*, *12*(9), 1931–1938.

Ding, C., Shi, J., Wang, Z., & Li, C. (2017). Photoelectrocatalytic Water Splitting: Significance of Cocatalysts, Electrolyte, and Interfaces. *ACS Catalysis*, *7*(1), 675–688.

Ding, C., Zhou, X., Shi, J., Yan, P., Wang, Z., Liu, G., & Li, C. (2015). Abnormal effects of cations (Li+, Na+, and K+) on photoelectrochemical and electrocatalytic water splitting. *Journal of Physical Chemistry B*, *119*(8), 3560–3566.

Dulian, P. (2016). Solid-State Mechanochemical Syntheses of Perovskites. *Perovskite Materials - Synthesis, Characterisation, Properties, and Applications*, 3–26.

Duret, A., & Grätzel, M. (2005). Visible light-induced water oxidation on mesoscopic α-Fe2O3 films made by ultrasonic spray pyrolysis. *Journal of Physical Chemistry B*,

109(36), 17184–17191.

Eghbali, P., Hassani, A., Sündü, B., & Metin, Ö. (2019). Strontium titanate nanocubes assembled on mesoporous graphitic carbon nitride (SrTiO3/mpg-C3N4): Preparation, characterization and catalytic performance. *Journal of Molecular Liquids*, *290*.

Elzayat, M. (1998). Photoelectrochemical properties of dye sensitized Zr-doped SrTiO3 electrodes. *International Journal of Hydrogen Energy*, *23*(4), 259–266.

Fuentes, S., Muñoz, P., Barraza, N., Chávez-Ángel, E., & Sotomayor Torres, C. M. (2015). Structural characterisation of slightly Fe-doped SrTiO3 grown via a sol–gel hydrothermal synthesis. *Journal of Sol-Gel Science and Technology*.

Fujishima, A., Hashimoto, K., & Watanabe, T. (1999). *TiO2 photocatalysis : fundamentals and applications* (1st ed.). Tokyo Bkc.

Fujishima, A., & Honda, K. (1972). Electrochemical Photolysis of Water at a Semiconductor Electrode. *Nature*, *238*(5358), 38–40.

Gelderman, K., Lee, L., & Donne, S. W. (2007). Flat-Band Potential of a Semiconductor: Using the Mott–Schottky Equation. *Journal of Chemical Education*, *84*(4), 685.

Ginsburg, A., Priel, M., Barad, H. N., Keller, D. A., Borvick, E., Rietwyk, K., … Zaban, A. (2018). Solid state ITO|Au-NPs|TiO2 plasmonic based solar cells. *Solar Energy Materials and Solar Cells*, *179*, 254–259.

Gomes, W. P., & Cardon, F. (1982). Electron energy levels in semiconductor electrochemistry. *Progress in Surface Science*, *12*(2), 155–215.

Gong, M., Li, Y., Wang, H., Liang, Y., Wu, J. Z., Zhou, J., … Dai, H. (2013). An advanced Ni-Fe layered double hydroxide electrocatalyst for water oxidation. *Journal of the American Chemical Society*, *135*(23), 8452–8455.

Griffiths, P. R., & De Haseth, J. A. (2007). *Fourier Transform Infrared Spectrometry* (2nd

ed.). Wiley.

Grimoldi, A. (2015). Deposition and Patterning Techniques for Organic Materials. *Organic Electronics: Principles, Devices and Applications*, pp. 1–42. http://home.deib.polimi.it/sampietr/ESO/programma.html, accessed in June 2019.

Guan, C., & Wang, J. (2016). Recent Development of Advanced Electrode Materials by Atomic Layer Deposition for Electrochemical Energy Storage. *Advanced Science*, *3*(10), 1–23.

Guo, S., Zhao, X., Zhang, W., & Wang, W. (2018). Optimization of electrolyte to significantly improve photoelectrochemical water splitting performance of ZnO nanowire arrays. *Materials Science and Engineering B: Solid-State Materials for Advanced Technology*, *227*, 129–135.

Gupta, R. K., Ghosh, K., & Kahol, P. K. (2009). Fabrication and characterization of NiO/ZnO p-n junctions by pulsed laser deposition. *Physica E: Low-Dimensional Systems and Nanostructures*, *41*(4), 617–620.

Haber, J., Block, J., & Delmon, B. (1995). Manual of methods and procedures for catalyst characterization. *Pure and Applied Chemistry*, *67*(8/9), 1257–1306. http://old.iupac.org/publications/pac/1995/pdf/6708x1257.pdf, accessed in June 2019.

Han, K., Lin, Y. C., Yang, C. M., Jong, R., Mul, G., & Mei, B. (2017). Promoting Photocatalytic Overall Water Splitting by Controlled Magnesium Incorporation in SrTiO3 Photocatalysts. *ChemSusChem*, *10*(22), 4510–4516.

Hanaor, D. A. H., & Sorrell, C. C. (2011). Review of the anatase to rutile phase transformation. *Journal of Materials Science*.

Hara, M., Kondo, T., Komoda, M., Ikeda, S., Kondo, J. N., Domen, K., … Tanaka, A. (1998). Cu2O as a Photocatalyst for Overall Water Splitting under Visible Light Irradiation. *Chemical Communications*, (3), 357–358.

Hara, S., & Irie, H. (2012). Band structure controls of SrTiO3 towards two-step overall water splitting. *Applied Catalysis B: Environmental*, *115–116*, 330–335.

Haynes, W. M. (2016). *Handbook Chemistry and Physics*. CRC Press.

He, Y., Thorne, J. E., Wu, C. H., Ma, P., Du, C., Dong, Q., … Wang, D. (2016). What Limits the Performance of Ta3N5 for Solar Water Splitting? *Chem*, *1*(4), 640–655.

Higashi, M., Domen, K., & Abe, R. (2012). Highly stable water splitting on oxynitride TaON photoanode system under visible light irradiation. *Journal of the American Chemical Society*, *134*(16), 6968–6971.

Hilliard, S. (2016). *Water splitting photoelectrocatalysis : the conception and construction of a photoelectrocatalytic water splitting cell*. Université Pierre et Marie Curie.

Hisatomi, T., Kubota, J., & Domen, K. (2014). Recent advances in semiconductors for photocatalytic and photoelectrochemical water splitting. *Chemical Society Reviews*, *43*(22), 7520–7535.

Hou, T., Zhang, S., Chen, Y., Wang, D., & Cai, W. (2015). Hydrogen production from ethanol reforming: Catalysts and reaction mechanism. *Renewable and Sustainable Energy Reviews*, *44*, 132–148.

Hou, X., Shang, M., Bi, Y., & Jiao, Z. (2016). Synthesis of Ti3+ self-doped SrTiO3/TiO2 hetero-photoanodes with enhanced photoelectrochemical performances under visible light. *Materials Letters*, *176*, 270–273.

Huang, J. R., Tan, X., Yu, T., Zhao, L., & Hu, W. L. (2014). Enhanced photoelectrocatalytic and photoelectrochemical properties by high-reactive TiO2/SrTiO3 hetero-structured nanotubes with dominant {001} facet of anatase TiO2. *Electrochimica Acta*, *146*, 278–287.

Huang, S. T., Lee, W. W., Chang, J. L., Huang, W. S., Chou, S. Y., & Chen, C. C. (2014). Hydrothermal synthesis of SrTiO3 nanocubes: Characterization, photocatalytic

activities, and degradation pathway. *Journal of the Taiwan Institute of Chemical Engineers*, *45*(4), 1927–1936.

Indra, A., Menezes, P. W., & Driess, M. (2018). Photocatalytic and photosensitized water splitting: A plea for well-defined and commonly accepted protocol. *Comptes Rendus Chimie*, *21*(10), 909–915.

Iqbal, M. Z., & Siddique, S. (2018). Recent progress in efficiency of hydrogen evolution process based photoelectrochemical cell. *International Journal of Hydrogen Energy*, pp. 21502–21523.

Iwashina, K., & Kudo, A. (2011). Rh-doped SrTiO3 photocatalyst electrode showing cathodic photocurrent for water splitting under visible-light irradiation. *Journal of the American Chemical Society*, *133*(34), 13272–13275.

Jang, J. S., Joshi, U. A., & Lee, J. S. (2007). Solvothermal synthesis of CdS nanowires for photocatalytic hydrogen and electricity production. *Journal of Physical Chemistry C*, *111*(35), 13280–13287.

Jian, J., Jiang, G., van de Krol, R., Wei, B., & Wang, H. (2018). Recent advances in rational engineering of multinary semiconductors for photoelectrochemical hydrogen generation. *Nano Energy*, *51*, 457–480.

Jiang, C., Moniz, S. J. A., Wang, A., Zhang, T., & Tang, J. (2017). Photoelectrochemical devices for solar water splitting-materials and challenges. *Chemical Society Reviews*, *46*(15), 4645–4660.

Jing, D., Guo, L., Zhao, L., Zhang, X. X., Liu, H., Li, M., … Guo, P. (2010). Efficient solar hydrogen production by photocatalytic water splitting: From fundamental study to pilot demonstration. *International Journal of Hydrogen Energy*, *35*(13), 7087–7097.

Jing, J., Chen, Z., Bu, Y., Sun, M., Zheng, W., & Li, W. (2019). Significantly enhanced photoelectrochemical cathodic protection performance of hydrogen treated Cr-doped SrTiO3 by Cr 6+ reduction and oxygen vacancy modification. *Electrochimica Acta*,

304, 386–395.

Kalanoor, B. S., Seo, H., & Kalanur, S. S. (2018). Recent developments in photoelectrochemical water-splitting using WO3/BiVO4 heterojunction photoanode: A review. *Materials Science for Energy Technologies*, *1*(1), 49–62.

Kalyanasundaram, K. (2013). Photochemical applications of solar energy: Photocatalysis and photodecomposition of water. In *Photochemistry* (Vol. 41).

Kalyani, V., Vasile, B. S., Ianculescu, A., Buscaglia, M. T., Buscaglia, V., & Nanni, P. (2012). Hydrothermal synthesis of SrTiO3 mesocrystals: Single crystal to mesocrystal transformation induced by topochemical reactions. *Crystal Growth and Design*, *12*(9), 4450–4456.

Kanan, M. W., & Nocera, D. G. (2008). ChemInform Abstract: In situ Formation of an Oxygen-Evolving Catalyst in Neutral Water Containing Phosphate and Co 2+ . *ChemInform*, *39*(47), 1072–1076.

Kang, D., Kim, T. W., Kubota, S. R., Cardiel, A. C., Cha, H. G., & Choi, K. S. (2015). Electrochemical Synthesis of Photoelectrodes and Catalysts for Use in Solar Water Splitting. *Chemical Reviews*, *115*(23), 12839–12887.

Kelly, J. J., Kooij, E. S., & Meulenkamp, E. A. (1999). Luminescence studies of semiconductor electrodes. *Electrochimica Acta*, *45*(4–5), 561–574.

Khaselev, O., Bansal, A., & Turner, J. A. (2001). High-efficiency integrated multijunction photovoltaic/electrolysis systems for hydrogen production. *International Journal of Hydrogen Energy*, *26*(2), 127–132.

Khemakhem, O., Bennaceur, J., Cheikhrouhou-Koubaa, W., Koubaa, M., Chtourou, R., & Cheikhrouhou, A. (2017). Enhanced photoelectrochemical photocatalytic activities in hydrothermal synthesized SrTiO3/TiO2 heterostructure thin films. *Journal of Alloys and Compounds*, *696*, 682–687.

Kim, E. S., Nishimura, N., Magesh, G., Kim, J. Y., Jang, J. W., Jun, H., … Lee, J. S. (2013). Fabrication of CaFe2O4/TaON heterojunction photoanode for photoelectrochemical water oxidation. *Journal of the American Chemical Society*, *135*(14), 5375–5383.

Kitano, M., Takeuchi, M., Matsuoka, M., Thomas, J. M., & Anpo, M. (2007). Photocatalytic water splitting using Pt-loaded visible light-responsive TiO2 thin film photocatalysts. *Catalysis Today*, *120*(2), 133–138.

Kment, S., Riboni, F., Pausova, S., Wang, L., Wang, L., Han, H., … Zboril, R. (2017). Photoanodes based on TiO2 and α-Fe2O3 for solar water splitting-superior role of 1D nanoarchitectures and of combined heterostructures. *Chemical Society Reviews*, *46*(12), 3716–3769.

Kolodziejczak-Radzimska, A., & Jesionowski, T. (2014). Zinc oxide-from synthesis to application: A review. *Materials*, *7*(4), 2833–2881.

Konta, R., Ishii, T., Kato, H., & Kudo, A. (2004). Photocatalytic activities of noble metal ion doped SrTiO3 under visible light irradiation. *Journal of Physical Chemistry B*, *108*(26), 8992–8995.

Koroneos, C., Dompros, A., & Roumbas, G. (2008). Hydrogen production via biomass gasification - A life cycle assessment approach. *Chemical Engineering and Processing: Process Intensification*, *47*(8), 1267–1274.

Krol, R. Van de. (2012). Principles of PEC. In *Photoelectrochemical Hydrogen Production*.

Krol, R. Van De, & Grätzel, M. (2012). Photoelectrochemical Hydrogen Production. In *New York: Springer*.

Kuang, Y., Jia, Q., Nishiyama, H., Yamada, T., Kudo, A., & Domen, K. (2016). A front-illuminated nanostructured transparent BiVO4 photoanode for >2% efficient water splitting. *Advanced Energy Materials*, *6*(2), 2–8.

Kuang, Y., Yamada, T., & Domen, K. (2017). Surface and Interface Engineering for

Photoelectrochemical Water Oxidation. *Joule, 1*(2), 290–305.

Kudo, A., Omori, K., & Kato, H. (1999). A novel aqueous process for preparation of crystal form-controlled and highly crystalline BiVO4 powder from layered vanadates at room temperature and its photocatalytic and photophysical properties. *Journal of the American Chemical Society*, *121*(49), 11459–11467.

Kumari, S., Chaudhary, Y. S., Agnihotry, S. A., Tripathi, C., Verma, A., Chauhan, D., … Satsangi, V. R. (2007). A photoelectrochemical study of nanostructured Cd-doped titanium oxide. *International Journal of Hydrogen Energy*, *32*(9), 1299–1302.

Kuo, Y., & Klabunde, K. J. (2012). Hydrogen generation from water/methanol under visible light using aerogel prepared strontium titanate (SrTiO3) nanomaterials doped with ruthenium and rhodium metals. *Nanotechnology*, *23*(29).

Kurnia, F., Ng, Y. H., Amal, R., Valanoor, N., & Hart, J. N. (2016). Defect engineering of ZnS thin films for photoelectrochemical water-splitting under visible light. *Solar Energy Materials and Solar Cells*, *153*, 179–185.

Lana-Villarreal, T., Straboni, A., Pichon, L., & Alonso-Vante, N. (2007). Photoelectrochemical characterization of p-type silicon electrodes covered with tunnelling nitride dielectric films. *Thin Solid Films*, *515*(18), 7376–7381.

Lenser, C. (2013). *Investigation of Resistive Switching in Fe-doped SrTiO3 by Advanced Spectroscopy*. http://d-nb.info/985390468/34, accessed in June 2019.

Li, H., Zhu, J., Wu, Q., Zhuang, J., Guo, H., Ma, Z., & Ye, Y. (2017). Enhanced photovoltaic properties of PbTiO3-based ferroelectric thin films prepared by a sol-gel process. *Ceramics International*, *43*(16), 13063–13068.

Li, Z., Luo, W., Zhang, M., Feng, J., & Zou, Z. (2013). Photoelectrochemical cells for solar hydrogen production: Current state of promising photoelectrodes, methods to improve their properties, and outlook. *Energy and Environmental Science*, *6*(2), 347–370.

Liang, L., Li, K., Lv, K., Ho, W., & Duan, Y. (2017). Highly photoreactive TiO2 hollow microspheres with super thermal stability for acetone oxidation. *Cuihua Xuebao/Chinese Journal of Catalysis*, *38*(12), 2085–2093.

Lianos, P. (2011). Production of electricity and hydrogen by photocatalytic degradation of organic wastes in a photoelectrochemical cell. The concept of the Photofuelcell: A review of a re-emerging research field. *Journal of Hazardous Materials*, *185*(2–3), 575–590.

Lichterman, M. F., Shaner, M. R., Handler, S. G., Brunschwig, B. S., Gray, H. B., Lewis, N. S., & Spurgeon, J. M. (2013). Enhanced stability and activity for water oxidation in alkaline media with Bismuth Vanadate photoelectrodes modified with a cobalt oxide catalytic layer produced by atomic layer deposition. *Journal of Physical Chemistry Letters*, *4*(23), 4188–4191.

Lin, Y., Kapadia, R., Yang, J., Zheng, M., Chen, K., Hettick, M., … Javey, A. (2015). Role of TiO2 surface passivation on improving the performance of P-InP photocathodes. *Journal of Physical Chemistry C*, *119*(5), 2308–2313.

Liu, J., Sun, Y., Li, Z., Li, S., & Zhao, J. (2011). Photocatalytic hydrogen production from water/methanol solutions over highly ordered Ag-SrTiO3 nanotube arrays. *International Journal of Hydrogen Energy*, *36*(10), 5811–5816.

Liu, L., Yellinek, S., Valdinger, I., Donval, A., & Mandler, D. (2015). Important Implications of the Electrochemical Reduction of ITO. *Electrochimica Acta*, *176*, 1374–1381.

Liu, X., Wang, F., & Wang, Q. (2012). Nanostructure-based WO3photoanodes for photoelectrochemical water splitting. *Physical Chemistry Chemical Physics*, *14*(22), 7894–7911.

Liu, Y., Xie, L., Li, Y. Y., Yang, R., Qu, J., Li, Y. Y., & Li, X. (2008). Synthesis and high photocatalytic hydrogen production of SrTiO3 nanoparticles from water splitting under UV irradiation. *Journal of Power Sources*, *183*(2), 701–707.

Liu, Zhaoyang, Sun, D. D., Guo, P., & Leckie, J. O. (2007). One-step fabrication and high photocatalytic activity of porous TiO2 hollow aggregates by using a low-temperature hydrothermal method without templates. *Chemistry - A European Journal*, *13*(6), 1851–1855.

Liu, Zhendong, & Ma, Z. (2019). Ag-SrTiO3/TiO2 composite nanostructures with enhanced photocatalytic activity. *Materials Research Bulletin*, *118*.

Lobacheva, O., Chavarha, M., Yiu, Y. M., Sham, T. K., & Goncharova, L. V. (2014). The local structure and ferromagnetism in Fe-implanted SrTiO3 single crystals. *Journal of Applied Physics*.

Lopes, T., Andrade, L., Ribeiro, H. A., & Mendes, A. (2010). Characterization of photoelectrochemical cells for water splitting by electrochemical impedance spectroscopy. *International Journal of Hydrogen Energy*, *35*(20), 11601–11608.

Lopes, T., Dias, P., Andrade, L., & Mendes, A. (2014). An innovative photoelectrochemical lab device for solar water splitting. *Solar Energy Materials and Solar Cells*, *128*, 399–410.

Lü, X., Ding, S., Xie, Y., & Huang, F. (2011). Non-aqueous preparation of high-crystallinity hierarchical TiO2 hollow spheres with excellent photocatalytic efficiency. *European Journal of Inorganic Chemistry*, (18), 2879–2883.

Luo, X. L., He, G. L., Fang, Y. P., & Xu, Y. H. (2018). Nickel sulfide/graphitic carbon nitride/strontium titanate (NiS/g-C3N4/SrTiO3) composites with significantly enhanced photocatalytic hydrogen production activity. *Journal of Colloid and Interface Science*, *518*, 184–191.

Luttrell, T., Halpegamage, S., Tao, J., Kramer, A., Sutter, E., & Batzill, M. (2015). Why is anatase a better photocatalyst than rutile? - Model studies on epitaxial TiO2 films. *Scientific Reports*, *4*, 1–8.

Maeda, K. (2013). Z-scheme water splitting using two different semiconductor

photocatalysts. *ACS Catalysis*, *3*(7), 1486–1503.

Magesh, G., Kim, E. S., Kang, H. J., Banu, M., Kim, J. H. J. Y., Kim, J. H. J. Y., & Lee, J. S. (2014). A versatile photoanode-driven photoelectrochemical system for conversion of CO2 to fuels with high faradaic efficiencies at low bias potentials. *Journal of Materials Chemistry A*, *2*(7), 2044–2049.

Matsumoto, H. (2005). Application of Ionic Liquids to Photoelectrochemical Cells. In *Electrochemical Aspects of Ionic Liquids* (pp. 187–198).

McEvoy, A. J. (2011). *Photoelectrochemical Solar Cells*. Wiley

Memming, R. (2001). *Semiconductor Electrochemistry*. Wiley-VCH, Weinheim.

Mennig, M., Scmidt, H., & Berni, A. (2004). Doctor Blade. *Sol-Gel Technologies for Glass Producers and Users*, pp. 89–92.

Miller, E. L., Rocheleau, R. E., & Deng, X. M. (2003). Design considerations for a hybrid amorphous silicon/photoelectrochemical multijunction cell for hydrogen production. *International Journal of Hydrogen Energy*, *28*(6), 615–623.

Minggu, L. J., Wan Daud, W. R., & Kassim, M. B. (2010). An overview of photocells and photoreactors for photoelectrochemical water splitting. *International Journal of Hydrogen Energy*, *35*(11), 5233–5244.

Mishra, P. R., Shukla, P. K., Singh, A. K., & Srivastava, O. N. (2003). Investigation and optimization of nanostructured TiO2 photoelectrode in regard to hydrogen production through photoelectrochemical process. *International Journal of Hydrogen Energy*, *28*(10), 1089–1094.

Moniruddin, M., Kudaibergenov, S., & Nuraje, N. (2016). Hierarchical nanoheterostructures for water splitting. In *Green Chemistry* (pp. 142–167).

Monroy, E., Omnès, F., & Calle, F. (2003). Wide-bandgap semiconductor ultraviolet

photodetectors. *Semiconductor Science and Technology*, *18*(4).

Moreira, M. L., Volanti, D. P., Orlandi, M. O., Longo, E., Varela, J. A., Mambrini, G. P., … Paiva-Santos, C. O. (2008). Hydrothermal Microwave: A New Route to Obtain Photoluminescent Crystalline BaTiO3 Nanoparticles. *Chemistry of Materials*, *20*(16), 5381–5387.

Mourão, H. A. J. L., Lopes, O. F., Ribeiro, C., & Mastelaro, V. R. (2015). Rapid hydrothermal synthesis and pH-dependent photocatalysis of strontium titanate microspheres. *Materials Science in Semiconductor Processing*, *30*, 651–657.

Myamlin, V. A., & Pleskov, Y. V. (1967). *Electrochemistry of Semiconductors* (1st ed.).

Navarro, Y. R. M., Consuelo, Á. G. M., del Valle, F., Villoria de la Mano, J. A., & Fierro, J. L. G. (2009). Water splitting on semiconductor catalysts under visiblelight irradiation. *ChemSusChem*, *2*(6), 471–485.

Neumann, B., Bogdanoff, P., & Tributsch, H. (2009). TiO2-protected photoelectrochemical tandem Cu(In,Ga)Se2 thin film membrane for light-induced water splitting and hydrogen evolution. *Journal of Physical Chemistry C*, *113*(49), 20980–20989.

Nowotny, J., Bak, T., Nowotny, M. K., & Sheppard, L. R. (2007). Titanium dioxide for solar-hydrogen I. Functional properties. *International Journal of Hydrogen Energy*, *32*(14), 2609–2629.

Nozik, A. J. (1976). P-n photoelectrolysis cells. *Applied Physics Letters*, *29*(3), 150–153.

Nozik, A. J. (1980). Photoelectrochemical cells. *Philosophical Transactions of the Royal Society of London. Series A, Mathematical and Physical Sciences*, *295*(1414), 453–470. https://www.jstor.org/stable/36608, accessed in June 2019.

Obregón, S., & Colón, G. (2014). Improved H2 production of Pt-TiO2/g-C3N4-MnOx composites by an efficient handling of photogenerated charge pairs. *Applied Catalysis B: Environmental*, *144*, 775–782.

Ohno, H. (2005). Electrochemical Aspects of Ionic Liquids. In *Electrochemical Aspects of Ionic Liquids*.

Ohtani, B. (2010). Photocatalysis A to Z-What we know and what we do not know in a scientific sense. *Journal of Photochemistry and Photobiology C: Photochemistry Reviews*, *11*(4), 157–178.

Ong, C. K. (2013). *Design and performance of photo-electrochemical reactors with Fe2O3 photo-anodes for water splitting* (Imperial College London). https://spiral.imperial.ac.uk/handle/10044/1/12636, accessed in June 2019.

Osterloh, F. E. (2017). *Inorganic Materials as Catalysts for Photochemical Splitting of Water Partners*. *0*(August 2007), 2007–2008.

Öztaş, M., Bedir, M., Necmeddin Yazici, A., Vural Kafadar, E., & Toktamiş, H. (2006). Characterization of copper-doped sprayed ZnS thin films. *Physica B: Condensed Matter*, *381*(1–2), 40–46.

Paracchino, A., Laporte, V., Sivula, K., Grätzel, M., & Thimsen, E. (2011). Highly active oxide photocathode for photoelectrochemical water reduction. *Nature Materials*, *10*(6), 456–461.

Pareek, A., Gopalakrishnan, A., & Borse, P. H. (2016). Efficiency and stability aspects of CdS photoanode for solar hydrogen generation technology. *Journal of Physics: Conference Series*, *755*(1).

Park, D. W., Cañas, N. A., Wagner, N., & Friedrich, K. A. (2016). Novel solvent-free direct coating process for battery electrodes and their electrochemical performance. *Journal of Power Sources*, *306*, 758–763.

Patil, P. S. (1999). Versatility of chemical spray pyrolysis technique. *Materials Chemistry and Physics*, *59*(3), 185–198.

Paulauskas, I. E., Katz, J. E., Jellison, G. E., Lewis, N. S., & Boatner, L. A. (2008).

Photoelectrochemical studies of semiconducting photoanodes for hydrogen production via water dissociation. *Thin Solid Films*, *516*(22), 8175–8178.

Peerakiatkhajohn, P., Yun, J.-H., Wang, S., & Wang, L. (2016). Review of recent progress in unassisted photoelectrochemical water splitting: from material modification to configuration design. *Journal of Photonics for Energy*, *7*(1), 012006.

Peter, L. M. (2016). Fundamental Aspects of Photocatalysis. In *Photocatalysis:Fundamentals & Perpectives*.

Petit, S., & Madejova, J. (2013). Fourier Transform Infrared Spectroscopy. In *Developments in Clay Science* (Vol. 5, pp. 213–231).

Phoon, B. L., Lai, C. W., Juan, J. C., Show, P. L., & Chen, W. H. (2019). A review of synthesis and morphology of SrTiO3 for energy and other applications. *International Journal of Energy Research*, (February), 1–24.

Phoon, B. L., Lai, C. W., Pan, G. T., Yang, T. C. K., & Juan, J. C. (2018). One-pot hydrothermal synthesis of strontium titanate nanoparticles photoelectrode using electrophoretic deposition for enhancing photoelectrochemical water splitting. *Ceramics International*, *44*(8), 9923–9933.

Pihosh, Y., Turkevych, I., Mawatari, K., Uemura, J., Kazoe, Y., Kosar, S., … Kitamori, T. (2015). Photocatalytic generation of hydrogen by core-shell WO3/BiVO4 nanorods with ultimate water splitting efficiency. *Scientific Reports*, *5*(June), 1–2.

Pinheiro, A. N., Firmiano, E. G. S., Rabelo, A. C., Dalmaschio, C. J., & Leite, E. R. (2014). Revisiting SrTiO3 as a photoanode for water splitting: Development of thin films with enhanced charge separation under standard solar irradiation. *RSC Advances*, *4*(4), 2029–2036.

Qu, Y., Zhou, W., & Fu, H. (2014). Porous cobalt titanate nanorod: A new candidate for visible light-driven photocatalytic water oxidation. *ChemCatChem*, *6*(1), 265–270.

Rajeshwar, K. (2007). Fundamentals of Semiconductor Electrochemistry and Photoelectrochemistry. *Encyclopedia of Electrochemistry*.

Ran, J., Zhang, J., Yu, J., Jaroniec, M., & Qiao, S. Z. (2014). Earth-abundant cocatalysts for semiconductor-based photocatalytic water splitting. *Chemical Society Reviews*, *43*(22), 7787–7812.

Rao, C. N. R., & Dey, S. (2017). Solar thermochemical splitting of water to generate hydrogen. *Proceedings of the National Academy of Sciences*, *114*(51), 13385–13393.

Rashid, M., Al Mesfer, M. K., Naseem, H., & Danish, M. (2015). Hydrogen Production by Water Electrolysis: A Review of Alkaline Water Electrolysis, PEM Water Electrolysis and High Temperature Water Electrolysis. *International Journal of Engineering and Advanced Technology (IJEAT)*, *4*(3), 80–93.

Read, C. G., Park, Y., & Choi, K. S. (2012). Electrochemical synthesis of p-type CuFeO 2 electrodes for use in a photoelectrochemical cell. *Journal of Physical Chemistry Letters*, *3*(14), 1872–1876.

Ren, K., Gan, Y. X., Nikolaidis, E., Sofyani, S. Al, & Zhang, L. (2013). Electrolyte Concentration Effect of a Photoelectrochemical Cell Consisting of TiO2 Nanotube Anode . *ISRN Materials Science*, *2013*, 1–7.

Rongé, J., Deng, S., Pulinthanathu Sree, S., Bosserez, T., Verbruggen, S. W., Kumar Singh, N., … Martens, J. A. (2014). Air-based photoelectrochemical cell capturing water molecules from ambient air for hydrogen production. *RSC Advances*, *4*(55), 29286–29290.

Said, N. D. M., Sahdan, M. Z., Ahmad, A., Senain, I., Bakri, A. S., Abdullah, S. A., & Rahim, M. S. (2017). Effects of Al doping on structural, morphology, electrical and optical properties of TiO2 thin film. *AIP Conference Proceedings*, *1788*(January).

Saito, R., Miseki, Y., & Sayama, K. (2012). Highly efficient photoelectrochemical water splitting using a thin film photoanode of BiVO4/SnO2/WO3 multi-composite in a

carbonate electrolyte. *Chemical Communications*, *48*(32), 3833–3835.

Sakata, Y., Miyoshi, Y., Maeda, T., Ishikiriyama, K., Yamazaki, Y., Imamura, H., … Domen, K. (2016). Photocatalytic property of metal ion added SrTiO3 to Overall H2O splitting. *Applied Catalysis A: General*, *521*, 227–232.

Sanwald, K. E., Berto, T. F., Jentys, A., Camaioni, D. M., Gutiérrez, O. Y., & Lercher, J. A. (2018). Kinetic Coupling of Water Splitting and Photoreforming on SrTiO3 -Based Photocatalysts. *ACS Catalysis*, *8*(4), 2902–2913.

Schields, P. J. (2004). Bragg's Law and Diffraction: How waves reveal the atomic structure of crystals. http://skuld.bmsc.washington.edu/~merritt/bc530/bragg/, accessed in July 2019.

Schoonen, M. A. A. A., & Xu, Y. (2000). The absolute energy positions of conduction and valence bands of selected semiconducting minerals. *American Mineralogist*, *85*(3–4), 543–556.

Schubert, D. W., & Dunkel, T. (2003). Spin coating from a molecular point of view: Its concentration regimes, influence of molar mass and distribution. *Materials Research Innovations*, *7*(5), 314–321.

Schwarz, J. A., Contescu, C., & Contescu, A. (1995). Methods for Preparation of Catalytic Materials. *Chemical Reviews*, *95*(3), 477–510.

Seabold, J. A., & Choi, K. S. (2011). Effect of a cobalt-based oxygen evolution catalyst on the stability and the selectivity of photo-oxidation reactions of a WO3 photoanode. *Chemistry of Materials*, *23*(5), 1105–1112.

Seifert, K., Waligorska, M., & Laniecki, M. (2010). Hydrogen generation in photobiological process from dairy wastewater. *International Journal of Hydrogen Energy*, *35*(18), 9624–9629.

Sharma, G. P., Upadhyay, A. P., Behara, D. K., Sivakumar, S., & Pala, R. G. S. (2017).

Fundamental aspect of photoelectrochemical water splitting. *The Water-Food-Energy Nexus: Processes, Technologies, and Challenges*, (August), 677–689.

Shen, S., Chen, J., Wang, M., Sheng, X., Chen, X., Feng, X., & Mao, S. S. (2018). Titanium dioxide nanostructures for photoelectrochemical applications. *Progress in Materials Science*, Vol. 98, pp. 299–385.

Shi, X., Cai, L., Ma, M., Zheng, X., & Park, J. H. (2015). General Characterization Methods for Photoelectrochemical Cells for Solar Water Splitting. *ChemSusChem*, *8*(19), 3192–3203.

Shi, X., Choi, I. Y., Zhang, K., Kwon, J., Kim, D. Y., Lee, J. K., … Park, J. H. (2014). Efficient photoelectrochemical hydrogen production from bismuth vanadate-decorated tungsten trioxide helix nanostructures. *Nature Communications*, *5*, 1–8.

Sin, N. D., Fuad Kamel, M., Alip, R. I., Mohamad, Z., & Rusop, M. (2011). The electrical characteristics of aluminium doped zinc oxide thin film for humidity sensor applications. *Advances in Materials Science and Engineering*.

Sivula, K. (2013). Metal oxide photoelectrodes for solar fuel production, surface traps, and catalysis. *Journal of Physical Chemistry Letters*, *4*(10), 1624–1633.

Sivula, K., & Grätzel, M. (2013). Tandem Photoelectrochemical Cells for Water Splitting. In *Photoelectrochemical Water Splitting: Materials, Processes and Architectures* (pp. 83–108).

Sivula, K., Le Formal, F., & Grätzel, M. (2011). Solar water splitting: progress using hematite (α-Fe2O3) photoelectrodes. *ChemSusChem*, *4*(4), 432–449.

Souza, A. E., Santos, G. T. A., Barra, B. C., MacEdo, W. D., Teixeira, S. R., Santos, C. M., … Longo, E. (2012). Photoluminescence of SrTiO3 : Influence of particle size and morphology. *Crystal Growth and Design*, *12*(11), 5671–5679.

Stavrides, A., Kunrath, A., Hu, J., Treglio, R., Feldman, A., Marsen, B., … Madan, A.

(2006). Use of amorphous silicon tandem junction solar cells for hydrogen production in a photoelectrochemical cell. *Solar Hydrogen and Nanotechnology*, *6340*(September 2006), 63400K.

Su, Z., & Zhou, W. (2011). Formation, morphology control and applications of anodic TiO2 nanotube arrays. *Journal of Materials Chemistry*, *21*(25), 8955–8970.

Sulaeman, U., Yin, S., & Sato, T. (2011). Effect of Sr/Ti ratio on the photocatalytic properties of SrTiO3. *IOP Conference Series: Materials Science and Engineering*.

Sun, W., Wang, D., Rahman, Z. U., Wei, N., & Chen, S. (2017). 3D hierarchical WO3grown on TiO2nanotube arrays and their photoelectrochemical performance for water splitting. *Journal of Alloys and Compounds*, *695*, 2154–2159.

Swapp, S. (2017). Scanning Electron Microscopy (SEM). https://serc.carleton.edu/ research_education/geochemsheets/techniques/SEM.html, accessed in July 2019.

Tahir, A. A., Wijayantha, K. G. U., Mazhar, M., & McKee, V. (2010). ZnFe2O4 thin films from a single source precursor by aerosol assisted chemical vapour deposition. *Thin Solid Films*, *518*(14), 3664–3668.

Tan, H., Zhao, Z., Zhu, W. Bin, Coker, E. N., Li, B., Zheng, M., … Sun, Z. (2014). Oxygen vacancy enhanced photocatalytic activity of pervoskite SrTiO3. *ACS Applied Materials and Interfaces*, *6*(21), 19184–19190.

Tayyebi, A., Soltani, T., & Lee, B. K. (2019). Effect of pH on photocatalytic and photoelectrochemical (PEC) properties of monoclinic bismuth vanadate. *Journal of Colloid and Interface Science*, *534*, 37–46.

Troyan, P., Zhidik, Y., & Zhidik, E. (2018). Investigation of temperature stability of ITO films characteristics. *MATEC Web of Conferences*, *143*, 03010.

Tryk, D. A., Fujishima, A., & Honda, K. (2000). Recent topics in photoelectrochemistry: Achievements and future prospects. *Electrochimica Acta*, *45*(15–16), 2363–2376.

Tseng, T. K., Lin, Y. S., Chen, Y. J., & Chu, H. (2010). A review of photocatalysts prepared by sol-gel method for VOCs removal. *International Journal of Molecular Sciences*, *11*(6), 2336–2361.

United States Department of Energy. (2015). *Hydrogen Production* (Vol. 11007, pp. 1–44). Vol. 11007, pp. 1–44.

Visuttipitukul, P., Sooksaen, P., & Yongvanich, N. (2013). Sol-gel synthesis of SrTiO3 nanoparticles using acetic acid as a chelating agent. *Ferroelectrics*, *457*(1), 82–88.

Walter, M. G., Warren, E. L., McKone, J. R., Boettcher, S. W., Mi, Q., Santori, E. A., & Lewis, N. S. (2010). Solar Water Splitting Cells. *Chemical Reviews*, *110*(11), 6446–6473.

Wang, B., Shen, S., & Mao, S. S. (2017). Black TiO2 for solar hydrogen conversion. *Journal of Materiomics*, *3*(2), 96–111.

Wang, Gongming, Wang, H., Ling, Y., Tang, Y., Yang, X., Fitzmorris, R. C., … Li, Y. (2011). Hydrogen-treated TiO2 nanowire arrays for photoelectrochemical water splitting. *Nano Letters*, *11*(7), 3026–3033.

Wang, Gui-yun, Qin, Y., Chen, J., & Wang, Y. (2010). Influence of Zn doping on the photocatalytic property of SrTiO3. *Journal of Fuel Chemistry and Technology*, *38*(4), 502–507.

Wang, J., Chen, R., Xiang, L., & Komarneni, S. (2018). Synthesis, properties and applications of ZnO nanomaterials with oxygen vacancies: A review. *Ceramics International*, *44*(7), 7357–7377.

Wang, Q., An, N., Bai, Y., Hang, H., Li, J., Lu, X., … Lei, Z. (2013). High photocatalytic hydrogen production from methanol aqueous solution using the photocatalysts CuS/TiO2. *International Journal of Hydrogen Energy*, *38*(25), 10739–10745.

Wang, W., Zhang, W., Hao, C., Wu, F., Liang, Y., Shi, H., … Hua, Y. (2016). Enhanced photoelectrochemical activity and photocatalytic water oxidation of NiO nanoparticle-decorated SrTiO3 nanocube heterostructures: Interaction, interfacial charge transfer and enhanced mechanism. *Solar Energy Materials and Solar Cells*, *152*, 1–9.

Wang, X., Shih, K., & Li, X. Y. (2010). Photocatalytic hydrogen generation from water under visible light using core/shell nano-catalysts. *Water Science and Technology*, *61*(9), 2303–2308.

Wang, Y., He, Y., Lai, Q., & Fan, M. (2014). Review of the progress in preparing nano TiO2: An important environmental engineering material. *Journal of Environmental Sciences (China)*, Vol. 26, pp. 2139–2177.

Wang, Z., Cao, D., Wen, L., Xu, R., Obergfell, M., Mi, Y., … Lei, Y. (2016). Manipulation of charge transfer and transport in plasmonic-ferroelectric hybrids for photoelectrochemical applications. *Nature Communications*, *7*, 1–8.

Watanabe, T., Fujishima, A., & Honda, K. (2006). Photoelectrochemical Reactions at SrTiO3 Single Crystal Electrode. *Bulletin of the Chemical Society of Japan*, *49*(2), 355–358.

Wender, H., Feil, A. F., Diaz, L. B., Ribeiro, C. S., Machado, G. J., Migowski, P., … Teixeira, S. R. (2011). Self-organized TiO2 nanotube arrays: Synthesis by anodization in an ionic liquid and assessment of photocatalytic properties. *ACS Applied Materials and Interfaces*, *3*(4), 1359–1365.

Wood, D. L., & Tauc, J. (1972). Weak absorption tails in amorphous semiconductors. *Physical Review B*, *5*(8), 3144–3151.

Wu, Y., & He, T. (2018). Ag loading induced visible light photocatalytic activity for pervoskite SrTiO3 nanofibers. *Spectrochimica Acta - Part A: Molecular and Biomolecular Spectroscopy*, *199*, 283–289.

Wu, Z., Su, Y., Yu, J., Xiao, W., Sun, L., & Lin, C. (2015). Enhanced photoelectrocatalytic

hydrogen production activity of SrTiO3-TiO2 hetero-nanoparticle modified TiO2 nanotube arrays. *International Journal of Hydrogen Energy*, *40*(31), 9704–9712.

Wysmulek, K., Sar, J., Osewski, P., Orlinski, K., Kolodziejak, K., Trenczek-Zajac, A., … Pawlak, D. A. (2017). A SrTiO3-TiO2 eutectic composite as a stable photoanode material for photoelectrochemical hydrogen production. *Applied Catalysis B: Environmental*, *206*, 538–546.

Xie, T. H., Sun, X., & Lin, J. (2008). Enhanced photocatalytic degradation of RhB driven by visible light-induced MMCT of Ti(IV)-O-Fe(II) formed in Fe-doped SrTiO3. *Journal of Physical Chemistry C*.

Xie, Y., Zhao, Q., Zhao, X. J., & Li, Y. (2007). Low temperature preparation and characterization of N-doped and N-S-codoped TiO2 by sol-gel route. *Catalysis Letters*, *118*(3–4), 231–237.

Xu, J., Wei, Y., Huang, Y., Wang, J., Zheng, X., Sun, Z., … Wu, J. (2014). Solvothermal synthesis nitrogen doped SrTiO3 with high visible light photocatalytic activity. *Ceramics International*, *40*(7 PART B), 10583–10591.

Yahya, M. S., & Ismail, M. (2018). Synergistic catalytic effect of SrTiO3 and Ni on the hydrogen storage properties of MgH2. *International Journal of Hydrogen Energy*, *43*(12), 6244–6255.

Yan, S., Liu, T., Zhang, Y., Sun, D., Li, X., Xie, G., … Xu, L. (2017). Enhanced photoelectrochemical performance of hydrogen-treated SrTiO3/TiO2 nanotube arrays heterojunction composite. *Journal of Electroanalytical Chemistry*, *807*, 213–219.

Yang, J., Wang, D., Han, H., & Li, C. (2013). Roles of cocatalysts in photocatalysis and photoelectrocatalysis. *Accounts of Chemical Research*, *46*(8), 1900–1909.

Yang, L. X., Luo, S. L., Cai, Q. Y., & Yao, S. Z. (2010). A review on TiO2 nanotube arrays: Fabrication, properties, and sensing applications. *Chinese Science Bulletin*, *55*(4), 331–338.

Yang, Yang, Lee, K., Kado, Y., & Schmuki, P. (2012). Nb-doping of TiO2/SrTiO3 nanotubular heterostructures for enhanced photocatalytic water splitting. *Electrochemistry Communications*, *17*(1), 56–59.

Yang, Ying, Han, J., Ning, X., Su, J., Shi, J., Cao, W., & Xu, W. (2016). Photoelectrochemical stability improvement of cuprous oxide (Cu2O) thin films in aqueous solution. *International Journal of Energy Research*, *40*(1), 112–123.

Yin, X. L., Li, L. L., Li, D. C., Wei, D. H., Hu, C. C., & Dou, J. M. (2019). Room temperature synthesis of CdS/SrTiO3 nanodots-on-nanocubes for efficient photocatalytic H2 evolution from water. *Journal of Colloid and Interface Science*, *536*, 694–700.

Yoon, K. H., Choi, W. J., & Kang, D. H. (2000). Photoelectrochemical properties of copper oxide thin films coated on an n-Si substrate. *Thin Solid Films*, *372*(1), 250–256.

You, Y., Zhang, S., Wan, L., & Xu, D. (2012). Preparation of continuous TiO2 fibers by sol-gel method and its photocatalytic degradation on formaldehyde. *Applied Surface Science*, *258*(8), 3469–3474.

Yourey, J. E., & Bartlett, B. M. (2011). Electrochemical deposition and photoelectrochemistry of CuWO4, a promising photoanode for water oxidation. *Journal of Materials Chemistry*, *21*(21), 7651–7660.

Yu, H., Ouyang, S., Yan, S., Li, Z., Yu, T., & Zou, Z. (2011). Sol-gel hydrothermal synthesis of visible-light-driven Cr-doped SrTiO3 for efficient hydrogen production. *Journal of Materials Chemistry*, *21*(30), 11347–11351.

Yu, H., Wang, J., Yan, S., Yu, T., & Zou, Z. (2014). Elements doping to expand the light response of SrTiO3. *Journal of Photochemistry and Photobiology A: Chemistry*, *275*, 65–71.

Yu, S. C., Huang, C. W., Liao, C. H., Wu, J. C. S., Chang, S. T., & Chen, K. H. (2011). A novel membrane reactor for separating hydrogen and oxygen in photocatalytic water splitting. *Journal of Membrane Science*, *382*(1–2), 291–299.

Zhang, C., Yu, K., Feng, Y., Chang, Y., Yang, T., Xuan, Y., … Liu, S. (2017). Novel 3DOM-SrTiO3/Ag/Ag3PO4 ternary Z-scheme photocatalysts with remarkably improved activity and durability for contaminant degradation. *Applied Catalysis B: Environmental*, *210*, 77–87.

Zhang, J., Tang, C., & Bang, J. H. (2010). CdS/TiO2 -SrTiO3 heterostructure nanotube arrays for improved solar energy conversion efficiency. *Electrochemistry Communications*, *12*(8), 1124–1128.

Zhang, Y., Zhong, L., & Duan, D. (2015). Single-step hydrothermal synthesis of strontium titanate nanoparticles from crystalline anatase titanium dioxide. *Ceramics International*, *41*(10), 13516–13524.

Zhao, W., Liu, N., Wang, H., & Mao, L. (2017). Sacrificial template synthesis of core-shell SrTiO3/TiO2 heterostructured microspheres photocatalyst. *Ceramics International*, *43*(6), 4807–4813.

Zhong, Q. dong, Wang, C., Lu, X. gang, & Zhou, G. zhi. (2008). Semiconducting behavior of no. 20 carbon steel in electrolyte solutions. *Corrosion Science and Protection Technology*, *20*(4), 265–267.

Zou, Z., Ye, J., Sayama, K., Arakawa, H., Zhigang, Z., Jinhua, Y., … Arakawa, H. (2001). Direct splitting of water under visible light irradiation with an oxide semiconductor photocatalyst. *Nature*, *414*(6864), 625–627.

Zsolt, P. (2011). *Synthesis , morpho-structural characterization and environmental application of titania photocatalysts obtained by rapid crystallization*. University of Szeged, Babes-Bolyai University.